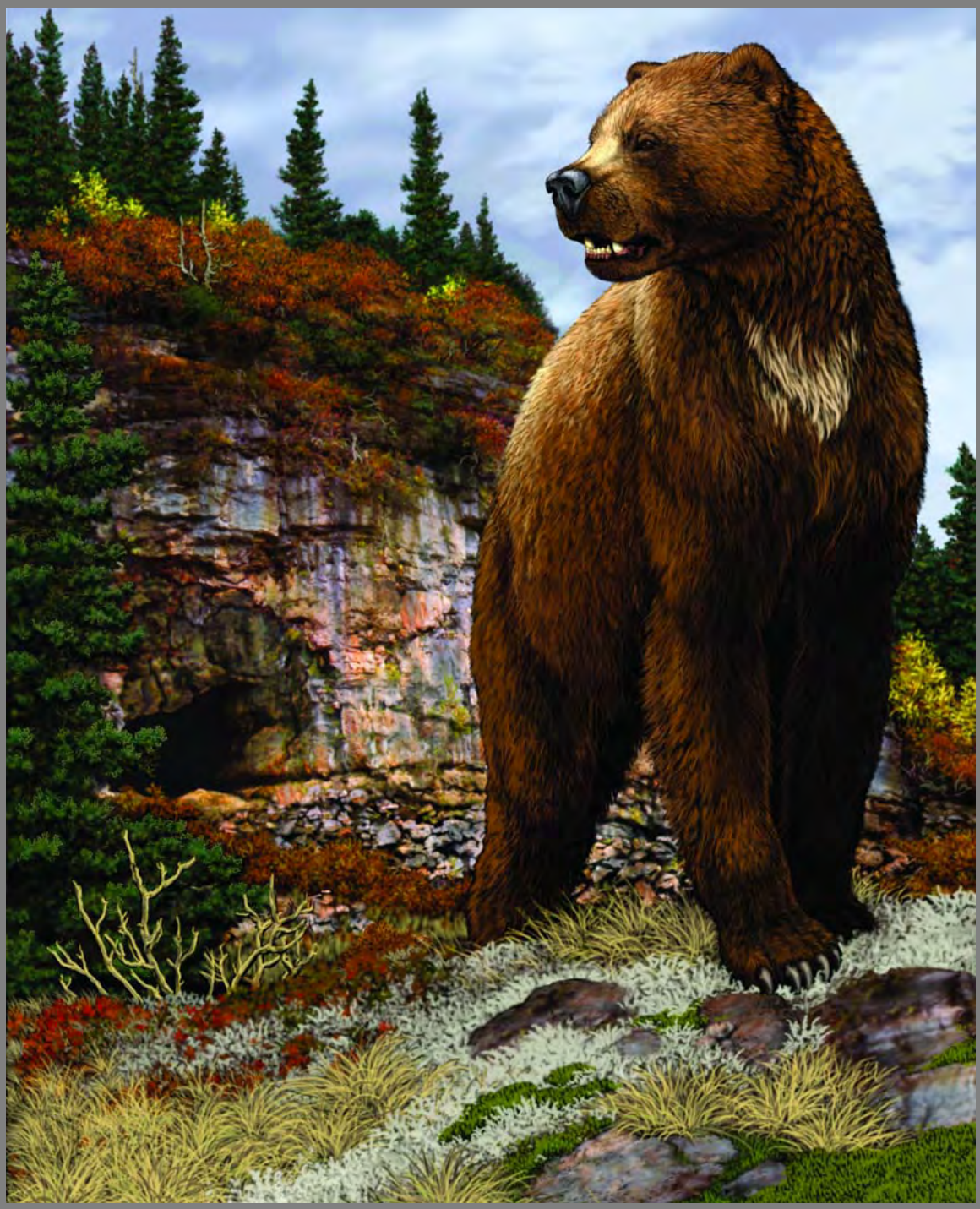
JOURNAL OF CAVE AND KARST STUDIES

August 2003
Volume 65 Number 2
ISSN 1090-6924
A Publication of the National Speleological Society



Journal of Cave and Karst Studies of the National Speleological Society

Volume 65 Number 2 August 2003

CONTENTS

Editorial

Science, the NSS, and the *Journal of Cave and Karst Studies*: Is it science without a journal?
William B. White 91

Articles

A troglomorphic sculpin (Pisces: Cottidae) population: Geography, morphology and conservaion status
Luis Espinasa and William R. Jeffery 93

A partial short-faced bear skeleton from an Ozark cave with comments on the paleobiology of the species
Blaine W. Schubert and James E. Kaufmann 101

Gypsum deposits in the Frasassi Caves, central Italy
Sandro Galdenzi and Teruyuki Maruoka 111

Detection of sinkholes developed on shaly Ordovician limestones, Hamilton County, Ohio, using digital topographic data: Dependence of topographic expression of sinkholes on scale, contour interval, and slope
Patrick Applegate 126

How speleothems grow: An introduction to the ontogeny of cave minerals
Charles A. Self and Carol A. Hill 130

Cave Science News 152

The *Journal of Cave and Karst Studies* (ISSN 1090-6924, CPM Number #40065056) is a multi-disciplinary, refereed journal published three times a year by the National Speleological Society, 2813 Cave Avenue, Huntsville, Alabama 35810-4431 USA; (256) 852-1300; FAX (256) 851-9241, e-mail: nss@caves.org; World Wide Web: http://www.caves.org/pub/journal/. The annual subscription fee, worldwide, by surface mail, is $18 US. Airmail delivery outside the United States of both the *NSS News* and the *Journal of Cave and Karst Studies* is available for an additional fee of $40 (total $58); The *Journal of Cave and Karst Studies* is not available alone by airmail. Back issues and cumulative indices are available from the NSS office. POSTMASTER: send address changes to the *Journal of Cave and Karst Studies*, 2813 Cave Avenue, Huntsville, Alabama 35810-4431 USA.

Copyright © 2003 by the National Speleological Society, Inc. Printed on recycled paper by American Web, 4040 Dahlia Street, Denver, Colorado 80216 USA

Front cover: Giant short-faced bear (*Arctodus simus*) in front of an Ozark cave, courtesy of natural history artist Carl Dennis Buell. Copyright Carl Dennis Buell, 2001. See article by Blaine W. Schubert and James E. Kaufmann, page 101.

Editor

Louise D. Hose
National Cave and Karst Research Institute
1400 University Drive
Carlsbad, NM 88220
505-234-5561 or 505-887-3051 FAX
lhose@cemrc.org

Production Editor

James A. Pisarowicz
Wind Cave National Park
Hot Springs, SD 57747
605-673-5582
pisarowicz@alumni.hamline.edu

BOARD OF EDITORS

Anthropology
Patty Jo Watson
Department of Anthropology
Washington University
St. Louis, MO 63130
pjwatson@artsci.wustl.edu

Conservation
Julian J. Lewis
J. Lewis & Associates, Biological Consulting
217 West Carter Avenue
Clarksville, IN 47129
812-283-6120
lewisbioconsult@aol.com

Earth Sciences-Journal Index
Ira D. Sasowsky
Department of Geology
University of Akron
Akron, OH 44325-4101
330-972-5389
ids@uakron.edu

Exploration
Vacant

Life Sciences
Steve Taylor
Center for Biodiversity
Illinois Natural History Survey
607 East Peabody Drive (MC-652)
Champaign, IL 61820-6970
217-333-5702
sjtaylor@inhs.uiuc.edu

Paleontology
Greg McDonald
Paleontology Program Coordinator
Geologic Resource Divison
National Park Service
P.O. Box 25287
Denver, CO 80225
303-969-2821
Greg_McDonald@nps.gov

Social Sciences
Marion O. Smith
P.O. Box 8276
University of Tennessee Station
Knoxville, TN 37996

Book Reviews
Ernst H. Kastning
P.O. Box 1048
Radford, VA 24141-0048
ehkastni@runet.edu

Proofreader
Donald G. Davis

JOURNAL ADVISORY BOARD

Malcolm Field
Chris Grove
Donald MacFarlane
Art Palmer
John Ganter
David Jagnow
Diana Northup
William White

SCIENCE, THE NSS, AND THE *JOURNAL OF CAVE AND KARST STUDIES*: IS IT SCIENCE WITHOUT A JOURNAL?

WILLIAM B. WHITE

Dept. of Geosciences and Materials Research Institute, The Pennsylvania State University, University Park, PA 16802 USA



Long, long ago in a college far, far away, I learned analytical chemistry from a hard-nosed professor who had no tolerance for sloppy data, sloppy concepts, or sloppy use of language. She would flunk you if you referred to an analytical balance as a "scale". She would flunk you if you referred to a scientific instrument as a "machine". And she would flunk you if you referred to a scientific journal as a "magazine". The NSS publishes the *Journal of Cave and Karst Studies*, which it claims is a scientific journal. Certainly it is not a magazine. From time to time, questions are raised as to what is a journal, anyway, and why is the NSS squandering its members dues by publishing one. In this editorial, I will try to explain what a journal is, how it differs from a magazine, and why the claim by the NSS that it is a scientific organization rests largely on the publication–and reputation–of the *Journal of Cave and Karst Studies*.

The essence of science is communication. Scientific discoveries must be communicated if they are to become part of the large and highly interconnected edifice we call scientific knowledge. Secret discoveries kept in locked file drawers are of no value to anyone. Leonardo Da Vinci wrote his voluminous and brilliant discoveries in secret code in notebooks that he showed to nobody. With his notebooks deciphered and published, today we see him as one of the great geniuses of the Renaissance, but his influence on the science of his day was essentially zero. Maybe, if the scientific journal had been invented in the 16th Century, he would have shared some of his observations and it would not have been necessary for them to be rediscovered later by others. The journal is the primary device for documenting, disseminating, and archiving scientific knowledge.

A journal, somewhat like a magazine, is composed of articles. The articles are written by scientists who use journal publication as their primary mode for communicating their discoveries. Journal articles are accepted for publication based on technical review by the author's peers, by the judgment of the editor, and by the appropriateness of the article to the subject matter of the journal. Because their primary purpose is to communicate new scientific discoveries, journal articles tend to be highly stylized. There is a statement noting the blank spot in human knowledge that is being investigated, there is a review of previous writings on the subject, there is a description of the field area and/or the laboratory methods being used, there are the main results–data, maps, photographs or whatever–presented as compactly as possible, and finally there is a discussion of the significance of the results and how much of the blank spot in human knowledge has been filled in. Journal articles are not literature. One learns nothing of the author's motivations in pursuing an investigation and nothing of his/her feelings and emotions as the study progressed. If one is intensely interested in the specific subject, a journal article may be very exciting. If one is not interested in the specific subject, a journal article will range from the stuffy to the downright boring. Journal articles are not written to entertain.

Journals have a range of intended audiences and a corresponding range of acceptable subject matter. There are broad audience journals, such as *Science* and *Nature*, that attempt to cover all of science. For articles to be accepted by these journals, they must appeal to a range of fields and, as might be expected, these journals are very picky about the articles they accept. Each field of science has its own leading journal – *Physical Review* for physicists, *Journal of the American Chemical Society* for chemists and the *Bulletin of the Geological Society of America* for geologists. To be taken seriously, physicists, chemists, and geologists must publish at least some of their work in their field's leading journal. But physics, chemistry, and geology are still too broad and there will be much research that is too specialized even for the leading journals in the field. Thus there are hundreds of subfields, most of which will have one or more niche journals. A niche journal caters to a highly specific subfield of science. The *Journal of Cave and Karst Studies* is a niche journal.

Being a niche journal means only that the subject matter is restricted to articles dealing with the geology, biology, and related aspects of caves and karst, subjects that make up only a tiny portion of the sciences of geology and biology. Niche journal status implies nothing about either the quality of the articles or the quality of the editing. With respect to quality of reviewing and editing, the *Journal of Cave and Karst Studies*

Copyright © 2003 by The National Speleological Society

and its predecessor, the *NSS Bulletin*, have had their ups and downs. Some editors tilted toward making the *NSS Bulletin* a magazine–for more reader appeal. Some editors didn't bother with external reviews and accepted more or less whatever showed up in the mailbox. However, for the past decade at least, the publication has followed the norms and standards of scientific journals generally. Based on personal experience with dozens of journals, I can say with confidence that the reviewing and editorial procedures are quite comparable to those of any of the leading journals.

In an age of rapid communication–telephones, e-mail, and the internet–it might reasonably be asked whether or not journals have become obsolete. After all, if communication is the objective, why wait for months for manuscripts to be reviewed, revised, printed, and distributed through the postal system? Why not just post the paper on a website which, indeed, is what is being done with many physics papers? We may be headed in that direction, but we're not there yet. Journal publication implies communication, documentation, and certification. It is the latter that gives journal publication its special status. Once a manuscript has survived review, revision, and editorial scrutiny, the version that is finally printed becomes, in effect, the official statement of what the author intended to say. This is the version that will be built into the fabric of scientific knowledge.

Niche journals at their best are a reservoir of highly detailed information on, for example, caves and karst, that is treated as an important resource by the entire scientific community. At their worst, they serve as a sort of newsletter for the handful of people interested in the topic and are totally ignored by everyone else. Where does the *Journal of Cave and Karst Studies* stand on this continuum? There is evidence that *JCKS* is a niche journal at its best. As anecdotal evidence, I have seen the *JCKS* cited frequently in papers in other professional journals by people who are not part of the cave and karst in-group. A current project of the Karst Waters Institute is to prepare a collection of "benchmark" papers that should be read by every graduate student interested in karst science. The list contains 39 papers. Five are from *Science*, three are from *Nature* (evidence in itself that caves and karst have a broad interest to the scientific community), and six are from the *NSS Bulletin/JCKS*. Some of the most fundamental investigations on caves have been published in the NSS's own journal. Even more quantitative evidence that researchers outside the little NSS-based scientific community read the *JCKS* is provided by the recent decision of the Institute for Scientific Information to add the *JCKS* to the list of journals covered in the Science Citation Index. This index provides a computer-searchable database of all papers published in the most cited of the thousands of journals published worldwide. For a journal to be included on the list means that it has a high citation rate, which in turn means that it is being read and taken seriously by many scientists outside its niche group of authors and readers.

To all of which many cavers may respond: So what? Even if the *JCKS* is a niche journal of the highest quality, does that justify the NSS membership being asked to pay for it? Why should a non-scientist NSS member be asked to pay for a publication–journal, magazine, whatever – that contains little that he/she is interested in reading? There are two answers to this question. One is that the NSS, with its steady support of its journal over the years, can take a great deal of credit for establishing the study of caves as a recognized subfield of science. It is mainly this contribution that permits the NSS to proclaim to the world (and the IRS) that it is a legitimate scientific organization. The second answer is another question. How is it that NSS members, many of whom are doing world-class caving in many places, do not see fit to write descriptions of their discoveries? The *NSS News* is full of outstanding articles describing the exploration. How is it that that there is no pressure to write a description of what was discovered? Good cave descriptions are good science. Good cave descriptions are the raw data that interpretation and theorizing follow. JCKS has an exploration editor. Make that person work harder. Science would benefit and the non-scientist NSS members might feel that they're getting more for their dues.

Luis Espinasa and William R. Jeffery - A troglomorphic sculpin (Pisces: Cottidae) population: Geography, morphology and conservation status. *Journal of Cave and Karst Studies 65*(2): 93-100.

A TROGLOMORPHIC SCULPIN (PISCES: COTTIDAE) POPULATION: GEOGRAPHY, MORPHOLOGY AND CONSERVATION STATUS

LUIS ESPINASA*
Centro de Educación Ambiental e Investigación Sierra de Huautla, Universidad Autónoma del Estado de Morelos, Avenida Universidad #1001, col. Chamilpa, Cuernavaca, Morelos, MEXICO
WILLIAM R. JEFFERY
**Department of Biology, University of Maryland, College Park, MD 20742-4415, USA*

In high latitudes, troglomorphic fish are absent despite the presence of caves. Glaciations during the Pleistocene may have prevented fish from colonizing this environment until very recent times. Here we present data on the northernmost cave adapted fish in the world, a troglomorphic sculpin (Cottus: Cottidae: Teleostei) from central Pennsylvania.

The characters normally used in recognizing troglomorphic fish, blindness and depigmentation, are not fully developed in this population. Nonetheless, these fish have a suite of modifications that readily identify them as cave-adapted: Elongated pectoral fins, more numerous and enlarged cephalic lateralis pores, a broader head, increased subdermal fat reserves, and in the brain, size reduction of the tectum opticum.

Individuals from this newly discovered troglomorphic population have been found only in a single cave at the lower end of the Nippenose Valley. Because of the significance and uniqueness of this population, we recommend that the U.S. Fish and Wildlife Service consider this troglomorphic sculpin for listing under the U.S. Endangered Species Act.

Despite the presence of large karst areas and long river cave systems in latitudes above 40° N (e.g., Baichtal 1995) troglomorphic fish have not been found in these habitats. A total of 88 species of troglomorphic fishes, belonging to 19 families, are known (Romero & Paulson 2001; Burr *et al*. 2001; Espinasa *et al*. 2001), but none has been reported from above 40° latitude. Europe has no described troglomorphic fish species, the northernmost species in Asia is *Nemacheilus starostini* from a cave in Turkmenistan (ca. 37° 55'N), and in North America the northernmost is *Amblyopsis spelaea*, found in Kentucky and southern Indiana (37-39°N). The latter is the most northern troglomorphic fish species described thus far (Romero & Paulson 2001).

One factor that probably contributes to the restricted distribution of troglomorphic fish is the extent of polar ice sheet migration during the Pleistocene. At the peak of the last Wisconsinan glacial advance ~20 ka ago, ice sheets covered most of the northern hemisphere above 40-50°N (Flint 1971). Therefore, most northern caves were not available for colonization by fish, at least until 12 ka ago, when the Wisconsinan ended. Restrictions in available underground habitats, as well as limited time to evolve distinct troglomorphic traits such as blindness and depigmentation, apparently confined the presence of troglomorphic fish to below 40°.

The second most northern troglomorphic fish in North America (Salem Plateau, Missouri: 37° 35'-37° 55'N) belongs to the *Cottus carolinae* species group (Burr *et al*. 2001). Although readily recognized as distinct from epigean fish by their body shape, reduction in pelvic fin ray number and enlarged cephalic lateralis pores (Burr *et al*. 2001), the "Grotto sculpins" are not fully eyeless or depigmented. They have small eyes (1-6% Standard Length vs. 6-10% SL in epigean samples) and significantly but not completely reduced pigmentation (Burr *et al*. 2001). Grotto sculpins are less troglomorphic than the cavernicolous amblyopsids, the archetypical North American hypogean fish group, which, with the exception of some localities for *Amblyopsis spelaea*, has a more southern distribution (32-39°N).

Here we present data on a previously unreported cave population of the *Cottus bairdi-cognatus* complex from a cave in central Pennsylvania (41° 9' N). This population represents the northern most cave adapted fish in the world.

MATERIALS AND METHODS

Troglomorphic sculpins were collected from Eiswert #1 Cave, Nippenose Valley, Lycoming County, Pennsylvania (41° 9' 23.2''N, 77° 12' 21.1''W, 212 m msl; Stone 1953). Fifteen individuals were collected in 2002 for study on 10, 11, and 17 August; 6 September; and 23-24 November (4, 1, 3, 4, 2, & 1 specimens, respectively). Surface sculpins were collected on 10 August, 2002 from nearby Lochabar Spring of Antes Creek, Lycoming County, Pennsylvania, also at the mouth of the Nippenose Valley (41° 9' 28.6''N, 77° 13' 13.6''W, 200 m msl). Antes Creek is a 4 km long tributary of the West Branch of the Susquehanna River. All samples were collected by

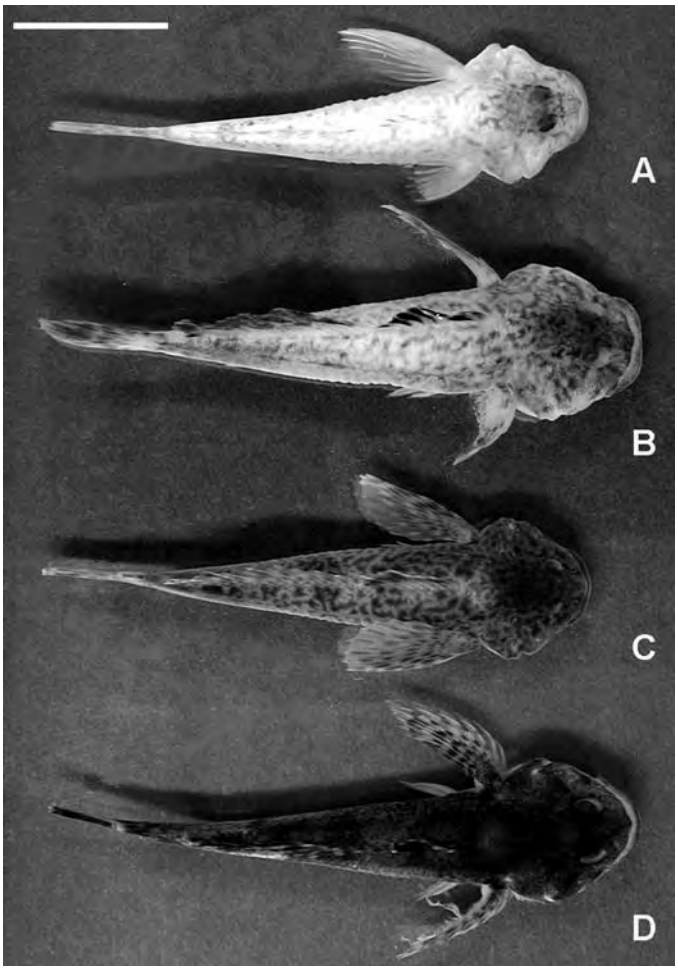


Figure 1. Dorsal view of Nippenose Valley troglomorphic (A-C) and epigean Antes Creek (D) sculpins showing patterns of coloration. A) Highly depigmented; B) Slightly depigmented; C) Pigmented; D) Highly pigmented. Scale bar: 2 cm.

James C.D. Lewis (Resident Pennsylvania Fishing License number R 703557). Samples were fixed either in the field or kept alive in the laboratory for a week before fixing. Fin clips were preserved in 100% ethanol and the body in 10% formaldehyde. Specimens used in the analyses will be deposited in the Pennsylvania State University Fish Collection.

Eye and mandibular canal pore #3 lengths were measured in 15 cave and 15 surface fish using a binocular microscope fitted with an eyepiece micrometer. Standard length, pectoral fin length, head width, and head length from mouth to base of pectoral fins were measured with dial calipers to the nearest 0.1 mm.

Heads from two cave and two surface sculpins were dissected using a scalpel and forceps under a binocular microscope. Skin of the head and the top of the skull were removed to expose brain, eyes and optic nerves. Eyes were then fixed in 10% formaldehyde, embedded in paraffin, and sagitally sectioned in slices, which in turn were stained with hematoxilin-eosin.

Level of pigmentation and its response to light were studied in the field by exposing 15 live cave and 15 live surface individuals to direct sunlight for 10 min and assessing changes in color. Four levels of pigmentation were assigned (Fig. 1). A) highly depigmented: skin color white with some groups of melanophores forming scattered dark spots of about 1 mm each. Some spots can be found in body and fins, but mostly on head. B) slightly depigmented: skin color also whitish but with spots found throughout whole body forming patterns and weak bands. C) pigmented: skin color tan to olive. Spots throughout whole body forming patterns and bands. D) highly pigmented: skin color dark green or black. Spots barely visible against dark background.

A Mann-Whitney test was used to look for possible differences in levels of pigmentation, number of mandibular pores and number of rays in the fins. Possible differences in the size of the eye, head, pectoral fin and mandibular pore #3 were examined using linear regressions and *t*-tests.

Visual response was studied in the field or in the laboratory by directly focusing a presentation pointer red laser beam (Limate corporation. Class IIIa laser product. Max. output <5 mW, 630-680 nm) in the eye of 7 individuals and assessing evasion reactions.

RESULTS

STUDY AREA

The Nippenose Valley is a nearly closed, anticlinal karstic valley. Surface water from the valley goes underground into a cave system that emerges at the mouth of the valley at Lochabar Spring, the origin of Antes Creek. Only 445 m from this spring, also at the lower end of the valley, is Eiswert #1 Cave. The cave, with a total of 167 m of explored passage, has a small stream that, in dry months, percolates under the gravel, leaving only an isolated sump pool at each end of the cave (Fig. 2). With about only 10 m of altitude difference between the downstream sump in the cave and the resurgence, it is likely that only partial isolation is in effect between the cave and surface populations.

Apart from the sculpins, the cave stream fauna included white isopods (5 mm long), amphipods (15 mm long), crayfish, and an unidentified teleost fish. None was collected or further identified. The isopod and amphipod appear to be cave adapted, and the presence of eggs in the marsupium of the isopods indicated they were reproducing. The crayfish and teleost fish appear to be surface taxa.

Surface sculpins were abundant around the spring and throughout Antes Creek, where they were found mainly under rocks. The Antes Creek fish population is isolated from the West Branch of the Susquehanna River during most of the year because its water is restricted to the hyporheic zone in the gravel of the creek bed. Only at high water levels is there continuous water contact between Antes Creek and the West Branch of the Susquehanna River.

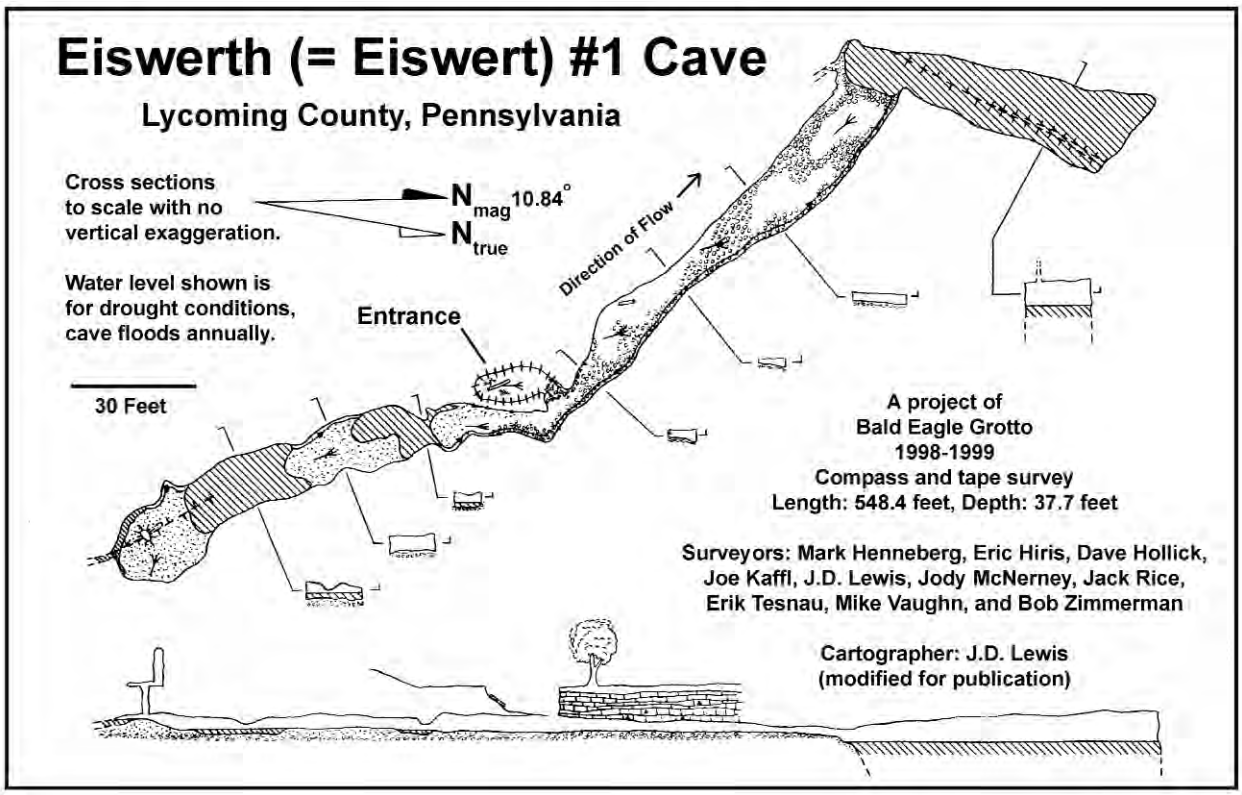


Figure 2. Eiswert #1 Cave map.

MORPHOLOGY

Mean standard length of the troglomorphic sculpins was 48.2 mm (n=15, SD=9.8, range=38.0-60.2 mm). All cavernicolous samples, except for one individual, had comparatively smaller eyes than epigean fish from Antes Creek (Fig. 3a). Their eye length was on average 5.7% (±0.8 SD) the standard length (SL). In the smallest eyed individual, the eye was 4.5% of the SL. Troglomorphic fish had eyes about 25% smaller ($P<0.001$) when compared to similar-sized surface fish (7.4% ±0.8 of the SL). The eyes themselves are positioned differently. In surface fish the eyes protrude conspicuously on the top of the head, while in troglomorphic fish they are half-sunken into the head (Fig. 4). Despite having smaller eyes, lens size was not reduced in cavefish. Both in surface and cavefish, the lenses were on average 1.3 mm (±0.3 SD) in diameter (Fig. 5).

Patterns and degree of pigmentation were variable in troglomorphic fish, but most individuals were conspicuously less pigmented than surface fish ($P<0.001$). Of the 15 troglomorphic fish studied, 3 were highly depigmented, 8 were slightly depigmented, and 4 were pigmented (Fig. 1). Of the 15 fish from Lochabar Spring, one was slightly depigmented, 12 were pigmented and 2 were highly pigmented. Reduction in eye size and pigmentation do not appear to be linked because pigmented fish could have highly reduced eyes and vice versa: Of the 4 pigmented cavernicolous fish, one of them had small eyes (4.8% of the SL), and of the 3 highly depigmented, one had big eyes (6.0% of SL). The other individuals had eyes roughly equal to the average in the Nippenose cave fish (5.7% ±0.8 SD of SL).

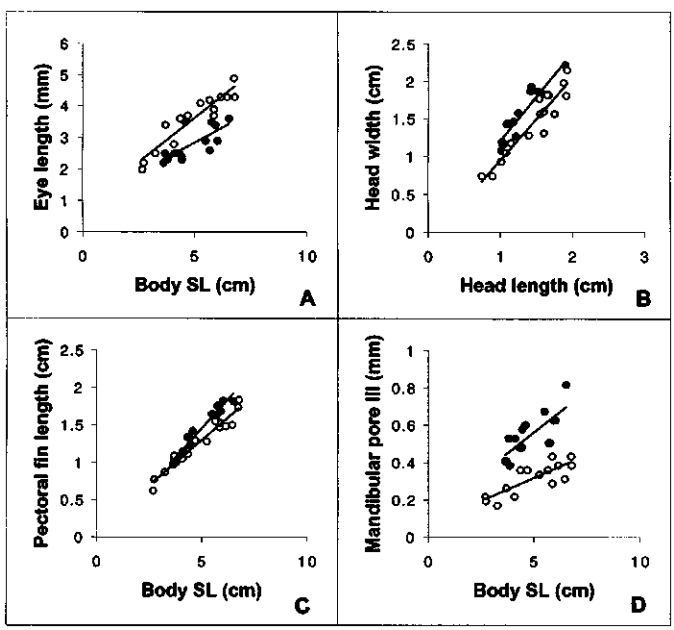


Figure 3. Morphometric comparisons between troglomorphic (closed circles, n=15) and epigean Antes Creek (open circles, n=15) sculpins. A) Eye length. B) Head width. C) Pectoral fin length. D) Mandibular pore III length. SL = Standard length. In C, linear regressions have significantly different slopes ($0.01<P<0.02$) and in A, B and D, linear regressions have significantly different elevations (all $P<0.001$).

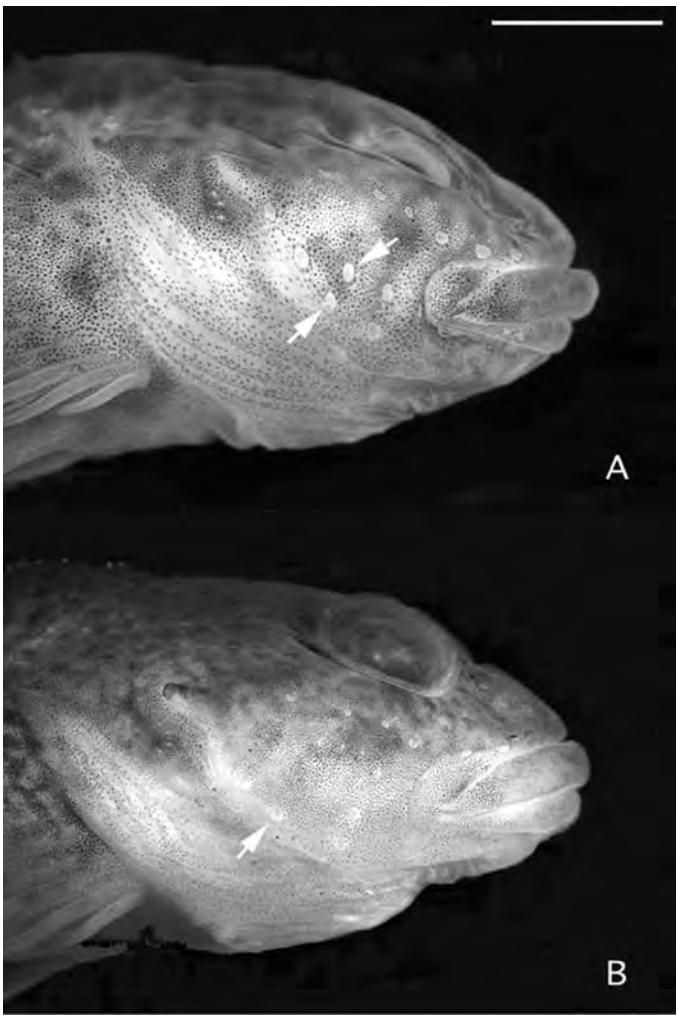


Figure 4. Lateral views of heads. Arrows point to mandibular pore VI (below) and the extra pore (above) found in most troglomorphic specimens. A) Pigmented troglomorphic sculpin; B) Pigmented epigean Antes Creek sculpin. Scale bar: 0.5 cm.

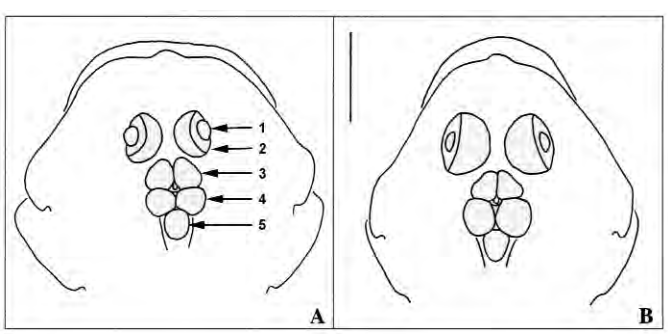


Figure 5. Drawing of dorsal views of heads showing the different eye size, tectum opticum and head width. A) Troglomorphic sculpin; B) Epigean Antes Creek sculpin. 1=Lens; 2= Eye; 3=Prosencephalon; 4= Mesencephalon (optic tectum); 5=Metencephalon. Scale bar: 0.5 cm.

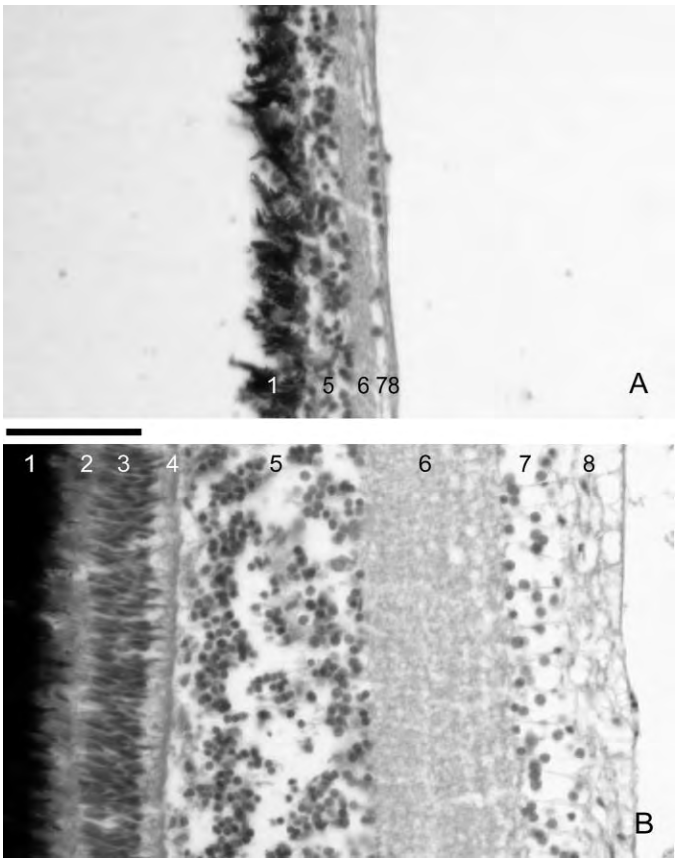


Figure 6. Histology of the retina. A) Troglomorphic sculpin; B) Epigean Antes Creek sculpin. Note absence of photoreceptors, outer nuclear layer, and outer plexiform layer in this troglomorphic individual. Other segments within the eye in this same individual had all retinal layers. 1=Pigmented epithelium; 2=Photoreceptors; 3=Outer nuclear layer; 4=Outer plexiform layer; 5=Inner nuclear layer; 6=Inner plexiform layer; 7=Ganglion cell layer; 8=Optic fiber layer. Scale bar for both images: 50 µm.

Histology of the eye from 2 cavernicolous individuals with small eyes (5.1% and 5.2% of SL) was performed. In these eyes, retina was present but its width was thinner. Cavefish retinal thickness, measured at the widest point in the eye, were 150 and 170 µm. Two similar-sized surface fish had retinas of 250 and 300 µm in width. Also, in one of the cavefish, almost half of the eye from one side of the optic nerve to the ciliary body showed a near absence of photoreceptor cells and outer nuclear layer (Fig. 6), and in this portion the thickness was only 50 µm. The other half of the eye had all the normal retinal layers. The optic nerve from the 2 cavernicolous individuals examined was 35% and 40% smaller in diameter compared to those of similar-sized surface fish, suggesting a reduced capacity to form connections to the brain.

Meristic features are presented in Table 1. Troglomorphic fish were not much different in their fin ray counts from Antes Creek surface fish and only slightly different from *C. cognatus* of Blockhouse Creek by averaging more rays in the first dorsal and pectoral fins. However, they were clearly different

Table 1. Comparison of percent frequencies of fin-ray counts. Data for *Cottus cognatus*, *Cottus bairdi* and hybrids are taken from Strauss' (1986) study of Blockhouse Creek fish.

	# of rays *	Troglomorphic (n=15)	Antes Creek (n=42)	Frequency *Cottus cognatus* (n=29)	Hybrids (n=8)	*Cottus bairdi* (n=42)
First dorsal fin						
	7	0.20	0.47	0.51	0.62	0.81
	8	0.73	0.42	0.48	0.37	0.19
	9	0.06	0.09			
Second dorsal fin						
	15	0.06		0.03		
	16	0.13	0.16	0.03		0.47
	17	0.66	0.69	0.65	0.37	0.45
	18	0.06	0.14	0.27	0.62	0.07
	19	0.06				
Pectoral fin						
	11.5			0.03		
	12			0.03		
	12.5		0.02			
	13	0.27	0.29	0.76		
	13.5	0.07	0.29			
	14	0.47	0.38	0.17		0.38
	14.5	0.13	0.02		0.13	0.05
	15	0.07			0.50	0.57
	15.5				0.13	
	16				0.25	
Pelvic fin						
	3	0.80	0.90	0.96		
	3.5	0.13	0.07	0.03	0.12	
	4	0.06	0.02		0.87	1.00
Anal fin						
	10			0.03		
	11	0.13	0.07	0.13		0.21
	12	0.62	0.57	0.58	0.50	0.66
	13	0.20	0.28	0.20	0.50	0.11
	14		0.07	0.03		

* values of .5 in # of rays indicates that the number of rays in the right and left fins is unequal, with one fin having one ray more than the other fin.

from *C. bairdi* and hybrids from Blockhouse Creek, particularly with respect to the first dorsal and pelvic fin ray counts (both $P<0.001$).

Bilateral asymmetry was high for both troglomorphic and Antes Creek surface fish. Right and left pectoral fins had different numbers of rays in 20% and 33% of the individuals respectively, while pelvic fin asymmetry was evident in 13% and 7% respectively (Table 1). This percentage of asymmetric individuals is an order of magnitude higher than for *C. bairdi* (pectoral 4.7%; pelvic 0.0%) and *C. cognatus* (pectoral 3.4%; pelvic 3.4%) from Blockhouse Creek, but is comparable to the bilateral asymmetry shown in hybrid individuals of that locality (pectoral 25.0%; pelvic 12.5%).

Head width measured both at the cheek level under the eyes or at its maximum width indicates that the troglomorphic fish head was about 20% wider ($P<0.001$) than in Antes Creek surface fish (Fig. 3b and 5). Pectoral fins in troglomorphic fish also differed ($0.01<P<0.02$) allometrically from Antes Creek. While small cave and surface fish had similar-sized pectoral fins, large cavefish individuals had 15% longer pectoral fins than similar-sized surface fish (Fig. 3c).

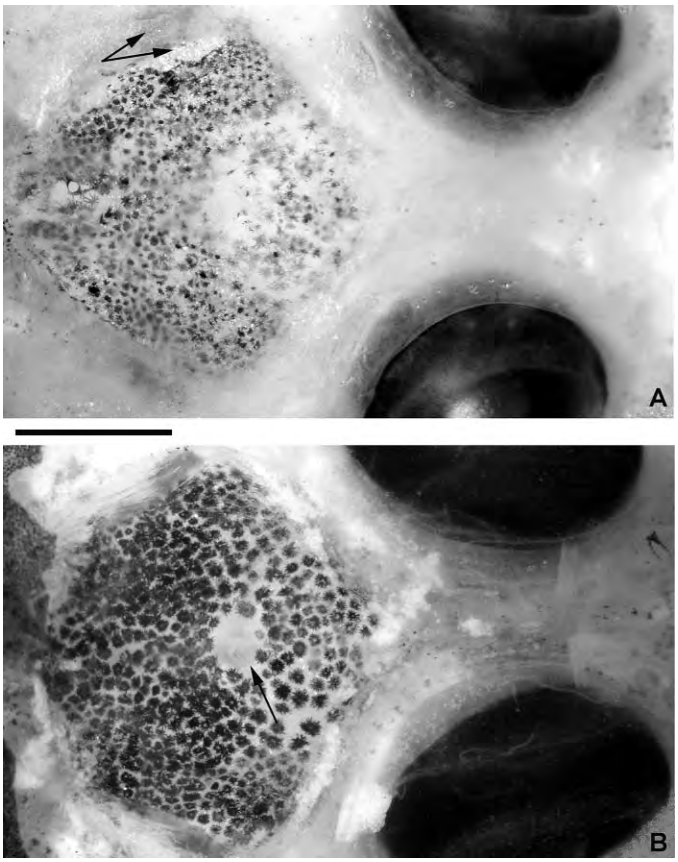


Figure 7. Dorsal view of head with skin removed. Melanophores in skull surround the pineal. A) Highly depigmented troglomorphic sculpin. Arrows point to subdermal fat layers. B) Pigmented epigean Antes Creek sculpin. Arrow points to pineal gland. Scale bar for both images: 2 mm.

Cephalic lateralis pore size was a clear discriminating feature between troglomorphic fish and surface fish. All cave individuals, including the most pigmented and large eyed individuals, had distinctly larger pore size than similar-sized surface fish ($P<0.001$). The mandibular pores of troglomorphic fish were readily visible with the unaided eye and, on average, were 1x-2x the size of those from epigean Antes Creek samples (Fig. 3d and 4). The number of pores also differed ($P<0.001$). In the mandibular canal above pore # 6 (counting from the chin backwards), 9 of 15 troglomorphic sculpins had an extra pore (Fig. 4). None of the 15 Antes Creek specimens had an extra pore.

Troglomorphic sculpins appear to have a thick subdermal layer of fat on the body. This was most clearly seen above the skull bones as a vacuolar matrix detachable from the skin and bone when dissecting (Fig 7a). A subdermal fat layer of this extent was not found in Antes Creek surface fish. Surface fish had abundant and orderly packed melanophores under the skin and above the skull, except for a window above the pineal gland (Fig 7b). Troglomorphic fish also showed these melanophores, but they were less abundant and disordered so that there are several uncovered sections and the window above the pineal was less obvious (Fig. 7a). The mesencephalon and prosencephalon also appeared to be different: troglomorphic fish brains had a comparatively smaller optic tectum than those of surface fish (Fig. 5). The mesencephalon in the two troglomorphic individuals examined was 1.01x and 1.03x the length of the prosencephalon while in similarly sized surface fish, mesencephalon was 1.20x and 1.40x the length of the prosencephalon.

RESPONSE TO LIGHT

Visual responses of the sculpins to the laser beam varied greatly among individuals. Two individuals evaded this stimulus instantly, 2 appeared never to notice it, and the remaining 3 were intermediate in their response, suggesting that vision capabilities are variable in the cavefish.

There were some changes in pigmentation levels after exposing live animals to direct sunlight for 10 minutes. Although pigment spots on troglomorphic sculpins were darker and more distinct, this general darkening was not intense enough to modify the level of pigmentation assigned originally to that individual while still in the darkness of the cave. After a week of living in the laboratory under illuminated conditions, a highly depigmented cave sculpin, although slightly darker, was still highly depigmented. Response to longer periods of light exposure could not be examined because fish failed to survive longer in the laboratory.

DISCUSSION

Two species of sculpins inhabit the West Branch of the Susquehanna River and its tributaries: Mottled sculpin (*Cottus bairdi*) and slimy sculpin (*Cottus cognatus*). These cottids display extreme variation in form and color between and within populations (Strauss 1986). Both species can overlap in meristic and morphometric traits and are known to hybridize with each other (Strauss 1986). One locality where the two species hybridize, Blockhouse Creek, is in the same county as Eiswert #1 Cave.

At the Blockhouse Creek locality, the number of pelvic fin rays, 3 in *C. cognatus* and 4 in both *C. bairdi* and the hybrids, can differentiate the species (Strauss 1986). Most individuals in the cave and in Antes Creek had 3 pelvic fin rays (Table 1), which would place them as *C. cognatus*. But Grotto sculpins in Missouri from the *C. carolinae* species group show a reduction in pelvic fin ray number from 4+4 elements to often 4+3, or 3+3 (Burr *et al*. 2001). If a reduction in pelvic fin number is a trend for cavernicolous cottids, the Nippenose Valley troglomorphic fish could be *C. bairdi* with a reduced pelvic fin ray number.

Because of the occurence of 2 *Cottus* species in this area and the potential for fin ray number reduction (see discussion earlier), assignment of the troglomorphic sculpins and the Antes Creek sculpins to *Cottus cognatus*, *Cottus bairdi*, or a

new taxon awaits more detailed assessments of characters and, perhaps, molecular studies. At this time, we restrict placement to the *Cotttus bairdi-cognatus* complex until further studies can be conducted.

Regardless of its final taxonomic position, the cave population has a unique set of morphological traits that permit their recognition as a distinct and unique population. We interpret these results as representative of losses and gains associated with cave habitation and evolution. Troglobitic characters found in other cavefish, such as elongated pectoral fins, more and enlarged cephalic lateralis pores, increased subdermal fat reserves, and modifications in the brain (Wilkens 1988) are also exhibited in these sculpins, but other characters, such as loss of pigmentation and blindness, are less developed.

Two contributing factors might explain why cave sculpins in the Nippenose Valley are not fully blind and depigmented. One could be that some genetic introgression with surface fish is still present, and second, that there has simply not been enough evolutionary time to fully regress these characters. These explanations are not mutually exclusive.

With a linear distance of 445 m between the cave and the spring, and only 10 m of altitude difference, it is unlikely that effective barriers prevent movement of sculpins between the surface and Eiswert #1 Cave. There is evidence suggesting that both the troglomorphic and Antes Creek fish populations are affected by hybridization. Bilateral asymmetry has been employed as a criterion of developmental instability on the assumption that coordination among loci within the genome protects the developing individual from developmental accidents (Felley 1980). Disruption of this coordination by hybridization with individuals having different coadapted gene complexes is expected to result in increased numbers of phenotypic variants and asymmetry (Strauss 1986). In the present study, the percentage of asymmetric individuals for both troglomorphic and Antes Creek fish is an order of magnitude higher than in *C. bairdi* and *C. cognatus* from Blockhouse Creek, but is comparable to the bilateral asymmetry shown in hybrid individuals of that locality. In this case, hybridization would not be between *C. bairdi* and *C. cognatus*, but instead, both Eiswert #1 Cave and Antes Creek populations could be an introgression gradient between an undiscovered troglobitic population that may exist deeper in the Nippenose karst and fish from the West Susquehanna River.

The other alternative, again not mutually exclusive, is that because of the northern location of the Nippenose karst, colonization of the cave environment could not be achieved until recent times due to Pleistocene glaciations. During the early Pleistocene (~850 ka BP), ice dammed the West Branch of the Susquehanna River at Williamsport, ~20 km east of the mouth of the Nippenose Valley, forming the 100-km-long Glacial Lake Lesley (Ramage *et al*. 1998). At that time, the Nippenose Valley would have been 100-150 m under water. The lake may have existed for ~4000 years, but it is likely that it ended abruptly by ice dam failure at maximum volume (~100 km^3), causing a flood of catastrophic proportions, perhaps one of the largest glacial floods in the eastern United States (Ramage *et al*. 1998). Even if sculpins had entered caves before this period, they would not have survived the catastrophic and abrupt change of pressure and conditions in the underwater caves. Therefore, the current population presumably colonized the cave environment less than 850,000 years ago.

During the late Illinoian and the Wisconsinan (198-17 ka BP), the southern limits of glacial advance were only 26 and 34 km north respectively of the Nippenose Valley (Sevon & Fleeger 1999). Although not under glaciers or lakes, tundra conditions with tens to even hundreds of meters of thick permafrost would have prevented surface sculpins from inhabiting the area. If all cave water froze during those times, and thus prevented occupancy, the sculpins could have inhabited the cave for <17 ka. If, on the contrary, the groundwater flow system in the valley is deep enough to absorb significant geothermal heat, it may not have frozen. In this case, sculpins could have taken refuge in the cave during the severest cold conditions while other surface fish migrated south. As such, the above glacial periods could be the isolating events.

CONSERVATION STATUS

Burr *et al*. (2001) noted that troglomorphic sculpin populations might be threatened both by their restricted distributions and the potential for impacts of human activities. Grotto sculpins of the *Cottus carolinae* species group from Missouri have been designated as Candidates for the Endangered and Threatened Wildlife and Plants list of the U.S. Fish and Wildlife Service. The designation may come too late for one of the six caves they inhabit, considering that a mass mortality was recently observed in one of the caves (Burr *et al*. 2001), and subsequent visits to that cave in 2002 failed to document any living Grotto sculpins.

The case for the troglomorphic sculpins of the *Cottus bairdi-cognatus* species group of the Nippenose Valley, Pennsylvania, is equally, if not more, alarming. Restriction to a single site locality is a criteria used by the International Union for the Conservation of Nature and Natural Resources (IUCN) to be included within the Red List of threatened animals (IUCN/SSC 1999), because any single point threat has the potential to bring extinction to the whole species. The troglomorphic sculpins are known only to exist in a single cave of the Nippenose Valley.

Proudlove (2001) lists 5 types of threats that cavefish can face: Hydrological manipulation, habitat degradation, overexploitation, impacts of introduced aquatic animals, and finally, environmental pollution by eutrophication and contamination from factory farms, agricultural, and/or industrial runoff. All 5 should be considered towards preserving the Nippenose troglomorphic sculpins.

Due to the distinctness and significance of this population, we recommend that the U.S. Fish and Wildlife Service consider this troglomorphic sculpin for listing under the U.S. Endangered Species Act.

ACKNOWLEDGMENTS

We thank all the concerned citizens of the Nippenose Valley, especially David Hollick, for all their encouragement, support, and friendship, without which this study could not have been done. We also would like to thank James C. D. Lewis for collecting the samples, Joan M. Ramage, Thomas W. Gardner, and Ira D. Sasowsky for clarifying the glacial history of the area, as well as Yoshiyuki Yamamoto for helping process the sculpins. Finally, we thank Monika Baker, Brooks M. Burr, Steve Taylor, and another anonymous reviewer for correcting the manuscript.

REFERENCES

Baichtal, J.F., 1995, Karstlands of southeastern Alaska: Recognition, exploration, and appreciation: American Caves, v. 7, n. 1, p.5-7.

Burr, B.M., Adams, G.L., Krejca, J.K., Paul, R.J., & Warren, M.L., 2001, Troglomorphic sculpins of the *Cottus carolinae* species group in Perry County, Missouri: Distribution, external morphology, and conservation: Environmental Biology of Fishes, v. 62, p. 279-296.

Espinasa, L., Rivas-Manzano, P., & Espinosa-Pérez, H., 2001, A new blind cave fish population of genus *Astyanax*: Geography, morphology and behavior: Environmental Biology of Fishes, v. 62, p. 339-344.

Felley, J., 1980, Analysis of morphology and asymmetry in bluegill sunfish (*Lepomis macrochirus*) in the southern United States: Copeia, v. 1980, p.18-29.

Flint, R.F., 1971, Glacial and Quaternary geology: Canada, John Wiley and Sons, Inc., p. 892.

IUCN/SSC Criteria Review Working Group, 1999, IUCN Red List criteria review provisional report: Draft of the proposed changes and recommendations: Species, v. 31-32, p. 43-57.

Proudlove, S.P., 2001, The conservation status of hypogean fishes: Environmental Biology of Fishes, v. 62, p. 201-213.

Ramage, J.M., Gardner, T.W., & Sasowsky, I.D., 1998, Early Pleistocene glacial Lake Lesley, West Branch Susquehanna River valley, central Pennsylvania: Geomorphology, v. 22, p.19-37.

Romero, A., & Paulson, K.M., 2001, It's a wonderful hypogean life: A guide to the troglomorphic fishes of the world: Environmental Biology of Fishes, v. 62, p. 13-41.

Sadoglu, P., 1967, The selective value of eye and pigment loss in Mexican cave fish: Evolution, v. 21, p. 541-549.

Sevon, W.D., & Fleeger, G.M., 1999, Pennsylvania and the Ice Age (2nd ed.): Pennsylvania Geological Survey Educational Series, n. 6, p. 30.

Strauss, R.E., 1986, Natural hybrids of the freshwater sculpins *Cottus bairdi* and *Cottus cognatus* (Pisces: Cottidae): Electrophoretic and morphometric evidence: The American Midland Naturalist, v. 115, p. 87-105.

Stone, R.W. 1953, Caves of Pennsylvania: The American Caver. Bulletin of the National Speleological Society, v. 15, p. 112-113.

Wilkens, H., 1988, Evolution and genetics of epigean and cave *Astyanax fasciatus* (Characidae, Pisces): Evolutionary Biology, v. 23 p. 271-367.

Blaine W. Schubert and James E. Kaufmann - A partial short-faced bear skeleton from an Ozark cave with comments on the paleobiology of the species. *Journal of Cave and Karst Studies* 65(2): 101-110.

A PARTIAL SHORT-FACED BEAR SKELETON FROM AN OZARK CAVE WITH COMMENTS ON THE PALEOBIOLOGY OF THE SPECIES

BLAINE W. SCHUBERT
Environmental Dynamics, 113 Ozark Hall, University of Arkansas, Fayetteville, AR 72701, and Geology Section, Research and Collections, Illinois State Museum, Springfield, IL 62703 USA
JAMES E. KAUFMANN
Department of Geology and Geophysics, University of Missouri-Rolla, Rolla, MO 65409 USA

Portions of an extinct giant short-faced bear, Arctodus simus*, were recovered from a remote area within an Ozark cave, herein named Big Bear Cave. The partially articulated skeleton was found in banded silt and clay sediments near a small entrenched stream. The sediment covered and preserved skeletal elements of low vertical relief (e.g., feet) in articulation. Examination of a thin layer of manganese and clay under and adjacent to some skeletal remains revealed fossilized hair. The manganese in this layer is considered to be a by-product of microorganisms feeding on the bear carcass. Although the skeleton was incomplete, the recovered material represents one of the more complete skeletons for this species. The stage of epiphyseal fusion in the skeleton indicates an osteologically immature individual. The specimen is considered to be a female because measurements of teeth and fused postcranial elements lie at the small end of the size range for* A. simus*. Like all other bears, the giant short-faced bear is sexually dimorphic. A review of* A. simus *records revealed that only small individuals have been recovered from cave deposits. This association of small* A. simus *specimens with caves suggests that females used these subterranean shelters for denning.*

In December 1998, Andy Free, a member of a cave mapping crew led by one of the authors (JEK), discovered the fragmentary remains of a large skeleton in the far reaches of a Missouri Ozark cave (Fig. 1). The survey crew was composed of members of the Missouri School of Mines Spelunkers Club from the University of Missouri-Rolla. This discovery led to a paleontological survey of the site in January 1999 by BWS. Following the preliminary identification of the specimen as *Arctodus simus*, excavations supported by the Illinois State Museum (ISM), the Missouri School of Mines Spelunkers Club, and the Cave Research Foundation, began in late February 1999. Due to logistical challenges associated with the site, excavations were not completed until March 2000. Here we present a description of this find from Big Bear Cave (BBC) and evaluate some aspects of the paleobiology of short-faced bears. A magazine article provided an informal account of this project (Schubert 2001).



Figure 1. Map of Missouri showing location of Big Bear Cave (black dot) and plan view sketch showing the cave passage where *Arctodus simus* remains were discovered, ~1.4 km from the modern entrance. The excavated area is indicated by a black rectangle. NSS standard map symbols follow Hedges *et al.* (1979).

SHORT-FACED BEARS

Although ursids first appear during the Miocene, their fossil record remains relatively meager until the Pleistocene. Two ursid subfamilies are represented in the New World, Tremarctinae and Ursinae. The earliest known tremarctine is the late Miocene *Plionarctos* (Tedford & Martin 2001). *Arctodus* appears during the Pliocene and is represented by *Arctodus pristinus* (lesser short-faced bear), a smaller, more gracile form with a proportionally longer snout than *A. simus* (giant short-faced bear) (Kurtén & Anderson 1980). Five species of short-faced bears have been described from the Pleistocene of South America (within the genus *Arctotherium*;

Copyright © 2003 by The National Speleological Society



Figure 2. Articulated *Arctodus simus* forearms *in situ* and forearm of caver for scale.

Soibelzon 2002). Another tremarctine genus, *Tremarctos*, appeared during the late Pliocene in North America (Tedford & Martin 2001). The only living representative of the tremarctine subfamily is *Tremarctos ornatus* (spectacled bear) of South America.

Arctodus simus was the largest Pleistocene terrestrial carnivore in North America (Churcher *et al.* 1993; Christiansen 1999). Recent estimates of body weight based on bone proportions place *A. simus* as heavier than other extant and extinct ursids, with large individuals weighing at least 700 kg, and perhaps more than a metric ton on occasion (Christiansen 1999).

The giant short-faced bear previously was reported from over one hundred localities in North America, ranging from Mexico to Alaska and from the Pacific to the Atlantic coasts (Richards *et al.* 1996). Eight of these localities are Ozark caves (Hawksley 1965; Hawksley 1986; Hawksley *et al.* 1973; Puckette 1976; Hawksley & Weaver 1981; Schubert 2001). Temporally this species ranged from the middle Irvingtonian North American Land Mammal Age (NALMA) through the Rancholabrean NALMA, becoming extinct near the end of the Pleistocene in an extinction event that killed off most large North American mammals (Grayson 1989; Kurtén & Anderson 1980).

MATERIALS AND METHODS

Excavation was carried out during the winter months to avoid contact with the extensive gray bat (*Myotis grisescens*) maternity colony located between the entrance and the excavation site. Reaching the bear bones required a great deal of crawling and wading through streams and muddy crawlways. A typical excavation round trip lasted from 13-16 hours. For these reasons, the skeleton was exposed (Fig. 2), mapped (Fig. 3), and divided into sections that were removed from the cave in plaster jackets. Quick setting plaster bandages were used for the removal process. Only remains that could be removed in a single trip were excavated at one time. In all, 13 excavation trips were made to the short-faced bear locality.

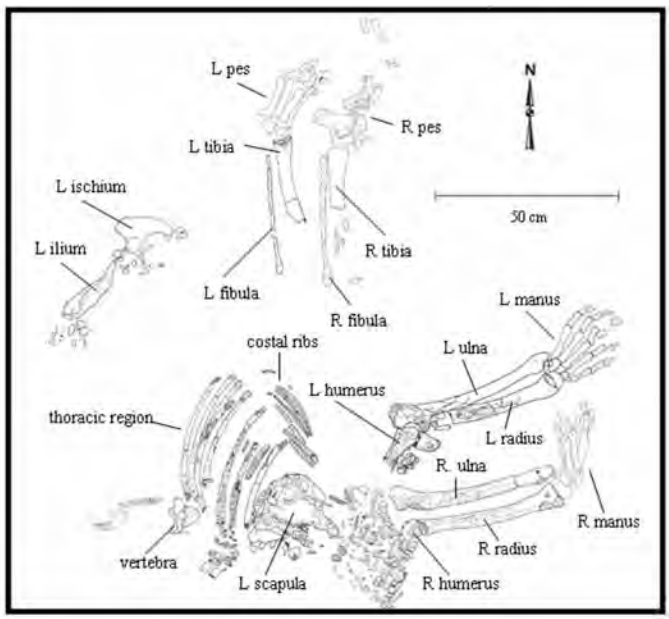


Figure 3. Plan view sketch of the excavated area showing *Arctodus simus* skeletal material *in situ*. Loose disturbed surface bones and teeth not shown on sketch.

The inner portions of BBC are typical of many caves in the central Ozarks, having streams, slick clay sediments, large sediment banks, and a constant high humidity. These characteristics present logistical challenges for excavation. All bone at the site was saturated and most of the material was highly fragmentary. Adhering to the bones was wet, sticky sediment, which proved difficult to remove without the sediment pulling off bone fragments.

The bear site (Figs. 1 & 3) was mapped by using survey station F9 from the original cave survey as a primary datum. This datum is a rock (with F9 written on it) located on a ledge above the excavation site. A secondary datum (a survey flag) was placed in the floor near the bear remains and is still in place. This secondary datum was used for vertically and horizontally mapping the skeleton with a tape measure, string, and line-level. Because of the poor condition of the skeletal material and distance from the cave entrance, plaster jackets were used to stabilize and transport most of the remains out of the cave. These plaster jackets were then transported to the ISM and prepared in the laboratory. Some of the remains were exposed but not removed from the sediment. These are currently conserved in plaster jackets (for example, see Fig. 4). Butvar™ was used as the consolidant for preserving nearly all the remains. Molds and casts of much of the articulated skeleton were also made in the ISM preparation laboratory. Digital calipers were used for measuring the smaller remains and sliding metal calipers for the larger specimens. Where possible, dimensions follow Merriam and Stock (1925), Kurtén (1967), and Driesch (1976). Length and width for dental measurements were taken at the base of the enamel. Skeletal and dental measurements are reported in millimeters (mm). All



Figure 4. Plaster jacket opened to show articulated left manus of *Arctodus simus*. White scale bar = 1 cm.

remains collected are now curated in the Geology Collections at the ISM under catalog number ISM 496850.

Scanning electron microscope (SEM) images were taken, and the energy dispersion spectrum (EDS) analysis was performed, at the Electron Microscopy Laboratory at UMR. X-ray diffraction analyses (XRD) were carried out in the Geochemistry and Clay Mineralogy Lab at UMR. Bone chemistry was analyzed at Stafford Laboratories, Boulder, Colorado, but, as noted below (under Chronologic Age), the specimen lacked sufficient bone protein for dating. Computed tomography (CT) scans were preformed at Memorial Medical Center, Springfield, Illinois.

LOCALITY

Big Bear Cave formed in the Ordovician Gasconade dolomite. The entrance to the cave faces south and lies at the base of an 11 m tall bluff at the top of a steep slope ~26 m above the Gasconade River in Pulaski County, Missouri. The entrance is 25 m wide by 7 m high but the entrance passage narrows to 6 m wide by 3 m high after 55 m and soon becomes a crawlway only 1 m high. The layout of the cave is a series of 3 north-northwest-trending trunk passages connected by crawlways. The *Arctodus* remains were in a side passage (now termed "Arctodus Avenue"), ~150 m from the Bat Room and 1400 m from the current entrance of the cave. The Bat Room is the site of a large maternity colony of gray bats (*Myotis grisescens*) that roost in at least 5 separate locations. Arctodus Avenue continues for ~380 m, ending at a large rubble pile that blocks the passage. This appears to be the closest potential entrance that the short-faced bear might have used. Many side passages have not been mapped or explored and, the total length of all the cave passages is certainly much longer than the currently known 6500+ m length.

A cursory paleontological survey of a small portion of the cave by the authors revealed numerous black bear (*Ursus americanus*) bones, bear beds, claw marks, tracks, and possible bear scat. Further investigation is needed to better understand the use of the cave by bears. The cave is currently closed to all visitations by the landowners. To respect the owner's wishes for privacy we renamed the cave for this publication. The exact location and other names for the cave are on file in the Geology Section archives at the ISM and the Missouri Speleological Survey database, Missouri Department of Natural Resources, Geological Survey and Resource Assessment Division, Rolla, Missouri.

DEPOSITIONAL SETTING

The passage where the *Arctodus simus* specimen was located is ~10 m wide and 3 m high. The entrenched stream flows in a channel along the north wall where the ceiling along that side of the passage lowers to within 1 m of the stream. A sediment bank rises some 1 m from the stream bed level to the ceiling level and forms a 2 m wide terrace at that level before another 1 m high slope. Immediately downstream from the site, the sediment bank rises abruptly to meet the descending ceiling level, thus constricting the stream in a small ~75 cm wide by ~50 cm high tunnel. This constriction forces flood waters to overflow the stream channel and flow on the terrace level, which serves as a flood-overflow channel (Fig. 1).

Excavation showed the bear to be lying on its right side (Fig. 3) with the distal portions of the hind limbs located on a sloping floor near the modern stream level beneath the overhanging ledge. Much of the surface in the excavation area was covered by highly fragmented and water saturated bone. The majority of the skeleton was located on a flood overflow channel that previously served as a footpath for cavers. The hind limbs were located on the sloping surface with the feet lying ~25 cm below the thoracic region. The hind feet were buried under ~20 cm of sediment while the thoracic region was buried by only a few centimeters of sediment.

The sediment immediately below and encasing the carcass is composed of banded silt and silty clay composed predominantly of quartz (Fig. 5). This banded sediment is only a few centimeters thick in the flood overflow channel but thickens to nearly 40 cm at the base of the bank near the stream. The banded sediment overlies a poorly consolidated, predominately red clay (7.5YR 4/4) unit (all Munsell colors were judged using dried sediments). The lower portion of the banded sediments is tinted red by inclusions of silt-sized clay particles, which are apparently eroded fragments of the red clay. The upper portion of the sediment immediately below the carcass is composed of light (10YR 7/4) and dark (10YR 6/4) tan layers with occasional thin reddish layers. The hind limbs, being lower in elevation, were subjected to more frequent flooding and hence were buried more rapidly and to a greater thickness than the torso.

Intimately associated with the skeleton is a prominent discontinuous layer from 1-2 mm thick containing a black (N 2.5/0) mineral (Fig. 5, white arrows). This black layer is composed of small tubules and strands (Fig. 6) that we interpreted



Figure 5. Cross-sectional view of sediments below ribs. White arrows indicate manganese deposits containing hair molds and casts.

to be hair. In many places an unstratified brown (10YR 5/3) sediment averaging 10 mm thick overlies the black layer. Associated with this layer are occasional clumps of red clay that match the most common older sediments in the cave. These clumps often contain nodules of the black mineralization. Like the thin black layer noted above, the nodules contain tubules and strands that appear to be fossil hairs (see Systematic Paleontology). EDS analysis indicates that the primary constituent of this black layer is manganese (Fig. 7) while XRD analysis failed to indicate any major crystalline component. This is typical of fine-grained manganese oxide/oxy-hydroxide mixtures. We suggest that the clumps of red clay containing the larger manganese nodules with fossil hair were enmeshed in the hair prior to, or near the time of, the bear's death.

Several authors (Nealson *et al.* 1992; Nealson & Stahl 1997; and Tebo *et al.* 1997) reported on the deposition of manganese oxide and oxy-hydroxides by microbial oxidation processes. The manganese oxide and oxy-hydroxide layer associated with the *A. simus* skeleton may have occurred during microbial decomposition of the decaying carcass. The cave stream, sediments, and carcass itself are potential sources of the manganese. The amount of potential manganese available from the bear and sediments has not been calculated. However, Imes *et al.* (1996) reported that typical spring water in the region of BBC contains from 1-3 µg/L of manganese, suggesting that the stream alone could have supplied the manganese. This process of microbially moderated manganese deposition may help explain the relatively common black staining on paleontological remains from wet caves.

CHRONOLOGIC AGE

A fragment of an incisor root was sent to Stafford Research Laboratories, Inc., Boulder, Colorado. Pretreatment techniques (Stafford *et al.* 1987; Stafford *et al.* 1991) indicated that the specimen had a non-collagenous amino acid composition containing 3nm/mg of protein, 0.1% of the protein found in modern tooth samples. Therefore, an AMS radiocarbon date attempt was not justified because of the low protein content of the dentine. This leaching of protein from the skeletal remains was probably the result of periodic inundation. Although an exact age could not be determined for the *A. simus* specimen, a Rancholabrean age is inferred based on the known time range of this species.

SYSTEMATIC PALEONTOLOGY

Order Carnivora Bowdich, 1821
Family Ursidae Gray, 1825
Subfamily Tremarctinae Kraglievich, 1926
Genus *Arctodus* Leidy, 1854
Arctodus simus (Cope), 1879
(Giant Short-faced Bear)
(Figs. 6 and 8; Tables 1-5)

Table 1. Measurements of *Arctodus* teeth. Dimensions after Driesch (1976) and Merriam and Stock (1925). (1) = M2 length dimension as in Driesch, (2) = M2 length dimension perpendicular to the midline. Observed ranges (OR) for *Arctodus pristinus* and *Arctodus simus* from Emslie (1995) and Richards *et al.* (1996). X = comparative measurements not reported in Richards *et al.* (1996). * = M2s may have been measured using either methodology noted here (1 or 2).

Measurement	BBC specimen	*Arctodus pristinus* OR (N)	*Arctodus simus* OR (N)
i2			
greatest transverse diameter	L 8.3, R 8.4	X	X
i3			
greatest transverse diameter	L 11.0	X	X
p4			
anteroposterior diameter	R 13.3	10.5-12.2 (9)	10.3-13.7 (13)
greatest transverse diameter	R 8.5	6.7-7.5 (7)	6.2-8.8 (12)
m1			
anteroposterior diameter	R 32.8	24.3-29.5 (15)	29.6-35.3 (32)
greatest transverse diameter of anterior half	R 16.1	X	X
greatest transverse diameter of heel	L 15.9, R 15.8	13.0-15.7 (15)	15.1-18.4 (6)
m2			
anteroposterior diameter	R 30.8	22.6-28.7 (18)	26.3-33.6 (45)
greatest transverse diameter	R 20.8	X	X
m3			
anteroposterior diameter	L 21.7	16.1-22.5 (14)	18.7-24.2 (33)
greatest transverse diameter	L 17.1	13.5-17.0 (14)	14.5-19.1 (33)
I1			
greatest transverse diameter	L 9.0, R 8.9	X	X
I2			
greatest transverse diameter	R 10.0	X	X
I3			
greatest transverse diameter	R 13.3	X	X
M2			
anteroposterior diameter (1)	R 38.5		
anteroposterior diameter (2)	R 37.3	*33.0-39.0 (9)	*33.3-42.9 (42)
greatest transverse diameter (anterior width)	R 22.8	19.6-22.5 (9)	20.8-26.6 (42)

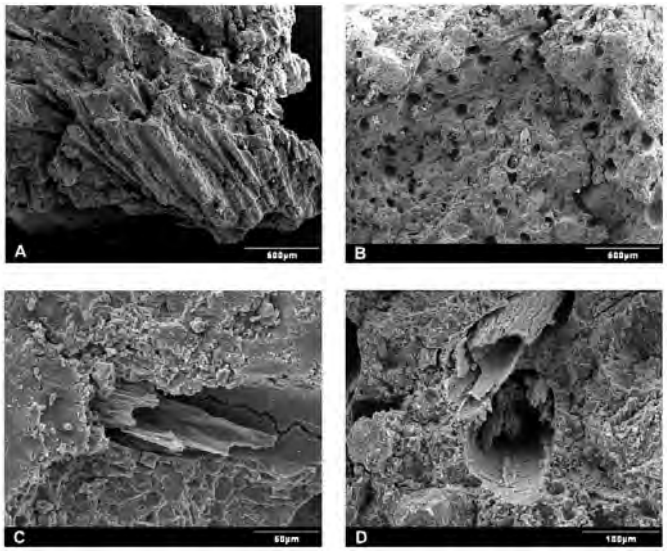


Figure 6. Scanning electron micrographs of *Arctodus simus* fossilized hair. A, hair molds; B, cross-sectional view of hair molds and hair; C and D, close-up of individual molds and hair.

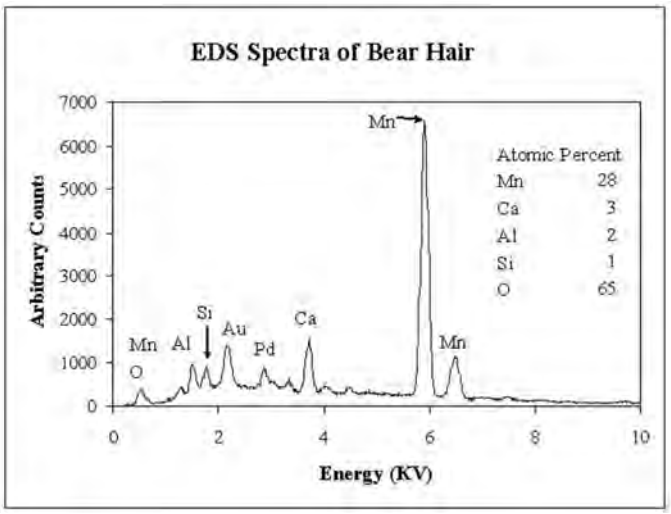


Figure 7. Energy Dispersion Spectral analysis (EDS) on black sediment containing fossil bear hair. Gold (Au) and palladium (Pd) were used to coat the sample to make it electrically conductive.

Table 2. Measurements of *Arctodus* calcanea and metacarpals. Dimensions after Driesch (1976). For the BBC specimen the greatest breadth of the distal end of the metacarpals was taken perpendicular to the shaft, not at an angle as shown in Driesch (1976). This measurement was taken at the widest point of the distal end, which is the contact between the shaft and the epiphysis. Observed ranges (OR) for *Arctodus pristinus* and *Arctodus simus* from Richards *et al.* (1996). X = comparative measurements not reported in Richards *et al.* (1996). * = pathological.

Measurement	BBC specimen	*Arctodus pristinus* OR (N)	*Arctodus simus* OR (N)
calcaneus			
greatest length	L 108.5, R 108.4	99.0 (1)	101.0-136.0 (16)
greatest width	L 72.4, R 71.7	65.0 (1)	67.0-92.8 (14)
metacarpal I			
greatest length	R 75.1	70.0 (1)	73.5-100.0 (10)
greatest breadth of distal end	R 19.2	18.7 (1)	17.4-27.2 (10)
metacarpal II			
greatest length	R 103.3	X	97.0-135.0 (9)
greatest breadth of distal end	R 24.4	X	23.5-34.0 (9)
metacarpal III			
greatest length	R 109.5	96.0 (1)	104.0-142.0 (10)
greatest breadth of distal end	R 24.4	22.9 (1)	24.8-35.4 (10)
metacarpal IV			
greatest length	*R 110.6	100.0 (1)	107.0-133.2 (8)
greatest breadth of distal end	*R 26.1	25.3 (1)	23.5-33.7 (8)
metacarpal V			
greatest length	R 111.1	X	98.0-130.0 (7)
greatest breadth of distal end	R 27.3	X	23.0-34.2 (7)

Table 3. Measurements of Big Bear Cave *Arctodus simus* proximal and middle phalanges, right manus. Dimensions after Driesch (1976).

Measurement	BBC specimen
proximal phalanx, digit II	
greatest length	49.0
greatest breadth of proximal end	25.2
least breadth of diaphysis	14.0
greatest breadth of distal end	18.7
proximal phalanx, digit III	
greatest length	51.2
greatest breadth of proximal end	25.8
least breadth of diaphysis	14.7
greatest breadth of distal end	19.6
proximal phalanx, digit IV	
greatest length	54.3
greatest breadth of proximal end	27.5
least breadth of diaphysis	15.4
greatest breadth of distal end	20.5
proximal phalanx, digit V	
greatest length	52.6
greatest breadth of proximal end	26.4
least breadth of diaphysis	14.1
greatest breadth of distal end	19.1
middle phalanx, digit II	
greatest length	36.2
greatest breadth of proximal end	19.9
least breadth of diaphysis	13.6
greatest breadth of distal end	18.1
middle phalanx, digit IV	
greatest length	38.7
greatest breadth of proximal end	20.5
least breadth of diaphysis	12.2
middle phalanx, digit V	
greatest length	34.5
greatest breadth of proximal end	19.9
least breadth of diaphysis	12.5
greatest breadth of distal end	16.7

MATERIAL

All the remains are cataloged within the same number, ISM 496850. The recovered elements include whole or partial specimens of L i2; R i2; L i3; R p4; L m1 fragments; R m1; R m2; L m3; L I1; R I1; R I2; R I3; R M2; enamel cap of p2/P2 or p3/P3; two M1? fragments; vertebral epiphyses; portions of 2 thoracic vertebrae; rib epiphyses; rib fragments; portions of at least 7 costal ribs; portions of L ilium and ischium; portions of L, R scapulae; L, R humeri, distal ends; L, R ulnae; L, R radii; L, R pisiforms; L, R scapholunars; L, R cuneiforms; L, R unciforms; L, R trapezoids; L, R trapeziums; L, R metacarpals I-V; L proximal phalanges of manus digits I-V; R proximal phalanges of manus digits II-V; L medial phalanges of manus digits II-V; R medial phalanges of manus digits II, IV, and V; L terminal phalanges of manus digits I-V; four R terminal manus phalanges (undifferentiated); 10 sesamoids from L manus; 8

Table 4. Measurements of *Arctodus* right and left metatarsals. Dimensions after Driesch (1976). Observed ranges (OR) for *Arctodus pristinus* and *Arctodus simus* from Richards *et al*. (1996).

Measurement	BBC specimen	*Arctodus pristinus* OR (N)	*Arctodus simus* OR (N)
metatarsal I			
greatest length	L 74.6	66.0 (1)	71.0-84.0 (7)
greatest breadth of distal end	L 18.0	17.7 (1)	16.7-25.0 (8)
metatarsal II			
greatest length	L 94.7	80.0-90.0 (2)	86.0-101.3 (3)
greatest breadth of distal end	L 23.6	22.4-23.0 (2)	23.6-25.6 (4)
metatarsal III			
greatest length	L 103.4, R 103.4	90.0-106.0 (2)	94.0-124.1 (12)
greatest breadth of distal end	L 23.3, R 24.2	24.2 (1)	23.2-35.8 (12)
metatarsal IV			
greatest length	L 114.1, R 114.1	98.0 (1)	105.0-132.3 (6)
greatest breadth of distal end	L 24.9, R 25.2	24.0 (1)	23.5-35.1 (6)
metatarsal V			
greatest length	L 113.1	98.0 (1)	85.0-135.0 (11)
greatest breadth of distal end	L 25.7	22.0 (1)	18.3-31.4 (11)

Table 5. Measurements of Big Bear Cave *Arctodus simus* proximal and middle pes phalanges. Dimensions after Driesch (1976).

Measurement	BBC specimen
proximal phalanx, digit I	
greatest length	L 39.5
greatest breadth of proximal end	L 19.6
least breadth of diaphysis	L 12.0
greatest breadth of distal end	L 14.8
proximal phalanx, digit II	
greatest length	L 39.9
greatest breadth of proximal end	L 22.8
least breadth of diaphysis	L 13.9
greatest breadth of distal end	L 16.2
proximal phalanx, digit III	
greatest length	L 42.2
greatest breadth of proximal end	L 23.1
least breadth of diaphysis	L 14.3
greatest breadth of distal end	L 17.3
proximal phalanx, digit IV	
greatest length	L 48.4
greatest breadth of proximal end	L 25.1
least breadth of diaphysis	L 14.6
greatest breadth of distal end	L 18.0
proximal phalanx, digit V	
greatest length	L 45.7
greatest breadth of proximal end	L 23.4
least breadth of diaphysis	L 12.6, R 12.7
middle phalanx, digit II	
greatest length	L 28.1
greatest breadth of proximal end	L 18.5
least breadth of diaphysis	L 13.0
greatest breadth of distal end	L 15.6
middle phalanx, digit III	
greatest length	L 30.7
greatest breadth of proximal end	L 19.0
least breadth of diaphysis	L 12.3
greatest breadth of distal end	L 16.2
middle phalanx, digit IV	
greatest length	L 32.4
greatest breadth of proximal end	L 19.6
least breadth of diaphysis	L 12.1
greatest breadth of distal end	L 15.9
middle phalanx, digit V	
greatest length	L 29.1
greatest breadth of proximal end	L 18.8
least breadth of diaphysis	L 12.0
greatest breadth of distal end	L 15.2

sesamoids from R manus; proximal end of L femur; proximal shaft of R femur; L, R patellae; L, R tibiae, proximal and distal portions for both sides; fragmentary L fibula; R fibula; L, R calcanea, L, R astragali; L, R mesocuneiforms; L, R naviculars; L, R ectocuneiforms; L, R entocuneiforms; L, R cuboids;

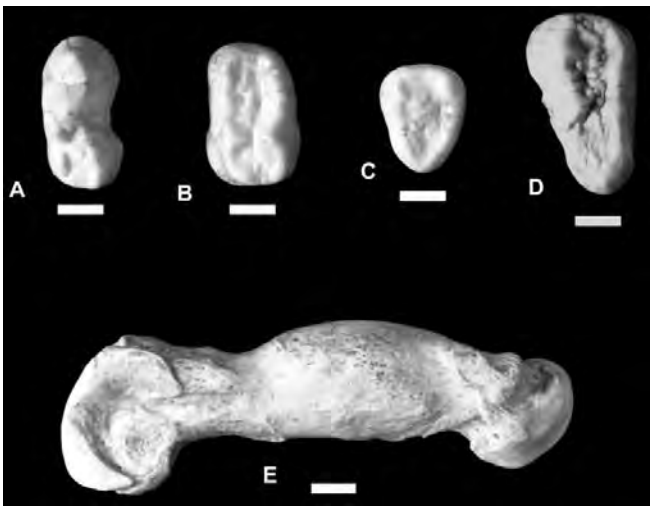


Figure 8. Selected elements from the BBC *Arctodus simus* skeleton. All teeth are shown in occlusal view. A, R m1; B, R m2; C, L m3; D, R M2. E, pathological R metacarpal IV. White scale bars = 1 cm.

L, R metatarsals I-V; L proximal phalanges of pes digits II-V; L medial phalanges of pes digits I-V; L terminal phalanges of pes digits I-III and V; R proximal phalanx of pes digit V; R terminal phalanx of pes digit V; 10 sesamoids from L pes; 3 sesamoids from R pes; one undifferentiated sesamoid; numerous bone and tooth fragments; sediment samples with fossilized hair and hair casts in manganese.

DIAGNOSIS

Tremarctine bears can be morphologically distinguished from ursine bears based on the presence of a premesseteric fossa on the mandible, an entepicondylar foramen on the humerus, and an extra lateral cusp between the talonid and trigonid on the m1 in the former (Kurtén & Anderson 1980). Although the dentaries and significant portions of the distal humeri were not recovered from the BBC specimen, the preserved R m1 has the extra lateral cusp aforementioned. Identification beyond the subfamily level has relied mostly on size differences. The genus *Arctodus* has higher crowned and considerably larger teeth than *Tremarctos. Arctodus pristinus* is distinguished from *A. simus* by its lesser size, greater prognathism, and smaller, narrower, and less crowded teeth (Kurtén & Anderson 1980; Emslie 1995). *Arctodus simus* is highly variable in size with the lower end of the observed range overlapping with *A. pristinus* in many measurements (Kurtén 1967; Richards *et al.* 1996). However, Kurtén (1967) concluded, and others have followed suit (e.g., Emslie 1995; Richards *et al.* 1996), that it is possible to distinguish *A. simus* from *A. pristinus* based on measurements and proportions of the teeth. Unfortunately, sample sizes for *A. pristinus* elements remain small (Richards *et al.* 1996: Appendix 2). Nevertheless, compared to compiled dental measurements (from Emslie 1995 and Richards *et al.* 1996), the BBC specimen is consistently within the range of *A. simus*, and 7 of the 9 measurements

taken lie above the range of *A. pristinus* (Table 1). Measurements on other skeletal elements also group the BBC specimen as a small *A. simus* (Tables 2 & 4).

DESCRIPTION

TEETH: No cranial or mandibular bones were identified from the site and the teeth were isolated and scattered. Numerous pieces of enamel were recovered, as well as root fragments. Tooth enamel is well preserved but the roots were saturated, fragmented, and have a purplish hue. The lack of tooth-bearing elements and cranial material is the likely result of long-term exposure of these remains in a depositional system with very slow sediment accumulation rates and a high humidity. A thin layer of clay and degraded bone on the current surface covered the teeth.

No hypoplasias or dental caries were found. However, supragingival dental calculus is relatively common and is present on most of the recovered teeth. This feature is most noticeable on the cheek teeth; the best example is seen on the R m2, where nearly half the labial surface is covered with supragingival calculus. Much of the calculus appears to have exfoliated over time; thus, the calculus that remains does not represent the exact coverage of calculus at the time of death.

Occlusal wear on the teeth is minimal (Fig. 8), but is described here for future comparison. Measurements of the dentine exposures are made from contact lines between the dentine and enamel on the occlusal surfaces. The L i2 has two wear facets with exposed dentine. The larger facet is more medially placed and has a maximum labiolingual width of 2.2 mm and a maximum mesiodistal width of 4.5 mm. The smaller facet with exposed dentine is near the lateral margin of the tooth. It has a maximum labiolingual width of 1.0 mm and a maximum mesiodistal width of 1.1 mm. The R i2 also has two wear facets with exposed dentine. The larger facet has a labiolingual maximum width of 2.0 mm and mesiodistal maximum width of 2.0 mm. The smaller wear facet is in contact with the lateral margin of the tooth and has a maximum labiolingual width of 2.0 mm and a mesiodistal width of 1.1 mm. On the R i3 dentine is exposed on the larger more proximal cusp but not on the smaller more lateral cusp. The maximum labiolingual width of the dentine on the larger cusp is 2.0 mm and the maximum mesiodistal width is 5.0 mm. The R p4 and the enamel cap (p2/P2 or p3/P3) displayed no wear facets with exposed dentine and appeared to be relatively unworn. The L m1 is not complete. The represented portion shows some wear and dentine exposure. The large protoconid has a wear facet with a maximum mesiodistal width of 1.5 mm and a maximum buccolingual width of 2.0 mm. The portion of the tooth containing the lateral accessory cusp was not recovered from the cave. The R m1, like the L m1, has a wear facet on the apex of the protoconid (Fig. 8A). The mesiodistal maximum width of the dentine exposure is 1.4 mm and the buccolingual exposure is 1.6 mm wide. The lateral accessory cusp between the trigonid and talonid also shows minor wear, with the mesiodistal maximum width of the facet being 1.5 mm and a buccolingual maximum width of 0.6 mm. The R m2 (Fig. 8B) and L m3 (Fig 8C) displayed no wear facets with exposed dentine and the teeth are relatively unworn.

Like the lower dentition, some of the upper teeth show wear, and the most extreme is on the incisors. The L I1 has one relatively large wear facet with exposed dentine. The labiolingual maximum width is 4.2 mm and the mesiodistal maximum width is 6.5 mm. At least one diminutive wear impression was apparent on a small cusp posterior and medial to the larger wear facet. The R I1 has one large wear facet with a labiolingual maximum width of 4.5 mm and a mesiodistal width of 6.6 mm. One smaller cusp, posterior and medial to larger cusp, has a small wear facet with a labiolingual maximum width of 0.5 mm and a mesiodistal maximum width of 0.6 mm. There is also a groove on the occlusal surface approximately 4.5 mm long and 0.5 mm wide that was not on the LI1. This attritional groove is u-shaped in cross-section, runs labiolingually, and is along the lateral margin of the occlusal surface. The R I2 has one large wear facet with a labiolingual maximum width of 3.5 mm and a mesiodistal length 6.4 mm. The R I3 has a wear facet with exposed dentine. The labiolingual maximum width is 1.0 mm and the mesiodistal width is 1.0 mm. The L M1? fragments and the R M2 (Fig. 8D) did not have any exposed dentine/wear facets and appeared to have little to no wear.

VERTEBRAE: The vertebral elements recovered consist of spinous and transverse processes, vertebral body fragments lacking epiphyses and isolated unfused vertebral epiphyses. One partial thoracic vertebra is curated with the surrounding sediment holding the specimen together.

RIBS: The ribs were smashed, cracked, and in very poor condition but many were preserved in sequence. This high level of fragmentation is probably the result of people walking over the site. Like the vertebral elements, these remains were near the modern surface (3-5 cm depth). All of the long rib segments lacked proximal articular ends. Some of these proximal ends were recovered and the proximal epiphyses were not fused at the time of death. Due to their poor condition nearly all the rib segments have been preserved within the original sediments. At least 7 segments of calcified costal cartilage were also recovered in sequence. These too have been preserved in their original position within matrix.

SCAPULAE: Both scapulae are highly fragmented and curated with matrix holding them together. The L scapula is on top of the left side of the ribcage and at least 4 ribs are preserved underneath it. The R scapula was in a semi-articulated position.

HUMERI: The distal half of the R humerus is represented by a block of sediment and highly degraded bone. Portions of the remaining distal end were articulated with the R ulna and radius. The L humerus is in poor condition, but the distal portion was articulated to the L ulna and radius.

ULNAE AND RADII: The L and R ulnae and radii are nearly complete. The shafts and proximal ends are highly fragmented, but the distal ends are intact. The proximal epiphyses on the ulnae could not be examined because of the poor preservation of these areas. On both distal ulnae, the epiphyseal suture is visible only on the radial surface. The epiphyseal sutures on

the distal radii are faint but visible.

MANUS: The L and R ulnae were articulated with their corresponding carpals. All epiphyseal plates in the metacarpals and phalanges are completely fused. The L manus was splayed out with palm down and was preserved in an articulated position within sediment. The second phalanx of digit II was out of orientation on the L manus and was discovered to be under the terminal phalanx of the same digit based on a CT scan. The CT scan also showed that the sesamoids between the metacarpals and phalanges are in their natural position within the sediment. The R manus was also articulated but was not complete. Its slightly higher position on the paleosurface and orientation made it more susceptible to erosion and disturbance than the L manus. The L manus is currently curated in sediment (see Fig. 4). The R manus was found on its side, with digit V being the lowest and digit I lying across the palm in a semi-closed position. The R fourth metacarpal possesses a well healed fracture (Fig. 7E). The R manus was also CT scanned to preserve the natural position of the bones prior to removal from the encasing sediments.

INNOMINATE: These remains were curated within sediment. Much of the L ischium is well preserved and some L iliac fragments are identifiable. The ischial tuberosity epiphysis is in contact with the ischium but is not fused. The acetabulum is obliterated. Additional innominate fragments were recovered from the disturbed surface area.

FEMORA AND PATELLAE: The proximal end of the L femur was found buried just west of the majority of the skeleton underneath a block of red clay. The recovered proximal end includes a small portion of the diaphysis and the complete fused capitular epiphysis. Although the epiphysis adheres to the diaphysis, the deep suture separating these parts indicates that fusion was in progress at the time of death.

The proximal end of the R femur shaft was recovered from the surface. The coloration of the fracture surfaces on the femur, and many other surface bones, indicated that these breaks were likely the result of earlier cavers. The recovered R femur lacks the capitular epiphysis, again indicating that this was an osteologically immature individual. The greater trochanter epiphysis is fused but the suture line is still visible. Both the L and R patellae were recovered from the surface near the R femur shaft and are complete.

TIBIAE/FIBULAE: The proximal ends of the L and R tibiae were recovered from the surface near the R femur and the patellae. Both tibiae have cut marks on the proximal ends. The much lighter coloration of these cut mark surfaces, compared to intact surfaces, indicates that other cavers discovered the site at some point in the recent past and some digging occurred.

The distal ends of the tibiae and fibulae were still articulated in sediments near the stream. The epiphyses are fused on the proximal R tibiae but a clear suture still exists along some portions of the contact. The distal epiphysis on the R tibia is completely fused and no suture line is visible. The stage of fusion of the proximal L tibia mirrors that observed on the R tibia. The distal epiphysis on the L tibia is well fused and the suture line is only visible in one location along the lateral surface. The fibulae are nearly identical in their stage of epiphseal closure. The distal epiphyses are completely closed and the proximal epiphyseal sutures are still visible, particularly on the lateral sides.

PES: The tarsals were articulated with their corresponding tibiae and fibulae. All epiphyses in the metatarsals and pedal phalanges are fused. The L pes was found articulated with the ventral side down. It is nearly complete and was CT scanned prior to removal of the surrounding sediment to record the original orientation of the foot. The R pes was partially articulated and lying on its lateral side, thus digit V was the lowest. Because of this orientation, most of the medial and central phalanges washed away prior to burial.

HAIR: As noted above, we interepreted tubular structures as *Arctodus simus* hair molds and hair. Scanning electron microscopy (SEM) revealed that these tubules and strands have a structure and size similar to hair (Fig. 6). These structures overlap one another but do not branch or intersect and were recovered only from beneath or right next to the bear's skeletal remains. The hydrophobic keratinaceous protein composition of hair is not easily degraded when compared to other soft tissues (Rowe 1997). Thus, the preservation of hair features near the articulated skeletal remains should not be overly surprising. Unfortunately, the fossilized hair material we analyzed was too degraded to retain the scale pattern of the surface, texture, and morphology of distinct regions, and diameter of the medulla. Numerous blocks of sediment containing fossilized hair are preserved and are available for further analysis.

DISCUSSION

We can only speculate about what caused the death of this relatively young bear in the depths of this cave. Other than the healed metacarpal fracture, there was no sign of trauma on the skeletal remains. The only evidence of disease is extensive supragingival calculus on some of the cheek teeth, but this is not a life-threatening condition.

The BBC *A. simus* specimen was not osteologically mature when it died because numerous epiphyses were unfused. However, the stage of fusion of the long bone epiphyseal plates indicate that this animal was, for the most part, full sized. The age of individual modern bears can be determined using a number of methods. The most reliable technique used by neontologists studying older individuals in modern bear populations is counting cementum annuli on thin-sectioned premolars and canines (Harshyne *et al.* 1998). Though cementum annuli analysis may prove useful in understanding the paleobiology of short-faced bears in the future, at this point no specimens have been aged using this destructive technique.

Because the BBC specimen is osteologically immature, comparisons with known epiphyseal fusion sequences in extant bears may be made. Epiphyseal closures of the fore-

limbs in *Ursus americanus* are discussed by Marks and Erickson (1966) as a tool for determining age. X-rays of known-age *U. americanus* showed that the stages of the closure of the long bone epiphyses and the development of the carpals are closely correlated to age (Marks & Erickson 1966). They found that the metacarpal epiphyses fused in both sexes around the age of 1-2 years and the proximal and distal epiphyses fused on the ulna and radius in females around the age of 4-6 years (6-8 years in males). At present it is not known whether *Arctodus* had a similar rate and sequence of epiphyseal fusion to any of the genus *Ursus*. However, on the basis of fusion rates and sequences in black bears, the BBC *Arctodus simus* may be placed at around 4-6 years of age if it is a female and around 6-8 if it is a male. Interestingly, the wear patterns on the BBC bear's teeth is similar to 4-6 year old black bears (Marks & Erickson 1966). Unfortunately no comparable data exists for the extant tremarctine, *Tremarctos ornatus*.

The late time of epiphyseal fusion noted above indicates that bears are sexually mature well before their epiphyseal fusions are complete. If short-faced bears were similar in their timing of sexual maturity to modern bears, the BBC specimen would have been sexually mature. Female *T. ornatus* reach sexual maturity as early as 4 years of age (Stirling 1993a). Extant North American bears follow a similar pattern. For example, female black bears become sexually mature between 2 and 4 years of age (Larivière 2001; Stirling 1993a) and female brown or grizzly bears (*Ursus arctos*) begin breeding in some portions of their range at around 3 years (Pasitschniak-Arts 1993).

The postcranial remains of *A. simus* described here are at the small end of the recorded size range (Tables 1, 2 & 4). Kurtén (1967), Harington (1991), and Richards *et al.* (1996) divide *A. simus* into 2 subspecies, small *A. s. simus* and large *A. s. yukonensis*. Lamb (1911) and Voorhies and Corner (1982) suggested a specific rather than a subspecific distinction for the large and small forms. It is now generally accepted that all of these specimens represent one species, *A. simus* (Richards *et al.* 1996). What is currently unknown is whether or not the bimodal size distribution in *A. simus* is a result of 2 subspecies or sexual dimorphism.

All extant bears are sexually dimorphic (Stirling 1993a) and this dimorphism increases as species become larger (Stirling & Derocher 1993). For species with a single mate sexual dimorphism is small, whereas in species whose males compete for females, males can be up to 100% heavier (Stirling & Derocher 1993). Kurtén (1967) and others (e.g., Hawksley 1965; Kurtén & Anderson 1980; Cox 1991; Churcher *et al.* 1993; Scott & Cox 1993) have discussed sexual dimorphism in *A. simus*. At Rancho La Brea, contemporaneous large and small forms of this species were recovered, and the largest specimen exceeded the smallest by approximately 25% (Scott & Cox 1993). Though 25% is relatively high, it is still lower than the documented sexual dimorphism in extant *Tremarctos ornatus*, where males are 30-40% larger than females (Saporiti 1949; Stirling 1993a). That sexual dimorphism alone could account for the size variation in this taxon removes any basis or justification for subspecific distinctions.

The problem with positively distinguishing males from females in the fossil record is that size has been the primary criterion. Though over 100 short-faced bear localities are known, only one site produced a baculum that could belong to a short-faced bear. This was reported from Potter Creek Cave, California, in a compiled list of specimens (Richards *et al.* 1996). The BBC excavation site did not produce a baculum. The lack of recovered *Arctodus* bacula likely reflects both taphonomy and behavior. The majority of skeletal remains representing large individuals are from open sites where only a few elements were recovered (see specimen list in Richards *et al.* 1996). In contrast, horizontal (walk-in) cave passages produced numerous examples of small, yet relatively complete individuals where bacula would likely be found if they had been present. Both the small size of recovered skeletal elements and the lack of bacula from cave deposits suggest that female individuals of *A. simus* were using caves.

The use of caves as dens is relatively common among ursids. In the Americas *Tremarctos ornatus*, *Ursus arctos*, and *U. americanus* use caves for denning when available (Pasitschniak-Arts 1993; Nowak 1999) and polar bears (*Ursus maritimus*) dig their own "caves" in snow (Stirling 1993b). In modern ursids, females spend more time in dens than males. In regions with cold winters, extended periods of denning are an adaptation to seasonal changes in food availability and for birth of tiny cubs incapable of regulating their own body temperature. While denning during the winter months, many ursine species enter a period of dormancy or torpor. All 4 ursid species that live in temperate or Arctic regions enter into a winter sleep (Ramsay 1993). In areas where ursine dormancy occurs, pregnant females enter the dens earlier and leave later. Polar bears are carnivorous and do not undergo winter food shortages like other bears. Because of this, only pregnant females den for extended periods of time (Stirling 1993b). Similarly, in southern populations of *Ursus arctos* and *U. americanus*, males remain active in winter while pregnant females usually den and go into dormancy (Pasitschniak-Arts 1993; Larivière 2001).

In karst regions, fossils of *Arctodus simus* have been recovered almost exclusively from cave sites. In the contiguous United States, 26 of 69 *A. simus* sites (~38%) are in caves (based on data from Richards *et al.* 1996). That greater than one-third of all sites are caves suggests a close association between this species and cave environments. Further, over 70% of the smaller specimens (those assigned as *A. s. simus* by Richards *et al.* 1996) are from cave deposits. Not one of the specimens assigned to the larger morph (*A. s. yukonensis* by Richards *et al.* 1996) is from a cave passage. Taking into account the fact that female ursids are smaller and more prone to den in caves, it seems logical to conclude that the majority of *A. simus* from such deposits were females and may have been denning when they perished.

ACKNOWLEDGMENTS

We would like to thank the landowners, who wish to remain anonymous, for allowing us access to BBC and donating the remains to the Illinois State Museum. This project would not have been possible without the numerous cavers who assisted in the arduous excavations and removal of the remains from the cave, including George Bilbrey, Michael Carter, Amy McCann, Mona Colburn, Jeffrey Crews, Andy Free, Kally Gehly, Matt Goska, Sue Hagan, Dave Matteson, Christy Shannon, Kenny Sherrill, Trevor Stroker, Mick Sutton, Rick Toomey, Ryan Warnol, and David Wronkiewicz. Scott Miller, University of Missouri—Rolla, donated SEM time and instruction. Gary Andrashko, ISM, provided numerous photographs. The CT lab staff at Memorial Medical Center in Springfield IL provided scans and X-rays. Brian Bisbee, ISM, helped with the technical issues associated with the CT scans. Chris Bell and Chris Jass of the University of Texas—Austin, Rufus Churcher - University of Toronto, Greg McDonald - National Park Service, and Ron Richards - Indiana State Museum, provided helpful comments that improved this paper. This project was funded by an Illinois State Museum 1877 Club grant.

REFERENCES

Christiansen, P., 1999., What size were *Arctodus simus* and *Ursus spelaeus* (Carnivora: Ursidae)?: Annales Zoologici Fennici, v. 36, p. 93-102

Churcher, C.S., Morgan, A.V., & Carter, L.D., 1993, *Arctodus simus* from the Alaskan Arctic Slope: Canadian Journal of Earth Sciences, v. 30, p. 1007-1013.

Cox, S.M., 1991, Size range or sexual dimorphism in *Arctodus simus* from Rancho La Brea: Abstract #15, Annual Meeting of the Southern California Academy of Sciences.

Driesch, A. von den, 1976, A guide to the measurement of animal bones from archaeological sites: Peabody Museum Bulletin 1, Peabody Museum of Archaeology and Ethnology, Harvard University, 137 p.

Emslie, S.D., 1995, The fossil record of *Arctodus pristinus* (Ursidae: Tremarctinae) in Florida: Bulletin of the Florida Museum of Natural History, v. 37, p. 501-514.

Grayson, D.K., 1989, The chronology of North American late Pleistocene extinctions: Journal of Archaeological Science, v. 16, p. 153-165.

Harington, C.R., 1991, North American short-faced bears: Neotoma, v. 29, p. 1-3.

Harshyne, W.A., Diefenbach, D.R., Alt, G.L., & Matson, G.M., 1998, Error rates of estimated ages of black bears from tooth cementum annuli: Journal of Wildlife Management, v. 62, p. 1281-1291.

Hawksley, O., 1965, Short-faced bear (*Arctodus*) fossils from Ozark caves: Bulletin of the National Speleological Society, v. 27, p. 77-92.

Hawksley, O., 1986, Remains of Quaternary vertebrates from Ozark caves and other miscellaneous sites: Missouri Speleology, v. 26, p. 1-67.

Hawksley, O., Reynolds, J.F., & Foley, R.L., 1973, Pleistocene vertebrate fauna of Bat Cave, Pulaski County, Missouri: Bulletin of the National Speleological Society, v. 35, p. 61-87.

Hawksley, O., & Weaver, H.D., 1981, Quaternary vertebrates from Carroll Cave, Camden County, Missouri: Missouri Speleology, v. 21, p. 199-213.

Hedges, J., Russell, B., Thrun, B., & White, W.B.1979, The 1976 NSS standard map symbols: National Speleological Society Bulletin v. 41, p. 35-43

Imes, J.L., Schumacher, J.G., & Kleeschulte, M.J., 1996, Geohydrologic and water-quality assessment of the Fort Leonard Wood Military Reservation, Missouri, 1994-95: U.S. Geological Survey Water-Resources Investigations Report 96-4270.

Kurtén, B., 1967, Pleistocene bears of North America. 2. Genus *Arctodus*, short-faced bears: Acta Zoologica Fennica, v. 117, p. 1-58.

Kurtén, B., & Anderson, E., 1980, Pleistocene mammals of North America: Columbia University Press, New York, 442 p.

Lamb, L.M., 1911, On *Arctotherium* from the Pleistocene of Yukon: Ottawa Naturalist, v. 25, p. 21-26.

Larivière, S., 2001, *Ursus americanus*: Mammalian Species, v. 647, p. 1-11.

Marks, S.A., & Erickson, A.W., 1966, Age determination in the black bear: Journal of Wildlife Management, v. 30, p. 389-410.

Merriam, J.C., & Stock, C., 1925, Relationships and structure of the short-faced bear, *Arctotherium*, from the Pleistocene of California: Carniegie Institution of Washington Publication, v. 347, p. 1-35.

Nealson, K.H., Tebo, B.M., & Rosson, R.A., 1992, Occurrence and mechanisms of microbial oxidation of manganese: Advances in Applied Microbiology, v. 33, p. 279-318.

Nealson, K.H., & Stahl, D.A., 1997, Microorganisms and biogeochemical cycles: What can we learn from layered microbial communities?, *in* Banfield, J.F., & Nealson, K.H., eds., Geomicrobiology: Interactions between microbes and minerals: Reviews in Mineralogy, v. 35, p. 5-34.

Nowak, R.M., 1999, Walker's mammals of the world: Johns Hopkins University Press, Baltimore, 1936 p.

Pasitschniak-Arts, M., 1993, *Ursus arctos*: Mammalian Species, v. 439, p. 1-10.

Puckette, W., 1976, Notes on the occurrence of the short-faced bear (*Arctodus*) in Oklahoma: Proceedings of the Oklahoma Academy of Science, v. 56, p. 67-68.

Ramsay, M.A., 1993, Winter sleep, *in* Stirling, I., ed., Bears: Majestic creatures of the wild: Rodale Press, Emmaus, p. 68-69.

Richards, R.L., Churcher, C.S., & Turnbull, W.D., 1996, Distribution and size variation in North American short-faced bears, *Arctodus simus*, *in* Stewart, K.M., & Seymour, K.L., eds., Palaeoecology and palaeoenvironments of late Cenozoic mammals: Tributes to the career of C.S. (Rufus) Churcher: University of Toronto Press, Toronto, p. 191-246.

Rowe, W.F., 1997, Biodegradation of hairs and fibers, *in* Haglund, W.D., & Sorg, M.H., eds., Forensic taphonomy: The postmortem fate of human remains: CRC Press, New York, p. 337-351.

Saporiti, E. J., 1949, Contribucion al conocimiento de la biologia del oso de lentes: Anales de la Sociedad Cientifica Argentina, v. 147, p. 3-12.

Schubert, B.W., 2001, Discovery of an ancient giant in an Ozark cave: The Living Museum, v. 63, p. 10-13.

Scott, E., & Cox, S.M., 1993, *Arctodus simus* (Cope, 1879) from Riverside County, California: PaleoBios, v. 15, p. 27-36.

Soibelzon, L., 2002, A general review of the South American Pleistocene short-faced bears (Ursidae: Tremarctinae): Abstract from the 14th International Congress on Bear Research and Management, Steinkjer, Norway.

Stafford, T.W., Jr., Brendel, K., & Duhamel, R.C., 1987, Study of bone radiocarbon dating accuracy at the University of Arizona NSF Accelerator Radiocarbon Facility for Radioisotope Analysis: Radiocarbon, v. 29, p. 24-44.

Stafford, T.W., Jr., Hare, P.E., Currie, L., Jull, A.J.T., & Donahue, D.J., 1991, Accelerator radiocarbon dating at the molecular level: Journal of Archaeological Science, v. 18, p. 35-72.

Stirling, I., 1993a, The living bears, *in* Stirling, I., ed., Bears: Majestic creatures of the wild: Rodale Press, Emmaus, p. 36-49.

Stirling, I., 1993b, The polar bear, *in* Stirling, I., ed., Bears: Majestic creatures of the wild. Rodale Press, Emmaus, p. 98-107.

Stirling, I., & Derocher, A.E., 1993. The behavior of bears, *in* Stirling, I., ed., Bears: Majestic creatures of the wild. Rodale Press, Emmaus, p. 70-83.

Tebo, B.M., Ghiorse, W.C., van Waasbergen, L.G., Siering, P.L., & Caspi, R., 1997, Bacterially mediated mineral formation: Insights into manganese (II) oxidation from molecular genetic and biochemical studies, *in* Banfield, J.K., & Nealson, K.H., eds., Geomicrobiology: Interactions between microbes and minerals: Reviews in Mineralogy, v. 35., p. 225-266.

Tedford, R.H., & Martin, J., 2001, Plionarctos, a tremarctine bear (Ursidae: Carnivora) from western North America: Journal of Vertebrate Paleontology, v. 21, p. 311-321.

Voorhies, M.R., & Corner, R.G., 1982, Ice age superpredators: University of Nebraska State Museum, Museum Notes, v. 70, p. 1-4.

GYPSUM DEPOSITS IN THE FRASASSI CAVES, CENTRAL ITALY

SANDRO GALDENZI
Istituto Italiano di Speleologia, Frasassi Section, Viale Verdi 10, 60035 Jesi, ITALY sagalde@tin.it
TERUYUKI MARUOKA
Department of Geological Sciences, University of Vienna, Althanstrasse 14, A-1090 Vienna, AUSTRIA
Present address: *Laboratory for Space Sciences, Physics Department, Washington University, Campus Box 1105, One Brookings Drive, St. Louis, MO 63130-4899, USA teruyuki@wuphys.wustl.edu*

The Frasassi Caves are hypogenic caves in central Italy, where H_2S-rich groundwater flows in the lowest cave level. Near the water table, the H_2S is converted to sulfuric acid by biotic and abiotic processes, which have enhanced cave development. The sulfate generally deposits above the water table as a replacement gypsum crust coating limestone walls or as large gypsum crystals. Although the oxidation of sulfide also occurs below the water table, sulfate saturation is not achieved, therefore, sulfate does not precipitate below the water table.

In the upper dry levels of the cave, three main types of ancient gypsum deposits occurs: (1) replacement crusts, similar to the presently forming deposits of the active zone, (2) microcrystalline large and thick floor deposits, and (3) euhedral crystals inside mud. The study of the depositional setting and the analysis of sulfur isotopes in the gypsum and groundwater clearly demonstrate that all the sampled gypsum in the cave formed by H_2S oxidation above the water table. Some fraction of small sulfur isotopic differences between H_2S in the water and gypsum can be explained by isotopic fractionation during abiotic and/or biotic oxidation of H_2S.

Caves formed by sulfuric acid from the oxidation of H_2S are found in many different parts of the world and contain conspicuous gypsum deposits. A review of the concepts can be found in *The Caves of the Guadalupe Mountains Research Symposium* (DuChene *et al*. 2000). Oxidation generally involves bacterial activity, and these bacteria may represent the main source of organic matter inside the cave.

Many caves in carbonate bedrock contain small gypsum deposits formed by evaporation of sulfate-rich water on cave fills or walls. Water seeping into the cave picks up gypsum from oxidation of pyrite in the bedrock, which precipitates upon reaching the cave, or anhydrite (gypsum) is dissolved along the flow path and carried to the cave wall, where evaporation causes precipitation of gypsum. Large-size (up to m-scale) gypsum deposits are less common in carbonate caves, and are generally considered the result of H_2S-rich water circulation inside the cave. Such gypsum deposits are known in North America (Guadalupe Mountains: Hill 1987), in South America (Las Brujas Cave: Forti *et al.* 1993), and in Europe (Galdenzi & Menichetti 1995; Galdenzi 1990, 1997). Unfortunately, gypsum is not actively forming in most of these caves.

Some caves do include actively forming gypsum deposits (Egemeier 1981; Galdenzi 1990; Sarbu & Kane 1995; Hose *et al.* 2000), but these caves are generally short, and gypsum is forming only on the cave walls above the water table. No large bedded gypsum deposits have been found similar to the ones found in the Guadalupe Mountains caves (New Mexico) or in the Frasassi Caves (Italy).

The Frasassi Caves are unique in that they include both active and relict meter scale gypsum deposits. Therefore, we can compare both types of gypsum deposits directly from a single cave system, which is a great advantage in understanding how the gypsum forms. In this study, we will discuss the depositional setting and the sulfur isotopic compositions of the gypsum in the Frasassi Caves in order to understand how and where the gypsum forms.

GEOLOGIC SETTING

The Frasassi Caves make up one of the most famous Italian karst systems. They are the most visited show caves in Italy, and about 350,000 tourists visit the caves every year. The caves are in central Italy, on the eastern side of the Apennine Mountains, 40 km from the Adriatic Sea. This area is characterized by a mountainous landscape, with altitudes ranging between 200 m at the bottom of the valleys to ~1000 m in the surrounding mountains. The climate is Apenninic subcontinental, with an annual average temperature of about 13°C and an average annual rainfall of about 1000 mm/year. Precipitation generally reaches a maximum in autumn and spring, whereas evaporation exceeds precipitation in summer. About 100 caves are known in the Frasassi area: all these caves are developed in the small area around the step cliffs of the Sentino River Gorge, a 2 km long and 500 m deep canyon cut in the core of a small anticlinal ridge (Fig. 1). The major cave (i.e., Grotta del Fiume–Grotta Grande del Vento Cave System) consists of >20 km of cave passages located at altitudes between 200 and 360 m. Two important caves (Buco Cattivo, 5000 m long, and the Grotta del Mezzogiorno-Grotta di Frasassi System, 3500 m

Copyright © 2003 by The National Speleological Society

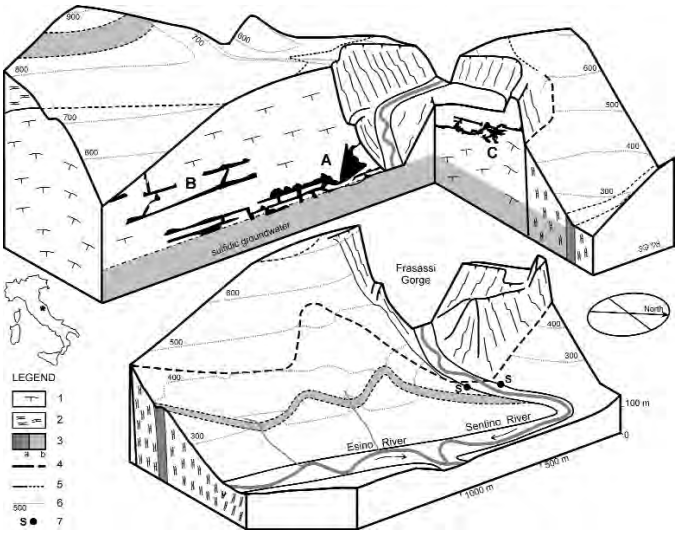


Figure 1. Block diagram of the Frasassi karst system. (1) Calcare Massiccio Formation; (2) cherty limestone; (3) Cretaceous marl: a – section; b – outcrops; (4) faults; (5) stratigraphic boundary; (6) contour intervals; (7) sulfidic spring. Caves: (A) Grotta del Fiume-Grotta Grande del Vento Cave System; (B) Buco Cattivo; (C) Grotta del Mezzogiorno-Grotta di Frasassi Cave System.

long) occur at a higher altitude, ranging from 360 to 500 m.

The Frasassi Gorge offers a spectacular cross-section of the core of the anticline, where the geology is well exposed. The caves are formed mainly in the Calcare Massiccio Formation, a thick Jurassic (Lower Lias) limestone unit exposed in the gorge. The Calcare Massiccio formed in an epicontinental platform setting, and it is a very pure limestone (over 99% calcium carbonate), consisting mainly of wackestone and packstone facies, without any significant clay or silica minerals. It is a very permeable limestone, due to high syngenetic porosity and to a well developed network of fractures.

The Calcare Massiccio makes up the lower part of the sedimentary sequence outcropping throughout the region (Fig. 2). The thickness of this formation can reach ~1000 m, and it overlies a buried 2000 m thick Upper Triassic evaporitic sequence, consisting mainly of anhydrite and dolomite (Burano Formation: Martinis & Pieri 1964). A 50 m thick Triassic limestone unit, rich in organics, is interbedded between the Calcare Massiccio and the Burano formations. Near the Frasassi Gorge, the Calcare Massiccio is overlain by a 60 m thick unit (Bugarone Formation) formed in the Jurassic after drowning of the carbonate platform in the shallower depositional areas. This condensed Jurassic unit is mainly micritic, nodular limestone with small amounts of pyrite, and makes up a 10 m thick interbedded marly layer. This formation represents a low permeable bed that is thin and discontinuous and can influence underground drainage. A Lower Cretaceous cherty limestone (Maiolica Formation), ~300 m thick, forms another permeable and karstified section. The Calcare Massiccio and the Maiolica formations host the main aquifer

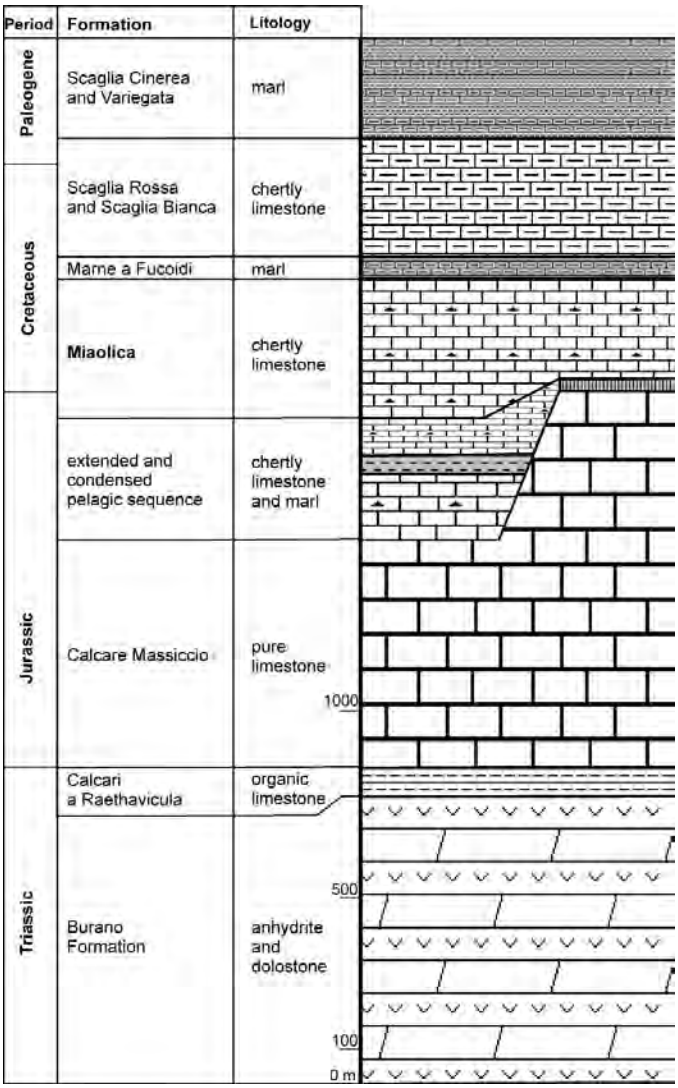


Figure 2. Simplified stratigraphic succession of the Frasassi area.

in the central Apennine chain. A 50 m thick Cretaceous marly formation (Marne a Fucoidi) forms a continuous aquiclude and isolates the lower section of the stratigraphic sequence from overlying permeable limestone formations of Late Cretaceous and Tertiary age.

The Frasassi Anticline was formed in the late Miocene during a tectonic compressive phase that also caused the Apennine uplift and emersion. The fold is asymmetric, with a main northeast vergence, and the caves are developed mainly in the eastern limb of the anticline, where a fault has concentrated the groundwater flow. The surface drainage formed at the end of the early Pleistocene, when entrenchment of the valleys cut into a preexisting "planation surface". At that time, the gorges cut into the anticlinal structures, and a landscape similar to the present one was formed (Ambrosetti *et al.* 1982; Ciccacci *et al.* 1985). During the Pleistocene, climate changes also heavily influenced geomorphic evolution. In the mountain areas, during glaciations, the valleys were filled with alluvial gravel

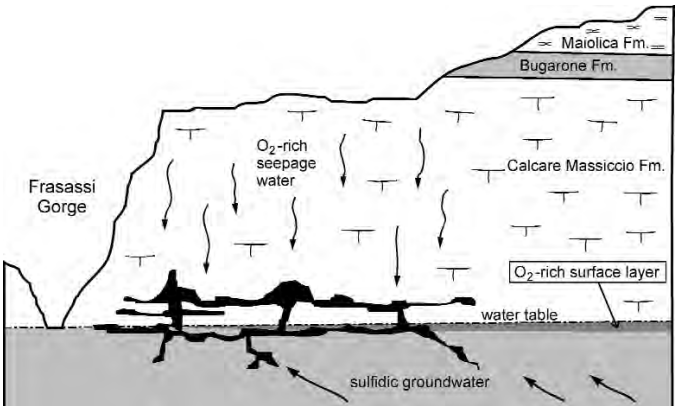


Figure 3. Hydrologic setting in the Frasassi Gorge. The significant recharge of O_2-rich freshwater increases water aggressiveness when it reaches H_2S at the water table. The very low water flow induces the stratification of groundwater in the inner parts of the cave.

deposits, while, during interglacials, the alluvial deposits and the bedrock were eroded by the river (Bisci & Dramis 1991).

GROUNDWATER

Groundwater in the Frasassi area consists of two types: Carbonate and sulfidic, which can be characterized by their chemical compositions and origin. The carbonate water is derived from diffuse infiltration of surface meteoric water through the limestone. It characterizes all the vadose zone and some small aquifers perched on interbedded marls (Fig. 3). This water has a low salinity (~200-400 mg/L: Cocchioni 2002) with a very low sulfate content and high dissolved oxygen (~0.32 mM/L). The sulfidic water characterizes the main aquifer, developed in the Calcare Massiccio and Maiolica formations at the core of the anticline (Fig. 1). This sulfidic groundwater is cold (~13°C), but shows a higher salinity, up to 2 g/L, than the carbonate water. It is enriched in sodium and chloride, and contains a high amount of sulfate (up to 2.5mM/L), but it is undersaturated with respect to gypsum. The most significant feature of this water is the presence of hydrogen sulfide. The H_2S concentrations reach up to 0.5 mM/L. These dissolved components are probably acquired as groundwater flows upward through the underlying anhydrite formation. Isotopic data on $\delta^{18}O$, δD, and tritium suggested a meteoric origin for the sulfidic groundwater (Tazioli *et al.* 1990). These authors estimated a recharge area located at altitudes of 600-1000 m, with a relatively brief residence time in the aquifer.

The sulfidic aquifer occurs at the core of the anticline in the Calcare Massiccio and Maiolica formations, where the mineralized groundwater can rise through the deep faults at the eastern limb of the anticline. Here groundwater flow is concentrated, and the main springs are located (Fig. 1). The water table can be reached in the lower section of the cave, at the same level as the river. The groundwater flow is generally very slow,

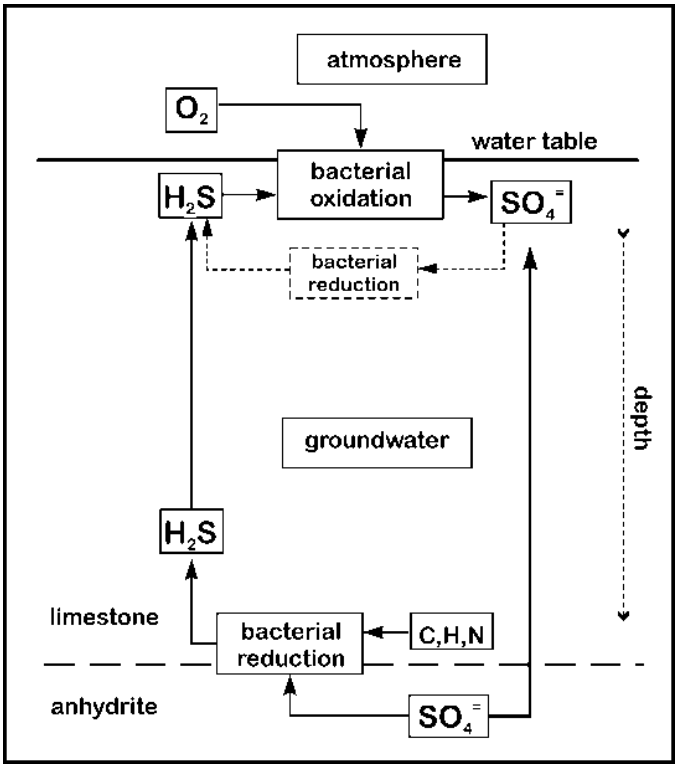


Figure 4. Sketch showing the redox processes involving sulfur in the Frasassi aquifer. Reduction of sulfate from underlying evaporites prevails in the deep phreatic zone, while sulfide oxidation occurs near the water table, causing cave development and limestone replacement with gypsum.

and flowing water is only found in the eastern part of the cave. The water levels are controlled by rainfall events, although river water enters the cave directly in narrow restricted zones near the spring. The conductivity and temperature of the sulfidic stream are also correlated with precipitation (Sarbu *et al.* 2000). These observations indicate that fresh water recharge, derived from surface precipitation, dilutes the sulfidic groundwater (Sighinolfi 1990; Tazioli *et al.* 1990).

The very low water flow in a large part of the cave leads to groundwater stratification. Fresh water seepage stays near the surface of the water table due to its lower salinity (Fig. 3). This surface layer can be rich in dissolved O_2, without any measurable H_2S. The thickness of this freshwater layer ranges from 20 cm up to 5 m (Galdenzi 2001). On the contrary, in some narrow zones the groundwater can have a higher salinity, because there is less dilution by the descending fresh water (Cocchioni 2002).

Hence the underground flow path is complex. The recharge area in the surrounding limestone is about 5 km². There infiltration quickly reaches the water table, dilutes the mineralized groundwater and flows toward the spring. Some meteoric water could reach the underlying evaporitic sequence, where it could pick up sodium chloride, sulfate, and sulfide (Fig. 4).

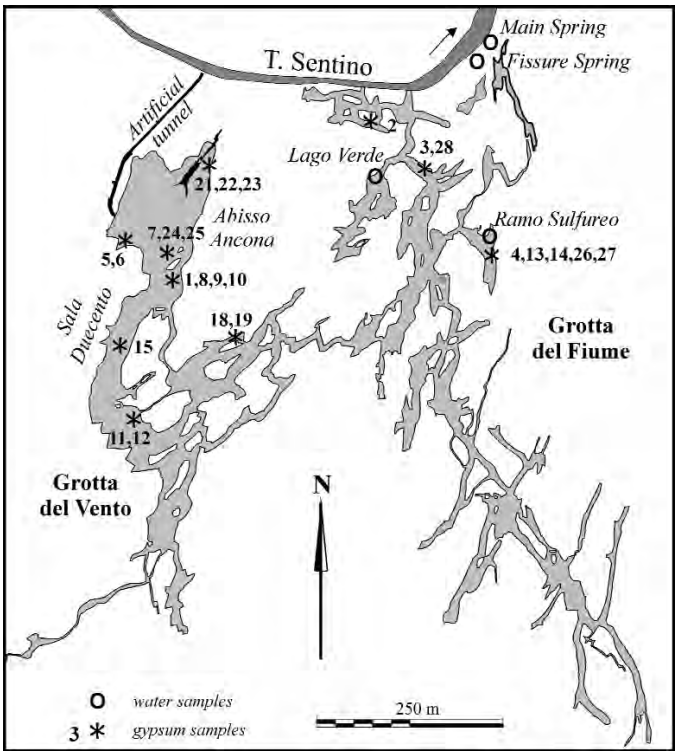


Figure 5. Map of Grotta del Fiume-Grotta Grande del Vento Cave System, with sample locations.



Figure 6. View of Abisso Ancona, the main room in Fiume-Vento Cave System. All photos by S. Galdenzi.

Sulfate reduction could occur in the underlying Triassic limestone rich in organic matter. Near the water table, oxygen in the fresh water causes oxidation of the sulfide in the sulfidic water. A small amount of sulfate could be reduced to sulfide in the shallow phreatic zone, mainly in the organic-rich mud covering the floor of the submerged passages.



Figure 7. Sala del Limone, a wide room in Grotta del Vento, with a shape similar to half a lemon. The rounded ceiling was formed by condensation corrosion. The flat rock floor is cut by shafts and fissures that formed below the sulfidic groundwater level.

CAVE FEATURES AND ORIGIN

The Frasassi Caves (Fig. 5) consist of a network of ramifying horizontal passages, where wide rooms alternate with smaller tubes and also with spongework zones. The major room, Abisso Ancona , has a volume of ~10^6 m^3 (Fig. 6). The system is clearly developed in several superimposed levels that are interconnected by short shafts or inclined passages. The genesis of the cave levels can be related to tectonic uplift and climatic changes that occurred during the Pleistocene. At least 4 main horizontal, often overlapping levels occur in the caves, whereas some further levels occur even lower (Fig. 1). The water table is in the lowest sections of the cave, where active sulfidic water is mainly in flooded passages.

The 2 lowest main levels, corresponding to the III and V level in Bocchini & Coltorti (1990), are between 200 and 300 m msl and occur mainly in the Fiume-Vento System (Fig.1). These passages developed in settings similar to the present, during the deposition of the surface alluvial gravel terraces in the Sentino River Valley, in the middle to late Pleistocene (Bocchini & Coltorti 1990). Ages were obtained by uranium series dating of speleothems (Taddeucci *et al.* 1992). In level V, those authors obtained stalagmite ages of up to 200 ka; in level III some stalagmites are 80 ka old, while a collapsed stalagmite has a range of ages between 170 ka and 120 ka. In the less-developed levels near the water table (e.g., I and II levels in Bocchini & Coltorti 1990), only Holocene dates were documented.

Each cave level has typical phreatic features with mainly horizontal tubes (1-10 m in diameter) that can form complex mazes or can alternate with large rooms characterized by flat, erosional rock surfaces at the floor and by rounded ceilings (Fig. 7). Shafts and fissures in the floor of the cave represent the original sources of H_2S-rich waters that formed the cave. Cupolas of different sizes are developed in the walls and ceil-



Figure 8. A bubble trail in Grotta del Vento. It consists of a rill that originates below the water table inside a pocket, a fissure or in a small side passage on the cave wall and rises upward. It can be some meters long and few decimeters deep, and can have also a meandering pattern.

ings of the cave. They could have formed either in the phreatic or vadose zones as a result of condensation corrosion. Bubble trails (Fig. 8) are common in many phreatic environments, indicating rising corrosive gas in the shallow phreatic zone. Some areas are covered by gypsum replacement crusts, while some thick floor deposits are common in the main rooms.

The two upper main levels are developed mainly in the Buco Cattivo and Mezzogiorno-Frasassi Caves at altitudes of 350 to 500 m (Fig. 1). The features of these caves are slightly different from those in the Fiume-Vento System. A few gypsum deposits indicate that sulfidic water circulation also occurred in this caves, but some important branches clearly developed in a deep phreatic zone. It may be supposed that during the formation of these upper caves, the hydrogeologic setting was different from the present one.

The oxidation of H_2S is considered the main cave-forming process (Galdenzi 1990). The oxidation of hydrogen sulfide to sulfate [1] can occur in the presence of oxygen from drip water, and can occur both in the shallow phreatic zone and during vadose conditions, causing the dissolution of limestone [2] and cave development.

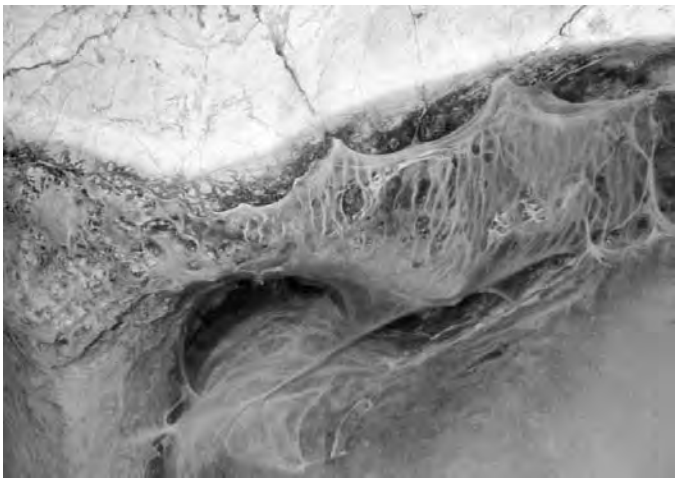


Figure 9. Microbial mats covering limestone walls in the sulfidic groundwater of Frasassi Caves.

$$[1]\ H_2S + 2O_2 \Leftrightarrow H^+ + HSO_4^- \Leftrightarrow 2H^+ + SO_4^=$$

$$[2]\ 2H^+ + SO_4^= + CaCO_3 \Leftrightarrow Ca^{++} + SO_4^= + H_2O + CO_2$$

Cave development by O_2-rich infiltrating meteoric water plays only a secondary role, and it is limited to a network of narrow passages formed in the vadose zone in the Frasassi karst area and in the surrounding mountains (Galdenzi 1996). Here, infiltrating meteoric water descends quickly to the water table. Similar networks can also facilitate sulfuric acid speleogenesis, by quickly delivering O_2-rich meteoric water to the groundwater, where H_2S oxidation can proceed (Fig. 3).

Recent investigations pointed out the role of microbial activity in speleogenesis. Chemoautotrophic microorganisms live near the redox interface between the sulfidic groundwater and the oxygen present in the atmosphere and in the seepage water, using the chemical energy resulting from the oxidation of H_2S. C and N stable isotopic results showed that the organic matter produced *in situ* by these microbial communities represents the trophic support for the rich community of invertebrates that inhabit the sulfidic sections of the caves (Sarbu *et al.* 2000). Biologic activity can significantly accelerate the oxidation of H_2S, causing the production of H_2SO_4 as a by-product of their metabolism. This has an important role in the cave development, increasing the water aggressiveness on the cave walls and accelerating the dissolution of the limestone. Therefore, cave development can be considered, at least partly, a consequence of bacterial activity (Galdenzi *et al.* 1999).

PRESENT GYPSUM DEPOSITION

The morphologic effects of the oxidation of H_2S can be directly observed in the lower parts of the Frasassi Caves, where the corrosive processes on the limestone are still active in the sulfidic water. Here, bacterial colonies cover the bottom

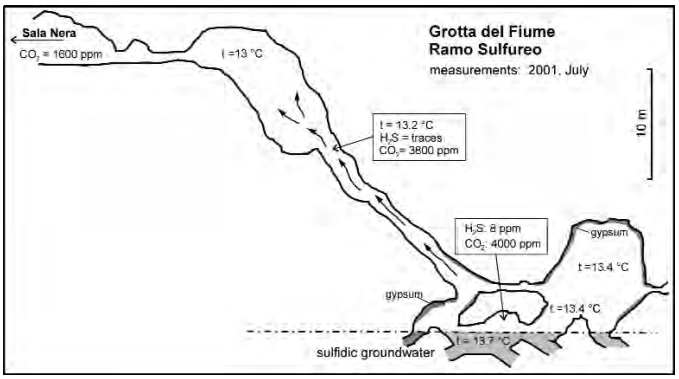


Figure 10. Schematic profile through the Frasassi sulfidic section. Small thermal differences cause water vapor to rise and condense at higher levels. CO_2 diffuses into the upper levels, while H_2S is present only near the water table. Gypsum replacement crusts are growing on the limestone walls directly exposed to H_2S (after Galdenzi 2001).



Figure 11. White, finely crystalline gypsum, growing on limestone pockets, Ramo Sulfureo, Grotta del Fiume. (Image width = 30 cm).

of the flooded galleries (Fig. 9) and cause the oxidation of H_2S, but gypsum deposition cannot occur in the water because saturation of sulfate is not achieved. In some pools and streams, H_2S and CO_2 are released to the cave atmosphere from the water and can diffuse to the nearby rooms. The concentration of H_2S and CO_2 reached peaks at 8 ppm and 5800 ppm, respectively, in the cave air near the sulfidic streams (Galdenzi 2001). The gas can rise toward the upper cave levels due to the small differences in the temperature (~1°C), but the H_2S concentration decreases quickly away from the water table (Fig. 10).

The gas concentration that can build up where air exchange is low was simulated by creating an air bell floating on the water table. Here the concentration of H_2S exceeded 120 ppm, while O_2 decreased to 7% (Galdenzi 2001). On the other hand, rapid air flow in the open cave disperses the H_2S and keeps the concentration low.



Figure 12. Organic "stalactites" growing on gypsum crystals coating the cave walls in Grotta del Fiume. They consist of mucous glycocalyx, secreted by sulfur-oxidizing bacteria to protect themselves from the very acidic environment. The droplets are rich in H_2SO_4 and their pH is always < 1.

The limestone walls exposed to H_2S vapors are highly corroded and partially or completely covered by gypsum crusts (Fig. 11), sometimes associated with small amounts of elemental sulfur. The gypsum crust generally consists of white, finely crystalline gypsum, whereas some large crystals grow on the gypsum crusts or directly on the limestone. The limestone surface under the gypsum crust is severely corroded, with hemispheric corrosion pockets some cm deep. The intensity of limestone corrosion was measured using limestone tablets (80 x 40 x 10 mm), exposed to acidic vapors in the cave atmosphere for 5 years (Galdenzi *et al.* 1997). At the end of the experiment, these tablets were completely covered with replacement gypsum, and the limestone surface under the gypsum crust was irregularly corroded, with incipient erosional pockets. The average weight loss, measured after gypsum removal, was about 15 mg/cm²/a, with significant variation due to small variations in the location of each tablet. This weight loss can correspond to an average loss of about 0.05 mm/a at the limestone surface. In the same experiment, quite similar values were obtained for limestone tablets placed in the sulfidic groundwater, where gypsum deposition did not occur.

Galdenzi *et al.* (1997) also discovered a biofilm at the limestone-gypsum interface. This means that bacterial communities played an important role in the H_2S oxidation. The microbial biofilm can grow and cover the walls with a layer of organic mucous matter, that forms organic "stalactites", secreting acidic drops, rich in H_2SO_4, with a pH < 1 (Galdenzi *et al.* 1999) (Fig. 12). Microbiologic studies of these biofilms found sulfur-oxidizing bacteria that play an important role both in limestone corrosion and in the cave food web (Vlasceanu *et al.* 2000). These organic formations are quite similar to those described in the Cueva de Villa Luz, Mexico, by Hose and Pisarowicz. (1999).

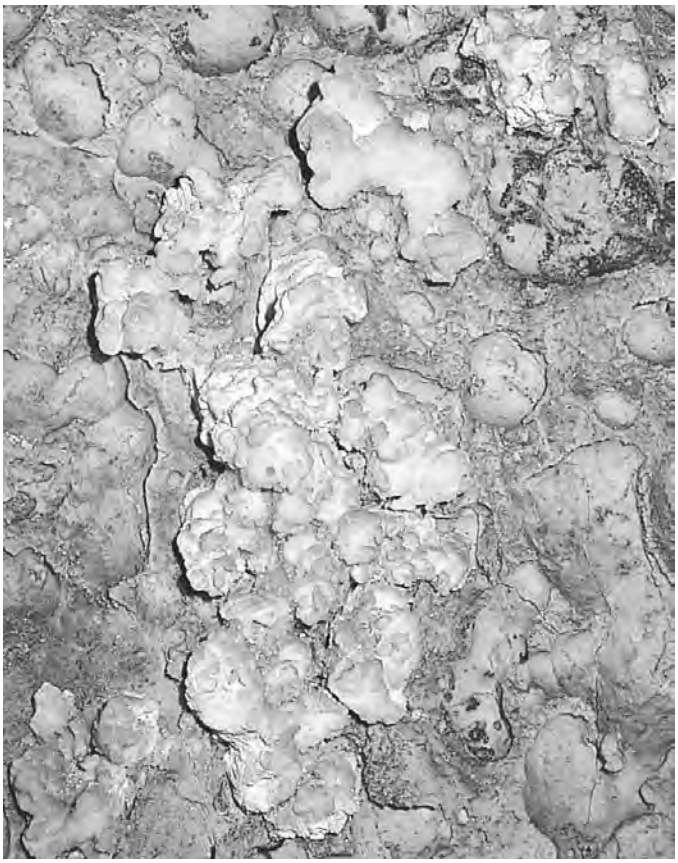


Figure 13. Limestone pockets on the cave walls after gypsum removal by dripping water and gravity, Abisso Ancona, Grotta del Vento. (Image length = 60 cm)



Figure 14. Evidence of the old water table in a dry passage of Fiume-Vento Cave System. Note the rough limestone surface above the water level and the rounded features in the flooded zone. A bubble trail is near the speleologist's head.

ANCIENT GYPSUM DEPOSITS

Gypsum deposition in limestone caves is fairly common in central Italy (Galdenzi & Menichetti 1995). Some large and interesting gypsum deposits are found particularly in the Faggeto Tondo Cave (Forti *et al.* 1989) and in the Monte Cucco Cave (~20 km to the west). Large gypsum deposits also occur in the dry, upper levels of Frasassi Cave. Three main types of deposits can be observed: (1) replacement crusts, (2) large floor deposits, and (3) gypsum crystals inside mud.

REPLACEMENT CRUSTS

This is the only type of ancient gypsum deposit that can be compared with gypsum presently forming in the cave. The old gypsum replacement crusts are quite common in many horizontal passages and rooms. Later seepage water often dissolved these old crusts, exposing small, rounded corrosion pockets on the limestone walls (Fig. 13). Commonly these corrosion pockets represent the only evidence of a preexisting gypsum crust. The replacement gypsum is generally recrystallized on the surface, but its characteristics are similar to the gypsum crusts that are forming in the sulfidic section of the cave, and they are believed to be a product of subaerial replacement of limestone (Bertolani *et al.* 1977; Ciarapica & Passeri 1978; Cigna & Forti 1986; Galdenzi 1990). In some passages, Galdenzi (1990) also reported that their lower parts show typical phreatic features such as rounded cupolas and bubble trails, while in the upper parts corrosion pockets or residual gypsum crusts cover the limestone walls (Fig. 14).

The distribution and thickness of gypsum forming today in the Frasassi Caves is much more limited than it was in the past. This may be due to the present hydrologic setting, because a free interface between groundwater and cave air generally exists only at the bottom of shafts or descending passages, where gypsum is forming in restricted areas (Fig. 3). Moreover, in most of these places, a layer of infiltration water overlies the sulfidic groundwater, preventing the release of H_2S and the subaerial growth of gypsum replacement crusts. In the past, the cave was an almost ideal water table cave, with many partly flooded rooms and passages formed as a result of degassing (Galdenzi 1990). At that time, condensation-corrosion could have been more important in enlarging the cave, as the wide distribution of old replacement crusts testifies.



Figure 15. Gypsum floor deposit below a wall covered by corrosional limestone pockets near Lago Cristallizzato, Grotta del Vento.



Figure 16. Piles of gypsum on the cave floor overlying mud with gypsum crystals, Sala Duecento, Grotta del Vento.

LARGE FLOOR DEPOSITS

Some large deposits of massive gypsum occur on the floor of the main rooms, where they are generally associated with replacement crusts that cover the limestone walls (Fig. 15). These floor deposits consist of white, finely crystalline gypsum, very similar to the replacement crusts. The floor deposits form mounds several meters thick, often below wide cupolas (Fig. 16), or form small gypsum "glaciers", similar to the ones described in Lechuguilla Cave (Davis 2000). Maximum thickness reaches 5 m, and volume exceeds 1000 m³ (Fig.17).

The large gypsum deposits in the Frasassi Caves were formerly thought to be the by-product of sulfate-saturated phreatic water (Bertolani *et al.* 1977; Ciarapica & Passeri 1978). Ciarapica & Passeri (1978) proposed that the massive gypsum deposition could be produced by the rapid cooling of warm water. Bertolani *et al.* (1977), based on cave mineral associations, excluded the possibility of thermal water flow in the cave, but believed the gypsum deposition was a result of super-

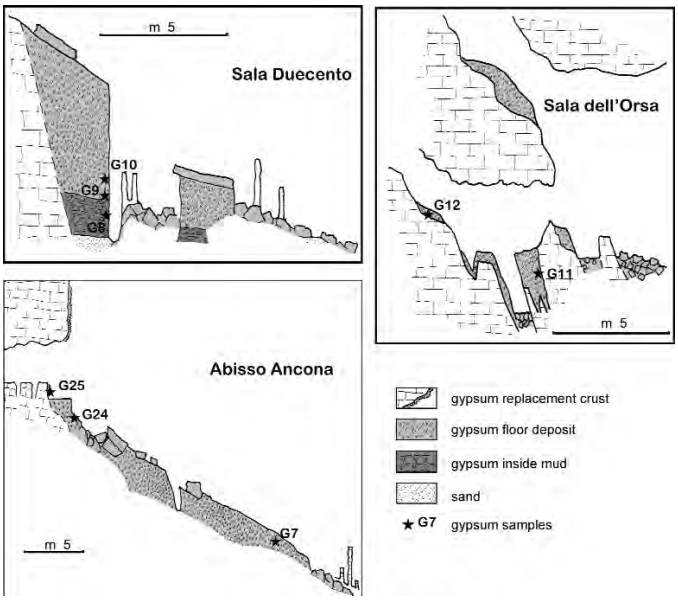


Figure 17. Profiles through some of the most significant gypsum deposits in Grotta del Vento.



Figure 18. Gypsum crystals growing inside mud in Frasassi Caves.

saturated groundwater. However, based on depositional settings and characteristics, Galdenzi (1990) concluded that these large gypsum deposits were produced above the water table.

Table 1. Mineralogical composition of sediment samples inside cave.

	dominant	abundant	present	scarce or trace
1- sand	calcite	quartz	feldspar, mica	illite
2- mud	quartz	calcite, gypsum	illite, mica	chlorite, feldspar, montmorillonite
4- mud	quartz	calcite	feldspar	kaolinite, amesite
6- mud	quartz	illite	mica, feldspar	chlorite, cristobalite
7- mud	quartz		illite, mica	chlorite

Galdenzi showed that these deposits lack any sedimentary structure or texture that can be attributed to a subaqueous environment. In particular, the gypsum is never interbedded with mud layers, while in the entire cave, mud deposits that originate below the water table are very common. Clear evidence of an origin above the water table also includes: (1) rare breccias of fallen gypsum crusts and (2) the corrosion runnels on bedrock below the floor deposit formed by flowing corrosive water. However, the main evidence for deposition above the water table is the depositional setting of these gypsum deposits in the western parts of the cave where recent gypsum is not forming. Here gypsum deposits in the lower part of the main rooms, below the old water table, are missing. Therefore, these large floor deposits were interpreted to have formed by the detachment and flow of slushy gypsum produced on the limestone walls as replacement crusts in zones exposed to intense H_2S vapors.

GYPSUM CRYSTALS INSIDE MUD

The last type of gypsum deposit typically occurs inside mud layers that, in places, underlie the large floor deposits. The quartz-rich mud (Table 1), contains authigenic, euhedral gypsum crystals that grew inside the sediments (Fig. 18). Ciarapica & Passeri (1978) proposed a phreatic origin for this type of gypsum via seepage and trapping of sulfate in solution inside mud sediments.

ISOTOPIC ANALYSIS: PURPOSE AND METHODS

Sulfur isotope ratios ($^{34}S/^{32}S$) can vary as a result of biologic and inorganic reactions involving the chemical transformation of sulfur species. Sulfur isotope studies have been useful in understanding the processes of sulfur cycling in many sulfur-related systems (see Canfield 2001, for a recent review). Here we use sulfur isotopes of gypsum to see whether gypsum formed by oxidation of H_2S or by precipitation of sulfate from saturated water.

Isotopic compositions of sulfur were measured in sulfides and sulfates using a helium-gas continuous-flow isotope-ratio mass spectrometer (CF-IR-MS: Micromass Optima; Maruoka *et al.* 2002, 2003). The samples were weighed into 12 x 5 mm tin capsules, together with a mixture of V_2O_5 and SiO_2 to promote full combustion (Yanagisawa & Sakai 1983). The sulfur isotopic compositions are expressed in terms of $\delta^{34}S$ (‰) relative to the Canyon Diablo standard. Results of three IAEA silver sulfide standards (IAEA-S-1, -0.30‰; IAEA-S-2, 22.67‰; IAEA-S-3, -32.55‰: Ding *et al.* 2001) were compared to constrain the $\delta^{34}S$ values. The isotopic compositions of sulfur were determined at a precision of ± 0.2‰ (1σ).

SAMPLING SITES

SULFIDIC WATER

The isotopic composition of sulfide and sulfate in the water can be used to discuss the origin of gypsum deposits inside the cave. Tazioli *et al.* (1990) also analyzed $\delta^{34}S$ in the water and in a gypsum sample, without discussing its characteristics and location, and confirmed its derivation from the H_2S dissolved in the water. Some water samples at different sites were collected November 11, 2000, at the end of a dry period when freshwater recharge to the groundwater and discharge were low. We sampled sulfate and sulfide in two different springs and in two cave pools with different water salinities (Fig. 5). The concentration of the oxidized and reduced sulfur in these water samples was determined by Cocchioni (2002).

The sulfide in the Main Spring water was collected from the main surface spring along the river, in the gorge. Here, many small springs have the same temperature and conductivity, about 13.5°C and 1600 µS, respectively. They can be considered to represent the "normal" sulfidic groundwater in the shallow phreatic zone, formed by the mixing of the rising mineralized water and the descending meteoric freshwater in the cave.

The Fissure Spring is a small emergence, very near the Main Spring. The sulfidic water in the Fissure Spring is significantly different compared to the "normal" sulfidic spring water. Throughout the year the temperature is ~0.5°C higher and the conductivity is ~30% higher. This spring is probably supplied by water rising from a deeper phreatic zone, with a lower dilution of descending freshwater (Cocchioni 2002).

The sulfide and sulfate of a sulfidic stream were sampled in the most studied cave room (Ramo Sulfureo: Galdenzi *et al.* 1997, 1999; Sarbu *et al.* 2000). Here, a direct influence from meteoric fresh water is well documented (Sarbu *et al.* 2000) and the chemical characteristics of the groundwater are similar to the Main Spring water (Cocchioni 2002). A large surface area of flowing sulfide water allows the release of H_2S into the cave air. The sulfide and sulfate of a stagnant sulfidic pool, Lago Verde, was also sampled. Here, groundwater has a chemical composition similar to the Fissure Spring (Cocchioni 2002).

The concentrations of sulfide in total sulfur range between 5.5 and 17.9% (Table 2). The Fissure Spring and the Lago Verde sulfidic pool, supplied by deeper water, appear to be more enriched in H_2S and have a higher ratio of sulfide/sulfate. The Main Spring and the Ramo Sulfureo water, on the contrary, has an higher value of oxidized sulfur owing to recharge by oxygen-rich freshwater. Sulfide $\delta^{34}S$ values in the water range between –13.30‰ and –15.03‰, while sulfate $\delta^{34}S$ val-

Table 2. Isotopic composition of sulfide and sulfate in the groundwater.

	sulfide–total sulfur ratio	$\delta^{34}S$ sulfide	$\delta^{34}S$ sulfate
Main Spring	12.1%	–14.47	+20.34
Fissure Spring	17.9%	–13.30	+22.06
Ramo Sulfureo	5.5%	–15.03	+20.11
Lago Verde	17.2%	–14.49	+22.17
Triponzo Spring		– 9.09	+17.45

ues range between +20.11 and +22.17‰ (Table 2). The sulfate $\delta^{34}S$ is lower in the Main Spring water than in the Fissure Spring water. As the Main Spring water mixed with the descending oxygen-rich freshwater, part of the H_2S, depleted in ^{34}S, in the Main Spring water would be oxidized to sulfate before degassing from the surface. This could cause the low sulfate $\delta^{34}S$ values in the Main Spring water.

GYPSUM DEPOSITS

Gypsum deposits were sampled in various areas of the cave system (Fig. 5) in order to analyze their isotopic compositions. Here they will be briefly described (Table 3).

Recent gypsum

Some gypsum, both microcrystalline and large crystals, up to several cm long, were collected at two different sites where gypsum is actively forming. A sample was also obtained from the surface of the limestone tablets described in previous experiments (Galdenzi *et al.* 1997).

Grotta del Vento, level III

This cave level is well developed in the Grotta del Vento: here a layer of freshwater over the sulfidic groundwater prevents the escape of H_2S, therefore all gypsum deposits can be considered inactive. Some of the largest gypsum deposits are located in this part of the cave.

Lago Cristallizzato. A small floor deposit in the Abisso Ancona, the main cave room, is under a limestone wall completely covered by corrosional limestone pockets with some residual replacement crusts (Fig. 15). Seepage water removed a large amount of the original deposit, while the replacement crust on the cave wall is almost entirely missing. Both the replacement crusts and the floor deposit were sampled.

Abisso Ancona. This is the largest gypsum deposit in the cave. It developed like a gypsum "glacier" under a high wall, completely covered by corrosional limestone pockets with some residual replacement crusts (Fig. 17). Both the replacement crusts and the floor deposit were collected for this study.

Table 3. Isotopic composition of sulfur in gypsum deposits in the caves.

Cave	sample	locality	karst level	depositional setting	fine-grained gypsum $\delta^{34}S$	gypsum crystals $\delta^{34}S$
Grotta del Fiume	G4	Ramo Sulfureo	active	limestone tablet	-19.17	
	G19-18	Laghi di Lucia	active	active wall crust	-19.62	-17.64
	G27-26	Ramo Sulfureo	active	active wall crust	-18.80	-10.79
	G14-13	Ramo Sulfureo	partly active	wall crust	-15.52	-13.90
	G2	old branches	II	wall crust	-14.07	
	G3	Pozzo Cristalli	unclear	wall crust	-7.82	
	G28	Pozzo Cristalli	unclear	wall crust	-10.33	
Grotta del Vento	G5	Lago Cristallizzato		III	floor deposit	-14.75
	G6	Lago Cristallizzato		III	wall crust	-16.06
	G7	Abisso Ancona	III	floor deposit	-12.14	
	G24	Abisso Ancona	III	floor deposit	-11.69	
	G25	Abisso Ancona	III	wall crust	-16.04	
	G8	Sala Duecento	III	floor mud		-14.05
	G9	Sala Duecento	III	floor deposit	-14.14	
	G10	Sala Duecento	III	floor deposit	-13.37	
	G1	Sala Duecento	III	floor deposit	-12.19	
	G12	Sala Orsa	III	floor	-11.69	
	G11	Sala Orsa	III	crevasse	-12.59	
	G15	Piano Superiore	V	floor deposit		-10.58
	G21	Abisso Ancona	V	floor deposit	-9.54	
	G22-23	Abisso Ancona	V	floor deposit	-7.93	-7.53
Triponzo Spring	T3-4	Triponzo		wall crust	-24.24	-22.52
	T5	Triponzo		wall crystals		-19.09

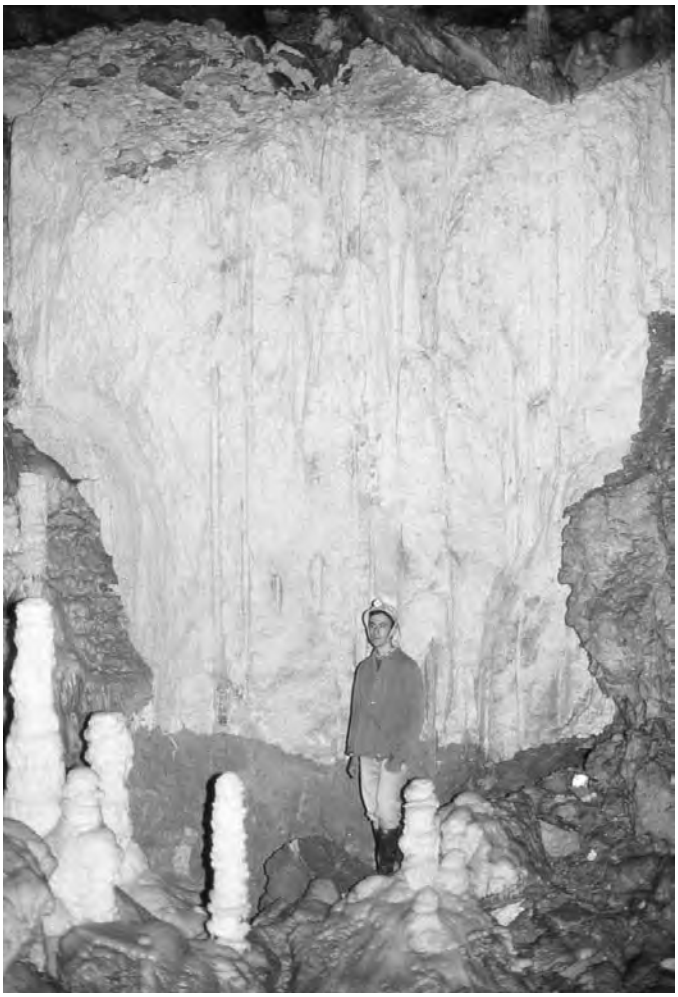


Figure 19. A natural section through one of the largest gypsum floor deposits of Sala Duecento, Grotta del Vento. Compare with the section in Figure 17.

Sala Duecento. This part of the cave consists of many interconnected rooms developed around a main large passage. This part of the cave includes two very interesting deposits, from which we collected samples. The first one represents the most spectacular natural section in the cave (Fig. 19). Here a small gypsum "glacier" is deeply dissected by dripping water. A succession of fine sand and mud with gypsum crystals (Table 1, samples G1 and G2), is overlain by thick, white, microcrystalline gypsum. The other deposit in Sala Duecento is on the floor of a wide room, cut by many shafts (Fig. 16). The gypsum overlies gray mud including small gypsum crystals (Table 1, samples G4 and G6), whereas the overhanging walls and roof are corroded by wide cupolas and by small pockets with a few residual gypsum replacement crusts. Gypsum is not present inside the shafts, which acted as vents for the sulfidic water when the cave level was forming.

Sala dell'Orsa. This room constitutes an intermediate part of a large shaft that opens in the flat rock floor of a big room at level V and reaches the actual water table. The lower part of this shaft, below level III, is deeply corroded by rounded phreatic features, while in its upper part scattered gypsum deposits occur inside the deeply corroded limestone wall or cover the floor. Three other cave minerals related to the sulfidic water (halloysite, barite, and jarosite) have been detected in this zone (Bertolani *et al.* 1977). Here we sampled a wall deposit and a nearby fissure filled with gypsum (Fig. 17).



Figure 20. Pile of gypsum cut by dripping fresh water in the level V, Grotta del Vento.

Grotta del Vento, level V

Some samples were collected in this upper dry level in a short, lateral branch of the Abisso Ancona Room. The gypsum lies on the floor, under wide cupolas in the roof. It is the typical, white, finely crystalline gypsum, recrystallized on the surface. It lies where a rising phreatic passage reaches the main room. A further sample of large gypsum crystals was collected from the top of piles in the large passage above Sala Duecento that are deeply dissected by dripping water (Fig. 20).

Grotta del Fiume deposits

In this part of the cave system, sulfidic water flows in the lower cave passages, therefore condensation-corrosion occurs near the sulfidic pools and in adjacent upper level passages. Moreover, in this zone two minor cave levels are well developed between level III and the water table. Therefore, H_2S can easily rise from the water table toward the upper dry level, and gypsum deposition can occur in the same cave level at different times.

Old Branch. This part of the cave represents a network of passages developed near the surface, ~10 m above the water table. Widespread replacement crusts can be observed on the cave walls. A few small floor deposits and gypsum crystals inside mud are also present (Table 1, sample G7).

Pozzo dei Cristalli. This shaft opens up below level III and is directly connected with the lower passages and with the water table. The walls are completely covered by a thick crust

of replacement gypsum, and the corrosional processes are still weakly active. The sulfidic water is the same as Lago Verde and the Fissure Spring.

Ramo Sulfureo. In this part of the cave, corrosion by the cave air is the most intense. Some deposits are still growing, and here the main research on the sulfidic zones was concentrated.

TRIPONZO SPRING: A COMPARISON

Triponzo Spring is a sulfidic thermal spring located ~60 km south of Frasassi. The deep valley of the Nera River cuts the Calcare Massiccio Formation in the northern periclinal termination of an anticline, where the spring reaches the surface, in a geologic setting similar to the Frasassi Gorge. Sulfide and sulfate in the Triponzo water were sampled in August 2000. The temperature of the water was 29-30°C, the conductivity was 2.14 mS/cm; the sulfate $\delta^{34}S$ value was +17.45‰, and the sulfide $\delta^{34}S$ was -9.09‰.

In this area, the deep karst is not well known. Only a few small caves were explored in the steep mountain sides, but an interesting room was encountered in a hydroelectric tunnel. This small cave is no longer accessible, but it was described during the drilling by an Italian geologist interested in cave origin (Principi 1931). He understood the importance of the cave and suggested that "the cave did not form by normal karst dissolution, but developed as a consequence of the sulfidic water action, that replaced limestone with gypsum, which could be easily removed by flowing water". The active corrosion of sulfidic water on the limestone walls could be observed until recently in a partly flooded artificial tunnel, where the sulfidic water flowed to the old thermal baths. The new thermal baths, built recently, reach the sulfidic water through boreholes, therefore the old flooded tunnel was destroyed. A remaining dry tunnel allowed a glimpse inside the karstified limestone near the spring. Here a network of open fissures and fractures is entirely covered by gypsum. In places, the limestone is replaced by a thin layer of finely crystalline gypsum, with small crystals on the surface. By turns, small gypsum crystals can grow directly on the limestone. These gypsum deposits were sampled to determine their sulfur isotopic composition (Table 3).

ORIGIN OF GYPSUM DEPOSITS

The Frasassi Caves make it possible to compare the isotopic content of sulfur in the water and in the gypsum deposits. It can help in the study of gypsum deposition and is very useful in deciphering the origin of the gypsum deposits in the upper dry levels. The $\delta^{34}S$ values of the gypsum collected in the cave range from –7.82 to –19.60‰. These are much lower than those of sulfate in the sulfidic groundwater (from +20.11 to +22.17‰). As it is impossible to produce such large isotopic fractionations during precipitation from water, the gypsum cannot have been produced by precipitation from saturationed groundwater. These low $\delta^{34}S$ values are related to H_2S ($\delta^{34}S$ = -13.30‰ and -15.03‰). Moreover, the sulfide oxidation occurred in the air. If the oxidation had occurred in the water, the sulfate from H_2S would mix with the abundant sulfate in the water, and the lower $\delta^{34}S$ values would not be preserved in the gypsum. This conclusion is consistent with the sub-aerial depositional settings of the gypsum (Galdenzi 1990).

REPLACEMENT CRUSTS

The gypsum replacement crusts in the upper dry levels have $\delta^{34}S$ values similar to those of sulfide now dissolved in the water. Therefore, the sulfur in the replacement crust came from H_2S released from groundwater. This conclusion is consistent with many observations, such as the gravity-controlled shape of the corrosion pockets on cave walls, the analogies with the present depositional setting, and the localization above the original old water table level in many passages.

FLOOR DEPOSITS

The massive floor deposits are not forming today in the cave, and they occur mainly in cave levels III and V, which formed in the middle and late Pleistocene (Bocchini & Coltorti 1990; Taddeucci *et al.* 1992). These gypsum deposits were considered the result of sulfate saturation in the groundwater (Bertolani *et al.* 1977; Ciarapica & Passeri 1978) or the result of collapse and flow of gypsum replacement crusts (Galdenzi 1990). In the Guadalupe Mountains caves, U.S.A., where past gypsum deposition is well documented, both phreatic and vadose gypsum deposition are described, although the largest deposits are generally considered the result of sulfate supersaturation in the groundwater (Hill 1987; Buck *et al.* 1994; Palmer & Palmer 2000). The sedimentary structures that suggest a phreatic deposition for gypsum in Guadalupe Mountains caves (Hill 1997) are not clearly developed in the Frasassi deposits, therefore the depositional setting is not necessarily the same.

In the Frasassi Caves, since we can compare the isotopic composition of sulfidic water and gypsum, we can easily see that the gypsum $\delta^{34}S$ values clearly exclude the possibility that these massive floor deposits formed by precipitation below the water table in sulfate-supersaturated groundwater. Furthermore, the $\delta^{34}S$ of the floor deposits is similar to the adjacent replacement crusts (i.e., Lago Cristallizzato, Abisso Ancona, Table 3), suggesting that the growth of the replacement crusts and the deposition of nearby floor deposits were related. Judging from their thickness, we can exclude direct limestone replacement of the cave floor by H_2S oxidation in the cave air. Therefore, these gravity piles or "gypsum glaciers", lying below walls or roofs covered with limestone pockets or replacement crust, can be considered the result of the detachment and flow of moonmilk-like replacement gypsum produced on the cave walls over a long time, as Galdenzi (1990) proposed.

GYPSUM IN MUD DEPOSITS

The low-$\delta^{34}S$ values of the euhedral gypsum crystals incorporated in mud also can be explained by the result of H_2S oxidation. Therefore, we can conclude that they could not form below the water table as a consequence of sulfate saturation inside the mud. Moreover, their values are quite similar to the overlying massive floor deposits. So these gypsum crystals grew by the seepage of sulfate-rich water from the overlying massive gypsum deposits. The chemical composition of this mud (Table 1) differs from the other mud deposits of the cave (Bertolani *et al.* 1977) and also implies etching by strong acid. The seepage of acidic water below the large gypsum deposits is also evidenced by meandering corrosional rills on the floor, formed where gypsum floor deposits directly overlie limestone, without interposed mud layers.

SULFUR ISOTOPIC FRACTIONATION

Although the low $\delta^{34}S$ values in the gypsum are related to H_2S, the values do not correspond exactly to those of H_2S. The $\delta^{34}S$ in the cave gypsum differs between deposits, and values can be lower or higher than values of present-day H_2S rising in the groundwater. The $\delta^{34}S$ in gypsum deposits ranges between –7.82‰ and –19.62‰, whereas in water the $\delta^{34}S$ values of H_2S rang from –13.30‰ to –15.03‰, with an average value of about –14.2‰. These differences in the $\delta^{34}S$ of gypsum and H_2S could represent the depositional setting in that the gypsum deposits formed in different places, over a period of ~200 ka.

ACTIVELY FORMING GYPSUM

The $\delta^{34}S$ values of actively forming microcrystalline gypsum are relatively constant. The $\delta^{34}S$ values of this gypsum on the active cave walls are ~5‰ lower than those of sulfide in the water. This depletion of ^{34}S may be related to kinetic isotopic fractionation during oxidation of sulfide (Fry *et al.* 1988). In the Triponzo aquifer, where gypsum growth is presently occurring, $\delta^{34}S$ in water sulfide is –9.09‰, while microcrystalline gypsum in the limestone fissure network is –24.24‰, with a depletion of about –14‰ of ^{34}S. Similar values were also obtained in other active H_2S caves: Hose *et al.* (2000) reported from Cueva de Villa Luz, Tabasco, Mexico, $\delta^{34}S$ values of –1.7‰ for H_2S and –23.4‰ for gypsum.

Isotopic fractionation of sulfur during abiotic oxidation is generally believed smaller than that measured from these caves (up to 5‰: Fry *et al.* 1988; Canfield 2001). Furthermore, sulfur oxidizing organisms are believed capable only of a small isotopic fractionation, even though this subject is not well explored (Canfield 2001). Therefore, a large fractionation should not be due only to isotopic fractionation during oxidation. Part of the isotopic fractionation might be explained by the additional production of H_2S in the shallow phreatic zone, which might be more depleted in ^{34}S than that rising in the aquifer. Although sulfate-reducing bacteria are not reported in those caves, they may be responsible for producing more depleted ^{34}S.

Sulfur isotope compositions of associated large and microcrystalline gypsums are shown in Table 3. The $\delta^{34}S$ values of the euhedral crystals are higher and closer to those of H_2S than those of the respective microcrystals. The $\delta^{34}S$ value of sample G26 is even higher than that of H_2S in the water. As biotic H_2S-oxidation is presently believed to cause a smaller isotopic fractionation than abiotic oxidation (Canfield 2001), the $\delta^{34}S$ values similar to those of H_2S may imply that the sulfate in those gypsums is mainly produced by sulfide-oxidizing bacteria rather than by abiotic oxidation. Actually, actively forming gypsum crystals are often covered with biofilms that contain sulfide oxidizing bacteria.

As mentioned above, the $\delta^{34}S$ value of sample G26 is even higher than those of H_2S in the water. This cannot be explained by only H_2S oxidation. Therefore, a more complex biologic activity affecting the gypsum should be considered. Sulfate-reducing bacteria are known to cause high isotopic fractionation, producing sulfide depleted in ^{34}S (Kaplan & Rittenberg 1964; Canfield 2001). Therefore, small amounts of sulfate in the gypsum might have been re-reduced to volatile H_2S. This process could have produced the ^{34}S-enriched sulfate because ^{34}S-depleted H_2S would have been released after the reduction. Similar considerations could explain the high $\delta^{34}S$ value of gypsum in the Pozzo dei Cristalli where finely crystalline gypsum is about +9‰ enriched in ^{34}S compared with gypsum forming in the other cave areas, and it is also +5‰ enriched in ^{34}S compared with water sulfide.

UPPER LEVEL DEPOSITS

In the upper dry III level of Grotta del Vento, where gypsum deposits probably formed before the Holocene, we observe some variation in the $\delta^{34}S$ values. The sulfur in the big floor deposits is enriched in ^{34}S compared to the associated replacement crusts. In the Lago Cristallizzato, the difference between the floor deposit and the nearby replacement crust is +1.3‰, while in the Abisso Ancona it is about +4‰. These differences between replacement crust and related floor deposit suggest that changes in the isotopic composition of gypsum might have occurred after gypsum formed on the walls.

Furthermore, the $\delta^{34}S$ values in the upper levels gypsum is generally higher than those in actively forming gypsum areas, and also in groundwater H_2S. In level V, all the 4 samples have a $\delta^{34}S$ value higher than –11‰; in level III the average value is –13.5‰ (11 samples), ranging between –11.69‰ and –16.06‰. These variations of isotopic composition might have been induced by the isotopic compositions of the H_2S released from the water. That could be caused by the activity of sulfate-reducing bacteria in the aquifer. As the bacterial activity should be influenced by environmental factors, such as the groundwater temperature, the amount of fresh water recharge, and the extension of the free interface between groundwater and cave atmosphere, the $\delta^{34}S$ values in the ancient gypsum may represent such factors at the time when the gypsum was produced.

CONCLUSIONS

The development of the Frasassi Caves can be clearly related to the oxidation of H_2S rising in the groundwater. H_2S oxidation can involve bacterial activity and occurs mainly in the shallow phreatic zone, utilizing oxygen dissolved in dripwater or diffusing from the cave atmosphere. At present, gypsum deposits form above the water table, where crusts of slushy gypsum including some large crystals replace the limestone walls. Below the water table limestone corrosion occurs without gypsum deposition, because sulfate saturation is not reached in the groundwater.

Three main types of gypsum can be observed in the dry upper levels of the cave: Replacement crusts similar to the actively forming deposits, large and thick microcrystalline floor deposits, and euhedral crystals in mud. The sulfur isotopic composition of these gypsum deposits shows that the sulfate was supplied by the oxidation of H_2S in the cave atmosphere. In the Frasassi caves, phreatic sulfate precipitation are (and were) prohibited due to the dilution of the groundwater by sulfate-poor meteoric water. These data agree with the sedimentary characteristics and the sub-aerial depositional setting of the gypsum.

The size of the old massive deposits and their distribution in the upper cave levels imply that there were some periods with a gypsum formation more intense than recent one. It probably can be related to the development of widespread interfaces between sulfidic groundwater and the cave atmosphere, which could exist while the cave was an almost ideal water table cave. Similar conditions repeatedly occurred during the cave history, depending on the surface geomorphic evolution. Small hydrologic changes inside the cave seem capable of influencing the solutional and depositional effects of the sulfidic water circulation inside the same cave system.

The sulfur isotopic data also confirm that large gypsum floor deposits could form by the flow of slushy gypsum from the walls and ceilings to the floor. This conclusion might be helpful in studying similar gypsum deposits, known in other dry caves of central Italy.

A comparison of the active and dry gypsum deposits made it possible to show the changes in the sulfur isotopic composition of the gypsum during limestone replacement. Because the sulfur isotope composition was related to the depositional setting of the gypsum deposit, H_2S caves could represent a good natural environment in order to study isotopic fractionation of sulfur for oxidation-reduction processes involving biologic activity.

ACKNOWLEDGMENTS

We wish to thank Arthur and Margaret Palmer for having kindly reworked the English and for their helpful suggestions; we also thank Christian Koeberl for allowing us to use the mass spectrometer for this study, Antonio Rossi who analyzed mud samples from the Frasassi Caves, and Mario Cocchioni who permitted us to utilize data on water chemistry. Helpful comments during the preparation of the manuscript are also due to Jennifer Macaledy and Alessandro Montanari. We should like to thank Carol A. Hill and George W. Moore for their helpful and constructive review of the paper.

REFERENCES

Ambrosetti, P., Carraro, F., Deiana, G., & Dramis, F., 1982, Il sollevamento dell'Italia Centrale tra il Pleistocene inferiore e il Pleistocene medio: C.N.R., Progetto Finalizzato "Geodinamica", Pubblicazione, v. 513, n. 2, p. 219-223.

Bisci, C., & Dramis, F., 1991, La geomorfologia delle Marche, *in* Marche, Regione, ed., L'ambiente fisico delle Marche: Firenze, S.E.L.C.A., p. 81-113.

Bertolani, M., Garuti, G., Rossi, A., & Bertolani-Marchetti, M., 1977, Motivi di interesse mineralogico e petrografico nel complesso carsico Grotta Grande del Vento-Grotta del Fiume: Le Grotte d'Italia, s. 4, v. 6, p. 109-144.

Bocchini, A., & Coltorti, M., 1990, Il complesso carsico Grotta del Fiume Grotta Grande del Vento e l'evoluzione geomorfologica della Gola di Frasassi, *in* Galdenzi, S., & Menichetti, M., eds, Il carsismo della Gola di Frasassi: Memorie Istituto Italiano Speleologia, s. II, v. 4, p. 155-180.

Buck, M.J., Ford, D.C., & Schwarcz, H.P., 1994, Classification of cave gypsum deposits derived from oxidation of H_2S, *in* Sasowsky, I.D., & Palmer, M.V., eds., Breakthroughs in karst geomicrobiology and redox geochemistry: Charles Town, WV, Karst Waters Institute, Special Publication, v. 1, p. 5-9.

Canfield, D.E., 2001, Biogeochemistry of sulfur isotopes: Reviews of Mineralogy and Geochemistry, v. 43, p. 607-636.

Ciarapica, G., & Passeri, L., 1978, Speleotemi solfatici e fasi sedimentarie carsiche: Congresso su Processi Neocarsici e Paleocarsici. Napoli, 1-3 aprile 1978. (unpublished)

Ciccacci, S., D'alessandro, L., Dramis, F., Fredi, P., & Pambianchi, G., 1985, Geomorphological and neotectonic evolution of the Umbria-Marche Ridge, Northern Sector: Studi Geologici Camerti, v. 10, p. 7-15.

Cigna, A., & Forti, P., 1986, The speleogenetic role of air flow caused by convection: 1st contribution: International Journal of Speleology, v. 15, p. 41-52.

Cocchioni, M., 2002, Chimismo delle acque del complesso ipogeo di Frasassi: Camerino University report, Camerino, Italy, 146 p.

Davis, D.G., 2000, Extraordinary features of Lechuguilla Cave, Guadalupe Mountains, New Mexico: Journal of Cave and Karst Studies, v. 62, n. 2, p. 147-157.

Ding, T., Valkiers, S., Kipphardt, H., De Bie'vre, P., Taylor, P.D.P., Gon¢antini, R., & Krouse, R., 2001, Calibrated sulfur isotope abundance ratios of three IAEA sulfur isotope reference materials and V-CDT with a reassessment of the atomic weight of sulfur: Geochimica et Cosmochimica Acta, v. 65, p. 2433-2437.

DuChene, H.R., Hill, C.A., Hose, L.D., & Pisarowicz, J.A., eds., 2000, The caves of the Guadalupe Mountains research symposium: Journal of Cave and Karst Studies, v. 62, n. 2, 159 p.

Egemeier, S.J., 1981, Cavern development by thermal waters: National Speleological Society Bulletin, v. 43, p. 31-51.

Forti, P., Benedetto, C., & Costa, G., 1993, Las Brujas cave (Malargue, Argentina): An example of the oil pools control on the speleogenesis: Theoretical and Applied Karstology, v. 6, p. 87-93.

Forti, P., Menichetti, M., & Rossi, A., 1989, Speleothems and speleogenesis of the Faggeto Tondo Cave (Umbria, Italy), *in* Hazslinszky, T. & Takacsne B.K. (eds.) Proceedings, International Congress of Speleology, 10th, Budapest: v. 1, p. 74-76.

Fry, B., Gest, H., & Hayes, J.M., 1988, $^{34}S/^{32}S$ fractionation in sulfur cycles catalyzed by anaerobic bacteria: Applied and Environmental Microbiology, v. 54, p. 250–256.

Galdenzi, S., 1990, Un modello genetico per la Grotta Grande del Vento, *in* Galdenzi, S., & Menichetti, M., eds, Il carsismo della Gola di Frasassi: Memorie Istituto Italiano di Speologia, s. II, v. 4, p. 123-142.

Galdenzi, S., 1996, Il carsismo profondo nell'Appennino Umbro Marchigiano (Italia), *in* Verico, P. & Zorzin, R. (eds.) Proceedings, 1992 International Congress: Alpine Caves: Alpine karst systems and their environmental context, Asiago, Italy, p. 229-242.

Galdenzi, S., 1997, First geological data on the caves around the Sibari Plain (South Italy): Journal of Cave and Karst Studies, v. 59, n. 2, p. 81-86.

Galdenzi, S., 2001, L'azione morfogenetica delle acque sulfuree nelle Grotte di Frasassi, Acquasanta Terme (Appennino marchigiano - Italia) e di Movile (Dobrogea–Romania): Le Grotte d'Italia, s. V, v. 2, p. 49-61.

Galdenzi, S., & Menichetti, M., 1995, Occurrence of hypogenic caves in a karst region: Examples from central Italy: Environmental Geology, v. 26, p. 39-47.

Galdenzi, S., Menichetti, M., & Forti, P., 1997, La corrosione di placchette calcaree ad opera di acque solfuree: Dati sperimentali in ambiente ipogeo, *in* Jeannin, P.Y. (ed.) Proceedings, International Congress of Speleology, 12th, Le Chaux-de-Fonds, Switzerland, v. 1, p. 187190.

Galdenzi, S., Menichetti, M., Sarbu, S., & Rossi, A., 1999, Frasassi caves: A biogenic hypogean karst system? *in* Audra, P. (ed.) Proceedings European Conference Karst 99, Grands Causses, Vercors, France: Cagep, Université de Provence, Etudes de Géographie physique, travaux 1999, suppl. n. 28, p. 101-106.

Hill, C.A., 1987, Geology of Carlsbad Cavern and other caves in the Guadalupe Mountains, New Mexico and Texas: New Mexico Bureau of Mines and Mineral Resources, Bulletin, v. 117, 150 p.

Hose, L.D.& Pisarowicz, J.A., 1999, Cueva de Villa Luz, Tabasco, Mexico: Reconnaissance study of an active sulfur spring cave: Journal of Cave and Karst Studies, v. 61, n. 1, p. 13-21.

Kaplan, I.R., & Rittenberg, S.C., 1964, Microbiological fractionation of sulphur isotopes: Journal of General Microbiology, v. 34, p. 195-212.

Martinis, B., & Pieri, M., 1964, Alcune notizie sulla formazione evaporitica del Triassico superiore nell'Italia centrale e meridionale: Memorie Società Geologica Italiana, v. 4, n. 1, p. 649-678.

Maruoka, T., Koeberl, C., Hancox, P.J., & Reimold, W.U., 2003, Sulfur geochemistry across a terrestrial Permian-Triassic boundary section in the Karoo Basin, South Africa: Earth Planetary Science Letters, v. 206, p. 101-117.

Maruoka, T., Koeberl, C., Newton, J., Gilmour, I., & Bohor, B.F., 2002, Sulfur isotopic compositions across terrestrial Cretaceous-Tertiary boundary successions, *in* Koeberl, C., & MacLeod, K.G., eds., Catastrophic events and mass extinctions: Impact and beyond: Geological Society of America Special Papers, v. 356, p. 337-344.

Palmer, A.N. & Palmer, M.V., 2000, Hydrochemical interpretation of cave patterns in the Guadalupe Mountains, New Mexico: Journal of Cave and Karst Studies, v. 62, n. 2, p. 91-108.

Principi, P., 1931, Fenomeni di idrologia sotterranea nei dintorni di Triponzo (Umbria): Le Grotte d'Italia, v. 5, p. 1-4.

Queen, J.M., Palmer, A.N., & Palmer, M.V., 1977, Speleogenesis in the Guadalupe Mountains, New Mexico: Gypsum replacement of carbonate by brine mixing, *in* Ford, T.D. (ed.) Proceedings, International Congress of Speleology, 7th, Sheffield (U.K.): p. 333-336.

Sarbu, S. M., Galdenzi, S., Menichetti, M., & Gentile, G., 2000, Geology and biology of the Frasassi Caves in Central Italy, an ecological multi-disciplinary study of a hypogenic underground ecosystem, *in* Wilkens, H., *et al.*, eds., Ecosystems of the world: New York, Elsevier, p. 359-378.

Sarbu, S.M., & Kane, T.C., 1995, A subterranean chemoautotrophically based ecosystem: National Speleological Society Bulletin, v. 57, p. 91-98.

Sighinolfi, G. P., 1990, Chimismo ed origine delle acque del sistema ipogeo "Grotte di Frasassi" (Ancona) Implicazioni speleogenetiche ed ambientali, *in* Galdenzi, S., & Menichetti, M., eds, Il carsismo della Gola di Frasassi: Memorie Istituto Italiano di Speleologia, s. II, v. 4, p. 109-122.

Taddeucci, A., Tuccimei, P., & Voltaggio, M., 1992, Studio geocronologico del complesso carsico Grotta del Fiume-Grotta Grande del Vento (Gola di Frasassi, AN) e indicazioni paleoambientali: Il Quaternario, v. 5, p. 213-222.

Tazioli, G. S., Cocchioni, M., Coltorti, M., Dramis, F., & Mariani, M., 1990, Circolazione idrica e chimismo delle acque sotterranee dell'area carsica di Frasassi nelle Marche, *in* Galdenzi, S., & Menichetti, M., eds, Il carsismo della Gola di Frasassi: Memorie Instituto Italiano di Speleologia, s. II, v. 4, p. 93-108.

Vlasceanu, L., Sarbu, S.M., Engel, A.S., & Kinkle, B.K., 2000, Acidic, cave-wall biofilms located in the Frasassi Gorge, Italy: Geomicrobiology Journal, v. 17, p. 125-139.

Yanagisawa, F., & Sakai, H., 1983, Thermal decomposition of barium sulfate-vanadium pentaoxide-silica glass mixtures for preparation of sulfur dioxide in sulfur isotope ratio measurements: Analytical Chemistry, v. 55, p. 985-987.

Patrick Applegate - Detection of sinkholes developed on shaly Ordovician limestones, Hamilton County, Ohio, using digital topographic data: Dependence of topographic expression of sinkholes on scale, contour interval, and slope. *Journal of Cave and Karst Studies* 65(2): 126-129.

DETECTION OF SINKHOLES DEVELOPED ON SHALY ORDOVICIAN LIMESTONES, HAMILTON COUNTY, OHIO, USING DIGITAL TOPOGRAPHIC DATA: DEPENDENCE OF TOPOGRAPHIC EXPRESSION OF SINKHOLES ON SCALE, CONTOUR INTERVAL, AND SLOPE

PATRICK APPLEGATE
Department of Geology, University of Cincinnati, Cincinnati, Ohio 45221 USA

The Ohio Geological Survey has recently published a map showing the locations of known and probable karst in Ohio. The map shows some areas of karst developed on the extremely shaly Ordovician limestone of Hamilton County, in the southwestern corner of the state. Detailed mapping of these sinkholes in Mt. Airy Forest, a municipal park near Cincinnati, shows that they occur only where the lower 10 m of the Corryville Member of the Grant Lake Formation is the surface bedrock. Of the many sinkholes in the study area, only one is evident on the 1:24,000 USGS topographic map. The expression of sinkholes on contour maps is dependent on the size of the sinkhole, as well as the scale of the map, the contour interval at which the topography is sampled, and the slope of the ground surface around the sinkhole. It is possible to determine the minimum size of sinkhole which will consistently be expressed on a given part of a contour map. Conversely, it is also possible to determine the scale and contour interval which will be necessary to consistently indicate the presence of sinkholes of a given minimum size.

The Ohio Geological Survey has recently published a map at a scale of 1:500,000 showing the locations of known and probable karst areas in Ohio (Pavey *et al.* 1999). Most of the karst areas in the state are underlain by relatively pure Silurian and Devonian carbonates; the units most prone to karstification are the Silurian Peebles Dolomite and the Devonian Columbus Limestone (Pavey *et al*. 1999). However, the map also shows a number of karst features developed on the interbedded shales and limestones of Upper Ordovician age in southwestern Ohio. In particular, the karst areas of Hamilton County, which are developed on some extremely shaly limestones, have never been described or mapped at any larger scale. This paper provides the results of some detailed mapping of sinkholes in a small area near Cincinnati.

The results of this mapping exercise have implications for the practice of locating sinkholes on US Geological Survey (USGS) 1:24,000 topographic maps. A qualitative comparison of the mapped locations of the sinkholes with 2 topographic data sets show that contours from the USGS quadrangle maps do not predict the presence of sinkholes as well as contours plotted at a scale of 1:100. Even this higher-resolution data set (from the Cincinnati Area Geographic Information System) does not give a true picture of the number, density, nor size of sinkholes in the field area.

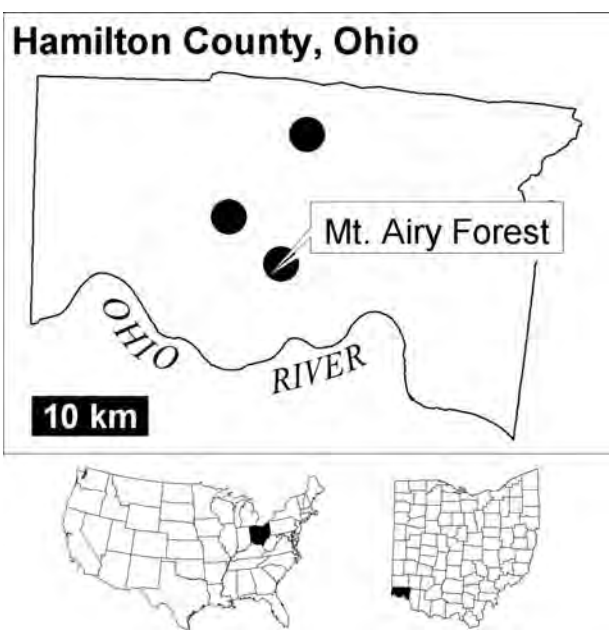


Figure 1. Map of Hamilton County, Ohio, showing the general locations of areas of known karst (black dots; simplified from Pavey *et al*. 1999). Sources: ESRI (US map) and Wells (2000; county outlines).

STUDY AREA

The Ohio Geological Survey's karst map identifies 3 general areas of known karst in Hamilton County (Fig. 1). These areas occur at the western end of Winton Lake (Greenhills 7.5-min. quadrangle), north of Taylor Creek (Addyston quad), and near West Fork Creek in Mt. Airy Forest (Cincinnati West quad).

The Mt. Airy Forest karst area lies almost completely within a large municipal park of the same name. The sinkholes there are well developed and accessible. The field observations

Copyright © 2003 by The National Speleological Society

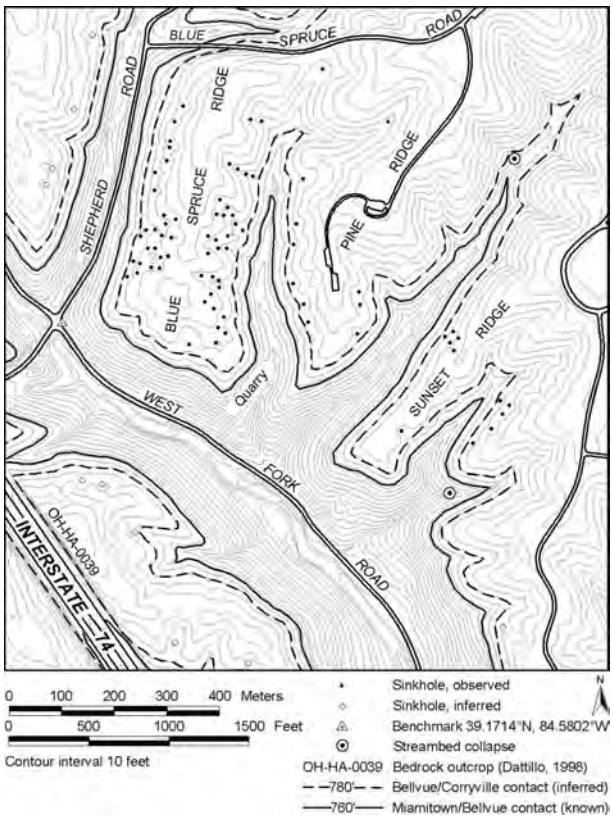


Figure 2. Mt. Airy Forest study area (Blue Spruce, Pine, and Sunset Ridges) and immediate surroundings; contour interval 10 ft. Topography from Cincinnati Area Geographic Information System (CAGIS).

for this paper were made in Mt. Airy Forest on Blue Spruce Ridge, Pine Ridge, and Sunset Ridge (Fig. 2).

Geologic maps of the Cincinnati West quadrangle (Ford 1974; Swinford & Ford 1996) show that the bedrock units listed in Table 1 are exposed in the study area. It is important to note that none of the units exposed in the study area are pure carbonates. Most are interbedded with considerable amounts of shale. The individual beds of limestone are thickest in the Fairview Formation, and even there they are rarely more than 0.3 m thick.

METHODS

All of the sinkholes in the Mt. Airy Forest study area (Fig. 2) were plotted by hand on a topographic base map prepared from the 10-ft contour interval topographic layer of the Cincinnati Area Geographic Information System (CAGIS). The contours in the CAGIS topographic layer were traced using a stereo plotter at a scale of 1:100, rather than the 1:24,000 scale used for USGS 7.5-min. maps (John Coulter, pers. comm., 2002).

For the purposes of this mapping, a sinkhole was considered to be any closed, localized depression in the ground surface. Where small depressions occurred within larger ones, the smaller depressions were mapped.

The elevation of the Bellvue/Miamitown contact was confirmed in the field. The Corryville/Bellvue contact is covered in the study area, but the thickness of the Bellvue was measured by Dattillo (1998) at a roadcut along Interstate 74 just outside of the field area (OH-HA-0039 on Fig. 2). Adding the 6.5-m thickness of the Bellvue at that roadcut to the 760-ft elevation of the Bellvue/Miamitown contact gives an elevation of about 780 ft for the Corryville/Bellvue contact.

RESULTS

All of the sinkholes in the Mt. Airy Forest study area plot between the 780- and 810-ft contours on the map, within the lower 10 m (30 feet) of the Corryville Member (Fig. 2). Field sheets from the Ohio Geological Survey show that the sinkholes in the other known karst areas in Hamilton County also occur in this stratigraphic interval (Dennis Hull, pers. comm., 2002).

In Mt. Airy Forest, the sinkholes tend to be <25 m across and 3 m deep. The single largest sinkhole observed in the study area is near the southern end of Blue Spruce Ridge, and is ~63 m across and 4 m deep.

DISCUSSION

Since the Corryville Member is mostly shale (65% on average; Swinford *et al*. 2001), it is surprising that the sinkholes are found only where it is the surface bedrock. Its high shale content suggests that it is probably not being removed solutionally. Instead, there may be a water table perched on the

Table 1. Descriptions of bedrock units exposed in the study area. The thickness of the Fairview Formation is estimated from Ford (1974) and Swinford and Ford (1996). The thicknesses of the Miamitown Shale and the Bellvue Member were measured by Dattillo (1998) at outcrop OH-HA-0039 (Fig. 2). Other values are from Swinford *et al*. (2001).

Formation	Member	Thickness	% Limestone	Description
Grant Lake	Corryville	19 m (60 ft)	35	Interbedded limestone and shale; poorly exposed in study area
	Bellvue	6.5 m (21 ft)	65	Wavy-bedded, nodular, shelly limestone, interbedded with minor amounts of shale
Miamitown Shale		2.7 m (9 ft)	10	Shale
Fairview	undivided	15 m (100 ft)	50	Limestone interbedded with shale; lower portion is less limestone-rich than upper portion
Kope	undivided	60 m (200 ft)	25	Interbedded limestone and shale; only about 9 m (30 ft) exposed in study area

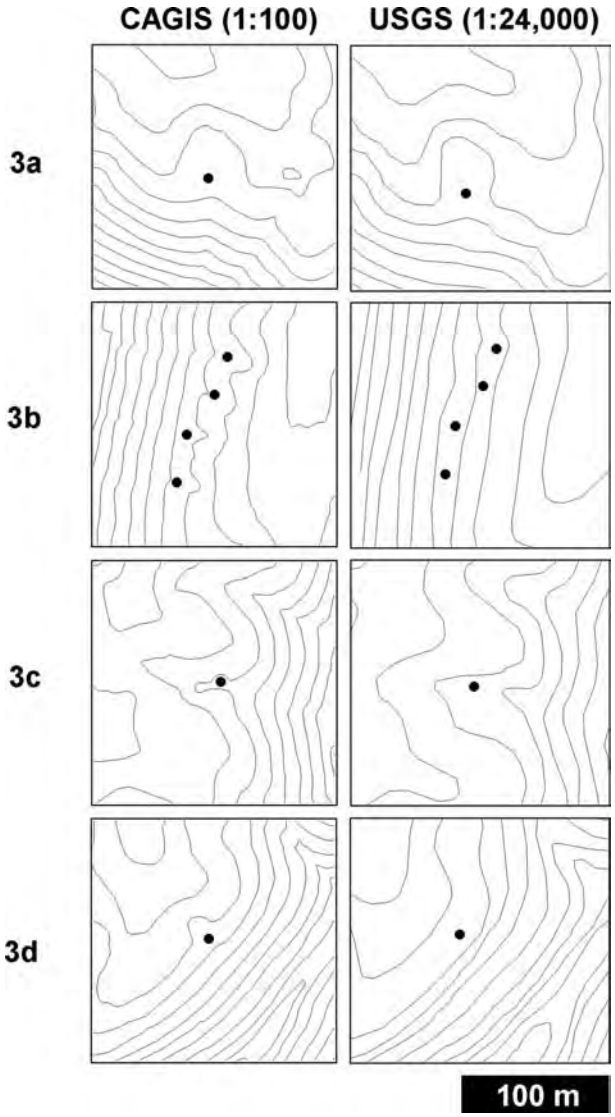


Figure 3. This figure shows the contour crenulations produced by selected sinkholes in the study area. Of all the sinkholes in the study area, only that in 3a is evident from the USGS contours. The contour interval is 10 ft for all eight maps.

Miamitown Shale that is dissolving the Bellvue Member, while the Corryville is collapsing into the cavities. It has historically been observed (Fenneman 1916) that the Bellvue Member is particularly resistant to erosion, and tends to mark a break in slope between itself and the overlying strata. It may be that no sinkholes appear where the Bellvue itself is the surface bedrock because the slopes it forms are too steep.

Most of the sinkholes in the study area do not hold water, even after heavy rains (though there are exceptions; one sinkhole on Blue Spruce Ridge is a seasonal pond). After prolonged periods of rain, many of the sinkholes show collapses at their bottoms, indicating that they have some way of passing sediment through themselves as well as water. The proximity of some of these sinkholes to gullies, and the presence in some of these gullies of collapses (Fig. 2), suggest that the gullies may be the surface expressions of conduits that drain the sinkholes. Without further study, however, this hypothesis must remain tentative.

Figure 3 shows the contour crenulations that represent selected field-verified sinkholes from the Mt. Airy Forest study area. Except in Figure 3a, which shows the largest sinkhole in the study area, the crenulations seen in the CAGIS contours are absent in the USGS contours. However, even the more detailed CAGIS data does not show all of the sinkholes (Fig. 2).

There are three factors that influence whether or not a sinkhole of a given size will be expressed on a contour map: 1) the scale at which the data is prepared; 2) the contour interval at which the topography is sampled; 3) the slope of the ground surface around the sinkhole.

We can assume that a circular topographic feature must be at least 2 mm across at the scale of the final map in order to be represented on that map. Therefore, the minimum sinkhole width that may be expressed on a USGS 7.5-minute quadrangle map is

$$2 \text{ map mm} \cdot \frac{24{,}000 \text{ ground mm}}{1 \text{ map mm}} \cdot \frac{1 \text{ m}}{1000 \text{ mm}} = 48 \text{ ground m}$$

In contrast, the minimum sinkhole width which may be expressed by the CAGIS contours, which were prepared at a scale of 1:100, is

$$2 \text{ map mm} \cdot \frac{100 \text{ ground mm}}{1 \text{ map mm}} \cdot \frac{1 \text{ m}}{1000 \text{ mm}} = 0.2 \text{ ground m}$$

The 1:100 scale is probably larger than necessary for sinkhole mapping, since a depression only 20 cm across would not be mapped as a sinkhole.

Sinkholes can be expressed on topographic maps as either contour crenulations, like those seen in figure 3, or as sets of closed, hachured contours. The style of expression of a particular sinkhole is dependent on the slope of the ground around it. On a steep slope, where the contours are close together, one or more of the contours may intersect the sinkhole, producing contour crenulations. Where the ground is flat and horizontal, however, the contours will be much further apart than the width of any sinkhole. In that case, the sinkholes will be expressed as hachured contours.

Figure 4 illustrates the importance of contour interval in the expression on contour maps of sinkholes developed on flat ground. Sinkholes that have a depth of twice the contour interval will always contain at least one hachured contour, and will usually contain two. By extension, the minimum sinkhole depth, D, which will consistently contain a given number of contours, n, on a flat surface is

$$D = nC$$

where C is the contour interval.

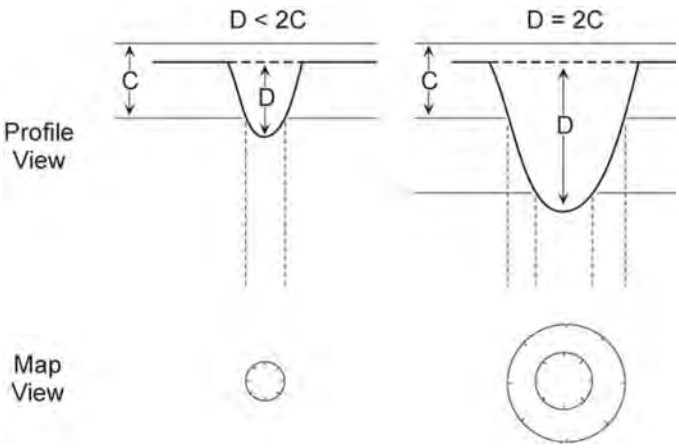


Figure 4. This figure shows the importance of sinkhole depth in the expression of that sinkhole on a contour map. The sinkhole on the right, which has a depth, D, equal to twice the contour interval, is better represented by the contours than the sinkhole on the left, which is much less deep. Contour interval, C, is held constant between the 2 drawings.

On a slope, however, the width of a sinkhole, rather than its depth, determines whether or not it will be expressed on a contour map (Fig. 5). Sinkholes that are twice as wide as the horizontal distance between contours will always be represented on a contour map by at least one crenulated contour, and will usually include two. The minimum sinkhole width, W, that will consistently be represented on a topographic map by a given number of crenulated contours, n, on a slope is

$$W = \frac{nC}{\tan \alpha}$$

where C is the contour interval and α is the angle that the slope forms with the horizontal.

Both these situations are present in the study area (Fig. 2). The shoulders of the ridges are relatively steep, and the sinkholes there tend to produce contour crenulations. On the other hand, the crests of the ridges are nearly horizontal, and the sinkholes near the crests are not evident from the contours because their depths are much less than the contour interval.

Thus, the expression of a sinkhole (or other circular topographic feature) on a contour map is dependent on the size (width and depth) of the sinkhole, the scale at which the map is prepared, the slope of the ground surface around the sinkhole, and the contour interval at which the topography is sampled. It is possible to determine, for any given location on a contour map, the minimum sinkhole size that will consistently be expressed by the contours. This minimum size will change over the extent of a contour map as the slope changes. Conversely, it is also possible to determine the scale and contour interval that will be necessary to consistently indicate the presence of sinkholes of a given minimum size.

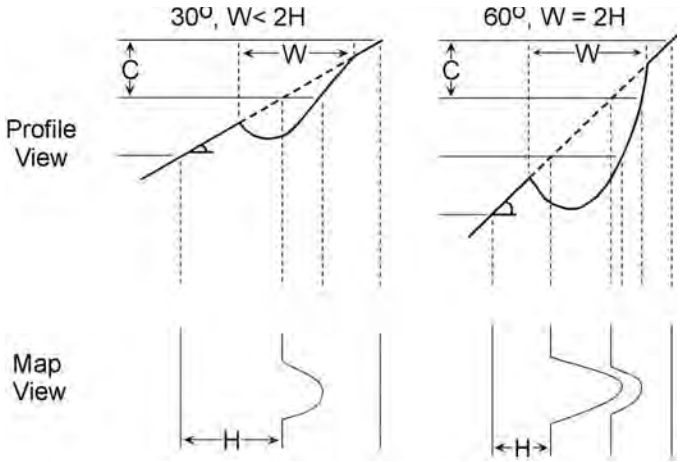


Figure 5. This figure shows the importance of slope in the expression of sinkholes of a given width on a contour map. Width, W, and contour interval, C, are held constant between the 2 drawings. Despite having the same width as the sinkhole on the right, the sinkhole on the left is represented by only one contour crenulation because the slope it is on is less steep than that on the right.

ACKNOWLEDGMENTS

Dennis Hull provided field sheets and other materials from the Ohio Geological Survey. John Coulter explained how the CAGIS topographic layer was made. Thomas Lowell suggested the idea of a perched water table and he, David Nash, and 2 anonymous reviewers commented on a draft of this paper.

REFERENCES

Dattillo, B. F., 1988, The Miamitown Shale: Stratigraphic and historic context (Upper Ordovician, Cincinnati, Ohio region), *in* Davis, R. A., & Cuffey, R. J., eds., Sampling the layer cake that isn't: The stratigraphy and paleontology of the type-Cincinnatian. Ohio Department of Natural Resources-Division of Geological Survey, Guidebook No. 13, p. 49-59.

Fenneman, N. M., 1916. Geology of Cincinnati and vicinity: Columbus, Ohio Department of Natural Resources-Division of Geological Survey, 207 p.

Ford, J. P., 1974, Bedrock geology of the Cincinnati West quadrangle and part of the Covington quadrangle, Hamilton County, Ohio: Ohio Department of Natural Resources-Division of Geological Survey, Report of Investigations No. 83, scale 1:24,000, 1 sheet.

Pavey, R. R., Hull, D. N., Brockman, C. S., Schumacher, G. A., Stith, D. A., Swinford, E. M., Sole, T. L., Vorbau, K. E., Kallini, K. D., Evans, E. E, Slucher, E. R., & Van Horn, R. G., 1999, Known and probable karst in Ohio: Ohio Department of Natural Resources-Division of Geological Survey, DCMS Map No. 24, scale 1:500,000, 1 sheet.

Swinford, E. M., & Ford, J. P., 1996. Bedrock geology of the Cincinnati West, Ohio quadrangle: Ohio Department of Natural Resources-Division of Geological Survey, Open-File Map BG-B5B5, scale 1:24,000, 1 sheet.

Swinford, E. M., Schumacher, G. A., Shrake, D. L., Larsen, G. E., & Slucher, E. R., 2001. Descriptions of geologic map units: A compendium to accompany Division of Geological Survey open-file bedrock geology maps: Ohio Department of Natural Resources-Division of Geological Survey Open-File Report 98-1.

Wells, T. L., 2000. County boundaries-statewide: ESRI ArcInfo GIS file. Ohio Department of Natural Resources, http://www.ohiodnr.com/gims/report.asp.

Charles A. Self and Carol A. Hill - How speleothems grow: An introduction to the ontogeny of cave minerals. *Journal of Cave and Karst Studies 65*(2): 130-151.

HOW SPELEOTHEMS GROW: AN INTRODUCTION TO THE ONTOGENY OF CAVE MINERALS

CHARLES A. SELF
4 Tyne Street, Bristol, BS2 9UA ENGLAND self@globalnet.co.uk
CAROL A. HILL
17 El Arco Drive, Albuquerque, NM 87123 USA carolannhill@aol.com

Speleothems are secondary mineral deposits whose growth in caves can be studied by mineralogic techniques. One of these techniques is the ontogeny of minerals, which is the study of individual crystals and their aggregates as physical bodies rather than as mineral species. Ontogeny of cave minerals as a scientific subject has been developed in Russia but is poorly understood in the West. This paper introduces the basic principles of this subject and explains a hierarchy scheme whereby mineral bodies can be studied as crystal individuals, aggregates *of individuals, associations of aggregates (termed* koras*), and as sequences of koras (*ensembles*).*

Speleothems are secondary mineral deposits that form in caves (Moore 1952). This distinguishes them from primary mineral bodies such as the bedrock that encloses the cave, mineral veins in the bedrock, and sediments accumulated in the cave. These primary minerals are important as sources of material from which new mineral bodies (speleothems) can grow in response to specific physical and chemical processes operating within the cave.

A *cave mineral* is a homogeneous solid having a definite chemical composition and a 3-D ordered atomic arrangement, growing naturally as a secondary mineral deposit within a cave. More than 250 cave minerals are known (Hill & Forti 1997) but only 3 (calcite, aragonite, and gypsum) can be considered common. The term *cave mineral* refers to the mineral species of a deposit, whereas speleothem terms (such as *stalactite*, *cave pearl*, etc.) are used to describe their morphology. Neither of these terminology systems defines the growth mechanisms of speleothems or their genetic history.

The study of the origin and evolution of mineral bodies is termed *genetic mineralogy* and includes nucleation, initiation (on a growth surface), development, alteration, and disintegration. Genetic mineralogy was formulated in Russia as a separate field of study within mineralogy during the 1920s (Fersman 1935). By the 1950s, Grigor'ev had divided genetic mineralogy into 2 separate branches: *ontogeny* and *phylogeny* (these terms are familiar from biology and are used in a broadly similar sense by Russian mineralogists). Ontogeny is the study of individual crystals (mineral *individuals*), how these crystals combine as *aggregates*, and their development as physical bodies. Phylogeny is the study of mineral species and their paragenesis (i.e., their association with contemporaneous mineral species). Phylogeny closely corresponds to the Western view of genetic mineralogy, whereas ontogeny (and even the term itself) is unfamiliar to most Western mineralogists. With the publication of 3 books devoted to the ontogeny of mineral veins and ore deposits (Grigor'ev 1961; Grigor'ev & Zhabin 1975; Zhabin 1979), this line of study has become a well-established science in Russia.

Although ontogeny as a subject has its origins in the Russian mining industry, caves prove to be ideal for ontogeny studies. There are few common mineral species, yet there is a great variety in the speleothem forms that these minerals can take. Also, the mineral-forming processes in caves are sufficiently slow in most cases to promote the development of clearly defined structures and textures. This has allowed far more complex mineral bodies to be studied in caves than has been possible in mines. The leading figure in this move to cave-based research was Stepanov (1965, 1970, 1971, 1973, 1997) of the Fersman Mineralogical Museum in Moscow. Other significant contributions have been made by Maleev (1971, 1972), Moroshkin (1976, 1986), Slyotov (1985), Korshunov and Shavrina (1998) and, most notably, by Maltsev (1989, 1993, 1996a, b, c; 1997a, b, c; 1998). This paper is an overview, based primarily on the ideas developed and promoted by the late Victor I. Stepanov, who died in 1988, and by Vladimir A. Maltsev.

In the West, comparatively little work has been done on the structure and texture of speleothems, and the papers that have been published (e.g., Folk 1965; Folk & Assereto 1976; Kendall 1977, 1985, 1993; Kendall & Broughton 1977, 1978; Broughton 1983a, b, c; Jones & Kahle 1993) have neither a unity of approach nor a common terminology. The Russians have a considerable advantage in this respect, and it is one of the main purposes of this paper to demonstrate the language and conceptual framework of ontogeny, so as to make Russian-authored work more accessible to Western scientists.

Ontogeny as a concept is important to mineralogy because the same mineral species can display different physical forms, depending on the specific environment in which growth occurs. In caves, it is possible to study the different forms of speleothems together with their depositional environments. This has resulted in a large number of mainly descriptive mineralogy texts, as documented in *Cave Minerals of the World* (Hill & Forti 1997). It is now necessary to study cave mineralogy from a genetic perspective. Ontogeny explains not only *how* speleothems grow, but *why* there are different speleothem types.

Copyright © 2003 by The National Speleological Society

The terminology of ontogeny can seem difficult to understand because it is unfamiliar to Western readers. Some terms are the same as in the West, some terms are new, while a third sort are familiar words that have been given a new and strictly limited sense. When the term *mineral* is used, it can mean several things. A mineral can be described by its chemical composition, its physical properties, or even its position in a classification scheme such as *A System of Mineralogy* (Dana 1837). Additionally, a view can be taken of minerals simply as material physical bodies. According to the thinking of Russian mineralogists, *minor mineral bodies* (MMBs) are physical mineral bodies that can be studied by mineralogic techniques, rather than by crystallographic or petrographic techniques. Specifically, MMBs have a "through" structure and/or texture and are a product of synchronous crystallization (or recrystallization) in some geometrically defined space. By *through* it is meant that the rules governing the growth of individual crystals also apply to aggregates composed of those individuals, and the rules that govern the growth of aggregates also apply to the higher hierarchical levels, so that a continuity of structure or texture can be traced all the way "through" the object. By *synchronous crystallization* it is meant that the crystallization (or recrystallization or destruction) of the individuals or aggregates that forms a MMB takes place at the same time over the entire body of the MMB.

The terms *structure* and *texture* have much tighter meanings in ontogeny than in western terminology, and cannot be used interchangeably or in a general sense. Structure describes the physical nature of crystal individuals and their bonding. Texture describes the geometric aspects of construction; i.e., the organization of mineral individuals or aggregates within a minor mineral body (Stepanov 1970, 1997). In the hierarchy of MMBs, structure and texture are contiguous regularities in that "through" structure links individuals with aggregates made of those individuals, while "through" texture can be traced from aggregates to the higher hierarchy levels. This continuity of structure and texture separates MMBs from more complex mineral bodies that have no such regularities. In the language of Russian mineralogy, such complex mineral bodies are termed *rocks* and are studied by petrographic techniques.

HIERARCHY OF MINOR MINERAL BODIES

The formulation by Stepanov (1970, 1997) of a specific and strictly defined term *texture* in mineralogy, separate from rock texture (as used in general geology), was a major advance that led directly to the development of the MMB concept. In turn, it became possible to see that MMBs could be organized into a hierarchical classification scheme. In mineral veins, only the first two hierarchy levels can easily be identified, but in caves 4 levels are discernable. This larger hierarchy–evident in the works of Stepanov (1971, 1997)–was outlined by Maltsev (1996b, 1997b). In this paper, we discuss the constituent parts of this hierarchy in more detail. This is not a complete analysis, and a fuller treatment is planned for sometime in the future.

Minor mineral bodies are classified according to their complexity of structure and texture. *Level* is used when MMBs of one level are built from MMBs of a previous level or levels. *Order* is used as a subdivision within a level and shows the level of complexity of the MMBs. Second-order MMBs are built from MMBs of the previous level, but in a more complicated manner than first-order MMBs. For example, multiaggregates (level 2, second order) are not built from aggregates (level 2, first order); they are built from individuals (level 1, either first or second order), but in a more complicated manner.

The hierarchy scheme of MMBs is *not* the same as the classification of speleothems into types and subtypes (e.g., Hill & Forti 1997). "Speleothem" is a descriptive term and can only be used to indicate the morphology of a MMB. In ontogeny, speleothems can appear on different organizational levels; i.e., they can be composed of individual crystals, crystal aggregates, or groups of aggregates. For example, selenite needles are individuals, flowstones and coralloids are both aggregates, but stalactites are multiaggregates.

(0) ZERO LEVEL: Subindividuals. The fundamental building block for all minor mineral bodies is the mineral individual (level 1). Simple (first-order) individuals are single crystals having no structure other than a crystallographic network. More complex (second-order) individuals, on the other hand, are composed of a number of different crystalline units known as *subindividuals*. Subindividuals also have no structure except for their crystallographic network, but they are at least partly separated by free space or a line of dislocation from neighboring crystal blocks. Inasmuch as subindividuals do not exist independently from each other, they are ascribed to a hypothetical "zero level" in the MMB hierarchy. A zero level is needed because complex (second-order) MMBs of the first level must be formed from MMBs of a previous level, not from first-order MMBs of the same level. Subindividuals (in the sense used here) are termed *crystallites* by some mineralogists, but in ontogeny the preferred use of this term is for the initial stage of crystallization of mineral individuals.

(1) FIRST LEVEL: Mineral Individuals. Individuals are mineral bodies that grow from a single crystal nucleus or embryo (crystallite), during one phase of crystallization, and which have a "through" crystallographic structure (Godovikov *et al.* 1989). Crystallites are minute crystal grains that represent the initial stage of crystallization, and which act as seeds for further crystal growth (Fig. 1). When crystallites are widely separated from each other, they grow freely into separate first-level mineral individuals. But when they grow close together, there is competition for growth space and a second-level MMB (a mineral *aggregate*) is formed. It should be emphasized that mineral individuals are *not* speleothems (except in a few special cases). They are the building blocks from which speleothems are made.

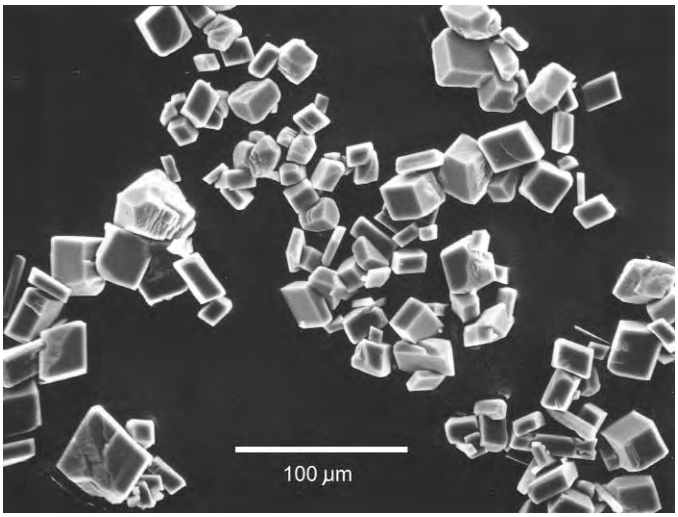


Figure 1. Calcite crystallites grown in the laboratory from a supersaturated solution by the degassing of CO_2. SEM photomicrograph by Art Palmer.

(1.1) First-Order Individuals. In the simplest case, mineral individuals are single crystals having no other structure except a standard crystallographic network, which is determined by the mineral species itself. First-order individuals can be described by their isometric, columnar, acicular, filamentary, or tabular habit, or by their euhedral, subhedral, or anhedral form. First-order individuals can, in some cases, be considered speleothems; for example, calcite, gypsum or fluorite crystals that have grown alone and independently from a hydrothermal water (Fig. 2A: p. 145) or subaerial environment (Fig. 2B: p. 145).

(1.2) Second-Order Individuals. Second-order individuals are single crystals that subdivide or split into a number of subindividuals, single crystals that have their growth inhibited on some crystal faces or edges, single crystals that incorporate crystallites into their crystal lattice, or single crystals that are twinned (Shafranovskiy 1961). In some cases second-order individuals can look as if there is a co-growth of several crystals, but this is an illusion. Subindividuals of second-order individuals are not separate from each other. They grow from the same nucleus and have a joined crystallographic network (Fig. 3: p. 145). Second-order individuals grow in response to certain environmental conditions, particularly oversaturation – a common occurrence in caves due both to CO_2 loss and evaporation of thin films. Many of the different subdivisions in this category depend on the degree of separation between subindividuals (Godovikov *et al.* 1989).

(1.2.1) Split Crystals. When a crystal individual splits apart during growth, it forms a number of subindividuals, a sheaf-like structure, or in its final form, a spherulitic structure (Fig. 4). Different minerals have a different "splitting ability" depending on their crystal structure. For example, aragonite has a higher splitting ability than calcite under usual cave conditions, and therefore it is almost always found in caves as split acicular crystals. Splitting in also quite common in calcite, but

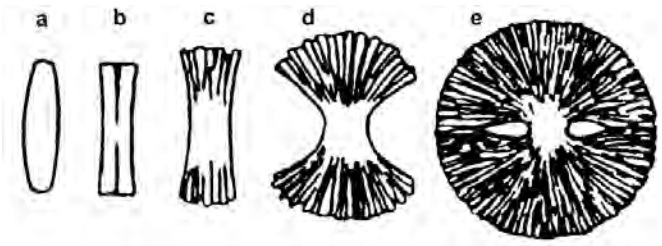


Figure 4. Drawing of successive stages of splitting during crystal growth: a = no splitting, b and c = simple splitting, d = "sheaf" structure, e = spherulite. From Grigor'ev (1961).

this splitting is not easily seen with the naked eye. Gypsum needs a rather high oversaturation to become split, but splitting can occur in some cases (e.g., growth from a porous sediment). Splitting may be due to a crystal receiving extra molecules in its layers (*mechanical splitting*), or to when certain ions (e.g., Mg as well as Ca) are present in the parent solution (*chemical splitting*) (Grigor'ev 1961). According to the level of supersaturation or impurity concentration (which can change during growth), splitting will take on different grades, which results in a number of subforms for split crystals (Fig. 5: p. 146).

(1.2.1A) Spherulites. Spherulites are second-order individuals having either a radial or curving radial structure due to the splitting of crystals. If growing in free space, they are spherical in form (Fig. 6: p. 145); if nucleated on a substrate, they grow as hemispheres (see Fig. 9a). Spherulites are composed of straight subindividuals, but often the subindividuals themselves continue to split. Constraints of growth space around the central axis of the crystal then direct this splitting outward to produce a curving radial structure (seen in the "twin leaf" splitting of Fig. 5c: p. 146). The shape of such spherulites is a property of both the crystal nucleus and its split branches. If part of the growth surface becomes mechanically blocked, the unobstructed "rays" will continue their growth in the form of a new spherulite (Fig. 7). This composite body is still a mineral individual, not an aggregate. Spherulites are widespread in caves as components from which many speleothems are built.

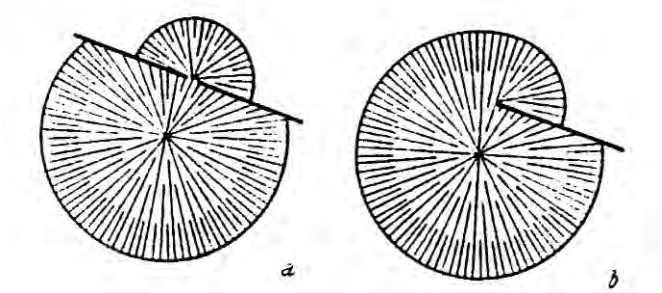


Figure 7. Spherulites encountering obstacles: (a) when a subindividual passes through a hole, it spreads out and grows into a new spherulite, and (b) when a spherulite is only partially obstructed, growth "goes around" the obstacle. From Maleev (1972).

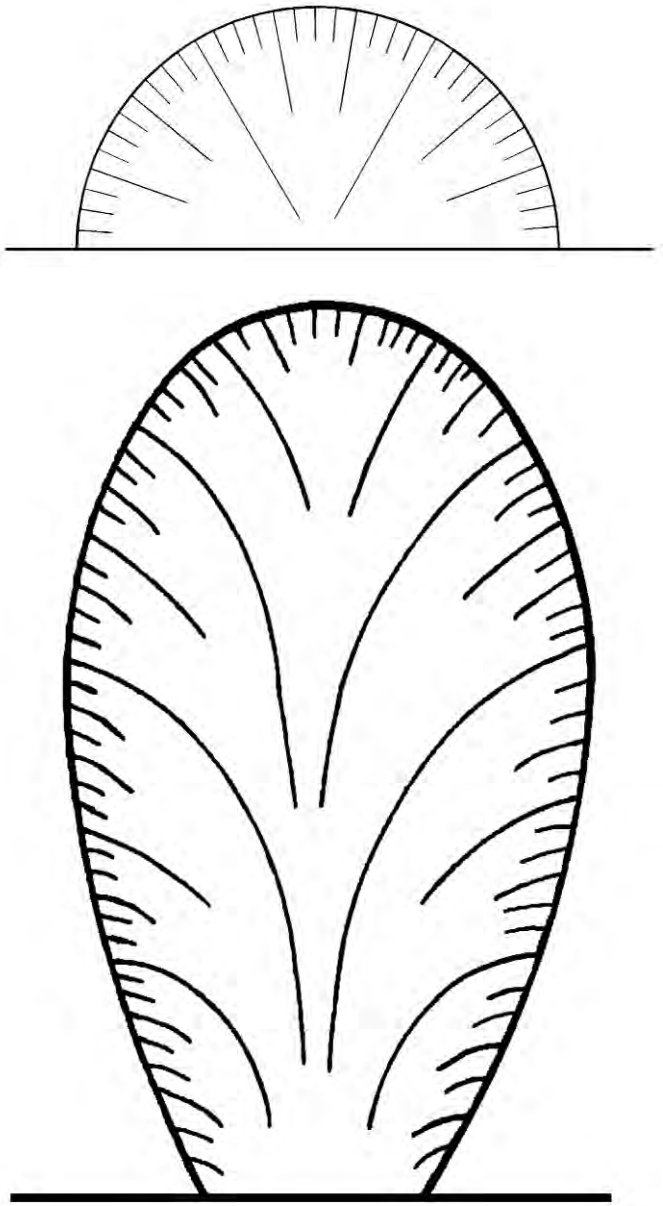


Figure 9. Comparison of spherulites and spheroidalites. (a - top) Spherulites are composed of straight subindividuals. If splitting occurs mostly at an early growth stage, a radial structure is produced. If there is continuous splitting, then structural lines will curve away from the central axis because of intense crowding of subindividuals (e.g., as in Fig. 5c). (b - bottom) Spheroidalites are composed of curved subindividuals and display asymmetric growth and growth layers of unequal thickness.

(1.2.1B) Spherulite Bunches. Spherulite bunches may be thought of as three-dimensional sectors of spherulites (their incomplete development being due to a strongly directional supply scheme). The subindividuals growing from a single nucleus form a stalk (a well connected bunch) or a splay of crystals (a poorly connected bunch). This shape depends on the growth speed of crystals. Slow growth results in well connected bunches, fast growth in poorly connected splaying bunches. Examples of speleothems built from spherulite bunches are most kinds of helictites and some kinds of anthodites and frostwork. Spathites and beaded helictites are sequences of spherulite bunch splays, with new bunches growing from subindividual "rays" of the previous bunch in the manner of a daisy chain (Fig. 8A, B: p. 146). If more than one "ray" becomes a focus of new growth, then branching will occur.

(1.2.1C) Discospherulites. Discospherulites are spherulites that have preferred crystal growth in two, rather than three, dimensions. Some kinds of cave rafts display discospherulitic growth, where the surface of a cave pool confines crystal growth to a plane. However, the supersaturation grade must be high enough to allow for split growth, or other types of rafts will form.

(1.2.1D) Spheroidalites. Spheroidalites are spherulites with nonsymmetrical structure (Godovikov *et al.* 1989). They have elongated and curved subindividuals, whereas spherulites have straight subindividuals (Fig. 9). Asymmetric growth of the fibers of a spheroidalite causes angular unconformities between the fiber orientations in different growth zones. Because of this asymmetry, growth layers in spheroidalites are of unequal thickness, whereas growth layers in a spherulite are always of the same thickness and display spherical concentric zonality. Most coralloids display spheroidalitic growth.

(1.2.1E) Spherocrystals. Spherocrystals are chemically split second-order individuals, so perfectly split that boundaries between subindividuals are at a molecular level, and physical properties (such as cleavage) become generalized across the whole crystal (Shubnikov 1935). This results in growth surfaces that are smooth and bright in appearance (e.g., botryoidal malachite or chalcedony; Fig. 10: p. 147). Although spherocrystals are composed of subindividuals, the separate fibers are not visible even under microscopic examination. However under crossed nicols (polarizers), spherocrystals display a "Maltese cross" extinction.

(1.2.2) Skeleton Crystals. Skeleton crystals are second-order individuals where preferred growth occurs along crystal edges or corners rather than on crystal faces (Fig. 11: p. 147). Such a growth pattern makes these crystals appear "lacy" or empty inside (e.g., "hopper" crystals). Skeleton crystals form where the supersaturation grade is high enough to promote rapid growth, but where the supply of material is insufficient to allow massive growth. For carbonate speleothems, it is possible to get skeleton growth without a high grade of supersaturation if CO_2 loss is oscillatory or periodic–for example, the actively dripping tips of stalactites (see Fig. 34: p. 150).

(1.2.3) Twin Crystals. A twin crystal begins as a simple individual, but at some point it continues its growth as two (or more) parts reflected across some definite plane called a *twin plane*. One part continues the "parent" crystallographic network, while the other(s) grows from the twin plane(s) with a reflected crystallographic network. Twin crystals typical of a cave environment are selenite needles (Fig. 12: p. 147) and the

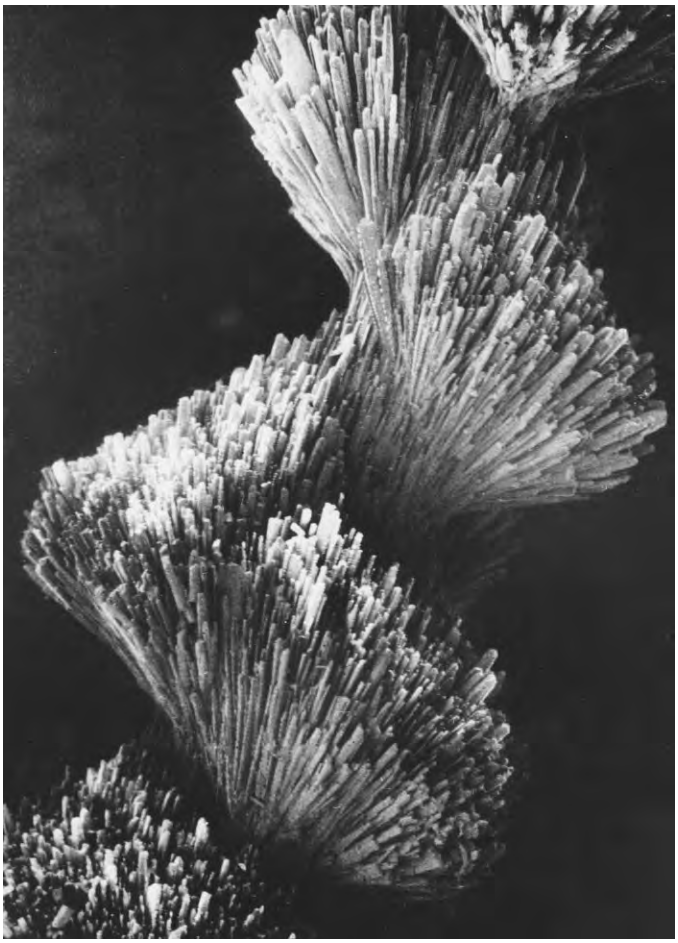


Figure 13. Scanning electron micrograph of an aragonite helictite from a cave in France, diameter 2 mm. Note how the split crystals are symmetrically screwed around the axis of the helictite. Photo by Patrick Cabrol.

twinned branches of gypsum chandeliers. (Note: There are other types of twins that look like an intergrowth of two or more individuals, but even these are thought to begin from a single nucleus.)

(1.2.4) Screw Crystals. Screw crystals are the result of screw dislocations in the crystallographic network where molecular layers have small regular rotations along a crystallographic plane so as to produce spiral layers (Fig. 13). In screw crystals, subindividuals cannot be separated because the dislocation is continuous (rotational around the greatest growth vector), and each molecular layer is a new crystal block fractionally rotated on the previous molecular layer. Screw dislocations are most common among filamentary crystals (e.g., gypsum cotton and selenite needles), but they can also occur in some types of helictite.

(1.2.5) Block Crystals. Block crystals (sometimes called "mosaic growth") are crystals whose separate parts (known as *blocks*) are slightly rotated in relation to each other (Grigor'ev 1961) (Fig. 14). When spatial nucleation continues around a growing crystal, crystallites of several-molecule size can become closely aligned to the growing crystal by electrostatic forces (Jushkin 1973). The crystallites become incorporated into the main crystal, with the crystallographic network of one block passing continuously into that of the next through a zone of dislocation. Block crystal growth is common for vein minerals such as pyrite and for subaquatic hydrothermal speleothems. Such mosaic growth has also been found in calcite and gypsum speleothems that have precipitated under normal cave conditions (B. Onac, pers. comm., 2002).

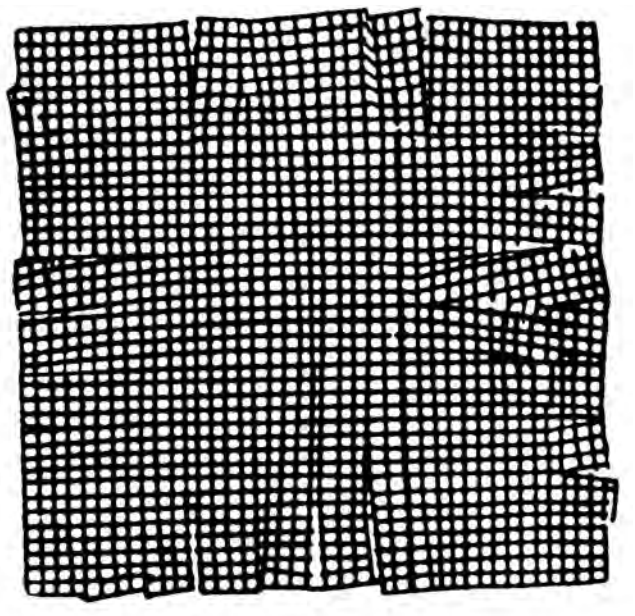


Figure 14. Schematic structure of a block crystal. The lattice of one "block" passes continuously into the lattice of another through a zone of dislocation. From Grigor'ev (1961).

(1.2.6) Complex Individuals. In some cases second-order individuals display two or more structural features at the same time. Dendrites display a branching pattern due to both crystal splitting and skeletonization (i.e., they are composite split-skeleton crystals; Fig. 15). In caves, dendritic crystals (e.g., frostwork and cave coral) usually form in the high evaporation conditions of a capillary film environment. Selenite needles are also complex individuals, inasmuch as they are skeletonized, twinned, and split–all at the same time (Maltsev 1996c).

(2) SECOND LEVEL: Mineral Aggregates. Mineral individuals very seldom occur singly; they grow multiply over a substrate surface as mineral *aggregates*. Aggregates are much more than simply a group of individuals of the same mineral species growing together. Interaction between individuals directly affects and limits the growth of each crystal. During such "group" or "common" growth, there is *competition* between the mineral individuals constituting the aggregate. Most speleothems are mineral aggregates.



Figure 15. Longitudinal (a - left) and transverse (b - right) sections of dendritic structure in an aragonite helictite, Cave of the Winds, Colorado, 20x, viewed in cross-polarized light. The "branches" are due to crystal splitting and skeletonization. Note the roughly triangular central feeding channel, which shows that this helictite is an aggregate of three crystals. Photos by George Moore.

Most aggregates form where growing individuals compete for space by physically contacting one another. In such a situation, contact faces (also called *induction surfaces*) develop between neighboring individuals, leaving a group growth front comprised of the crystallographic terminations of many individuals (Fig. 16: p. 147). However, aggregates do not necessarily have to be in direct physical contact for competition to occur. An example of indirect competition for the supply solution is when growth is in a plastic substrate such as porous clay, where interaction between crystals is due to the closure of feeding pores in the clay as a result of crystallization pressure. When growth is in a capillary film environment, there is competition for the loss of solvent molecules and interaction is by convection of water vapor and CO_2 between individuals. The mineral individuals constituting an aggregate have contact faces when they are in direct competition, but display true crystal faces when they are in indirect competition.

Competitive growth on a substrate surface normally leads to a reduction in the number of individuals constituting the aggregate, a situation called *selection*. The main selection mechanisms are:

(1) *Geometric selection*: The mineral individual whose greatest growth vector during competitive growth is best aligned for mass-transfer with the environment is the one that will continue its growth at the expense of neighboring individuals of other orientations.

(2) *Substrate selection*: The mineral individual (or mineral aggregate) growing from a convex substrate protrusion during competitive growth will continue its growth at the expense of its neighbors growing from flat or concave surfaces.

(3) *Primogeniture selection*: The mineral individual (or mineral aggregate) that nucleates on a substrate first has a better chance of continued growth than one that nucleates later.

(4) *Random selection*: In some cases, a mineral individual (or mineral aggregate) experiences a cessation of growth when it has no obvious natural disadvantage compared to its neighbors. Such selection is unpredictable.

The most influential process during the early stages of crystal growth is geometric selection. The crucial elements of this selection process are: (1) initiation of separate centers of crystallite growth; (2) the beginning of competition of these crystal individuals for growth space; (3) selection and a reduction in the number of competing individuals according to a geometric rule; and (4) continued growth with no further selection because the geometric rule forbids it (Fig. 17). There are several geometric rules for selection, but perpendicularity to the substrate is the most common. This rule applies to most mineral veins and to many common varieties of speleothems (e.g., dripstone, flowstone, pool spar).

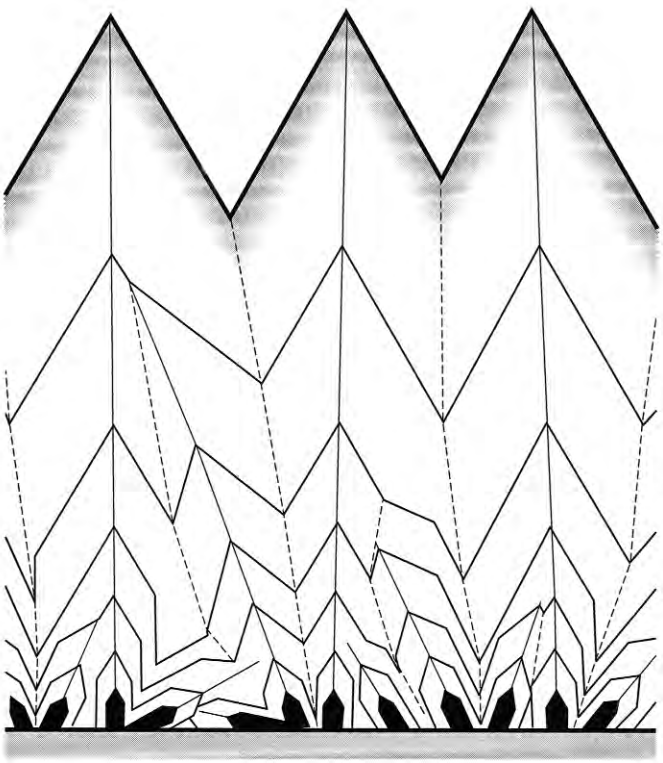


Figure 17. Geometric selection on a flat growth surface. From Kantor (1997).

(2.1) First-Order Aggregates. In ontogeny, first-order aggregates are simply termed *aggregates*, while second-order aggregates are termed *multiaggregates*. For cave minerals, aggregates can be defined as: "intergrowths or co-growths of individuals (either first- or second-order) of the same mineral species, which develop simultaneously on a common growth surface and which possess a homogeneous texture." (Note: aggregates can also form in free space by crystallization from viscous solutions and melts, but this is not relevant to speleothems in caves.) It is important to stress here that only simultaneous growth of similar individuals of the same mineral species can form first-order aggregates. Most speleothems are aggregates. Aggregates can be subdivided according to the different textures that are produced by competitive growth.

(2.1.1) Parallel-Columnar Aggregates. Examples of parallel-columnar texture, sometimes known in the West as "palisade fabric" (Folk 1965), dominate the collections of amateur mineralogists. Mostly these are groups of crystals with well-formed terminations, taken from vugs in simple mineral veins. If visible to the naked eye, these crystal aggregates are called *druses*, where each crystal is a mineral individual within a composite aggregate of crystals. These individuals only have crystallographic faces on their end terminations, with their sides being contact surfaces with other individuals (Fig. 17). Each druse crystal has had to compete with other individuals, and is a survivor of geometric selection at the aggregate druse growth front.

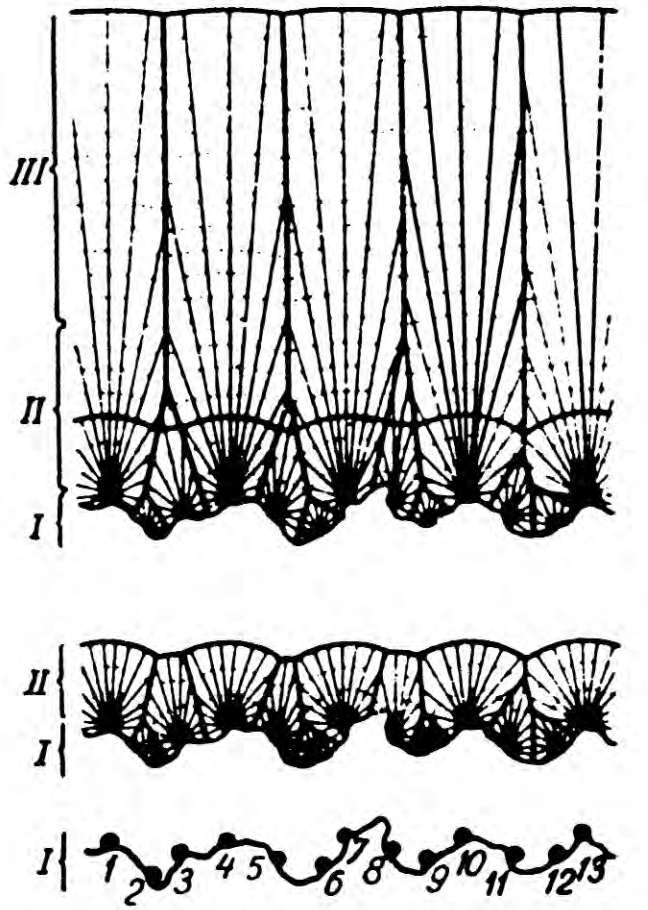


Figure 19. Diagram showing the group growth of spherulites on an irregular substrate: I) Growth of discrete spherulites; II) substrate selection between competing spherulite individuals; and III) geometric selection between competing subindividual spherulite rays. From Grigor'ev (1961).

Parallel-columnar aggregates grow by geometric selection perpendicular to nominally flat substrates, as described above and as shown in Figure 18 (p. 147). But in the natural world the substrate is seldom perfectly flat, and so a more complicated selection scheme operates. Geometric selection at first favors growth perpendicular to each irregularity of the substrate, but as the individuals reduce in number and increase in size, the most successful are those oriented toward the bulk volume of the solution. Where there are major irregularities of the substrate (compared with the size of the growing crystals), substrate selection also operates, and crystals growing in hollows become entrapped in the bulk growth of those growing from ledges and protrusions. The overall effect is a leveling out of the growth front and a progressive trend toward more closely parallel growth of the surviving crystals. When the individuals are themselves split, geometric selection determines which subindividuals survive at the growth front while sub-

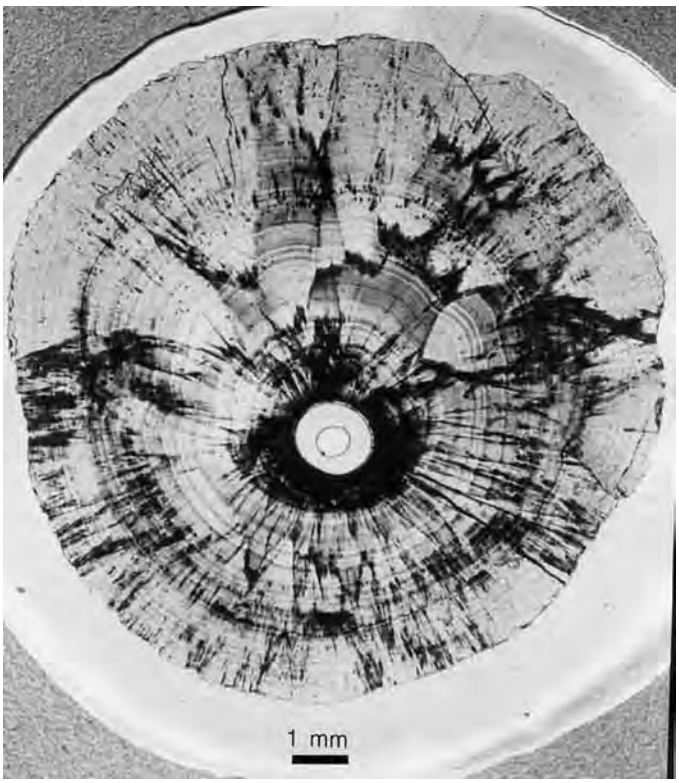


Figure 20. Cross-section of a cave pearl (a core spherulite) showing a radial arrangement of individuals due to geometric selection. Photo by Paolo Forti.

strate selection determines from which individuals they derive (Fig. 19).

(2.1.2) Spherulitic Aggregates. Spherulitic texture is a variant of parallel-columnar texture whereby the substrate, instead of being flat or slightly irregular, is sharply convex. Geometric selection produces crystals growing perpendicular to the substrate, but the curvature of this substrate produces a radiating fan of crystals rather than a roughly parallel growth of crystals. It is important to distinguish between spherulitic *structure* in mineral individuals (which is the result of crystal splitting) and spherulitic *texture* in mineral aggregates (which is the result of geometric selection). These are very different effects, and the term "spherulitic" simply refers to the external form of these quite different minor mineral bodies. Of the subtypes of spherulitic aggregates, the following two are particularly important:

(2.1.2A) Core Spherulites. Core spherulites are aggregates of mineral individuals growing in a radial manner away from a growth center (Godovikov *et al.* 1989). This radial arrangement is due to geometric selection between multiple individuals where only those crystals survive whose direction of maximum growth coincides with the radius of the core nucleus (i.e, a core spherulite is a spherical aggregate around a nucleus). A prime example is a cave pearl with a grain of sand at its center (Fig. 20).

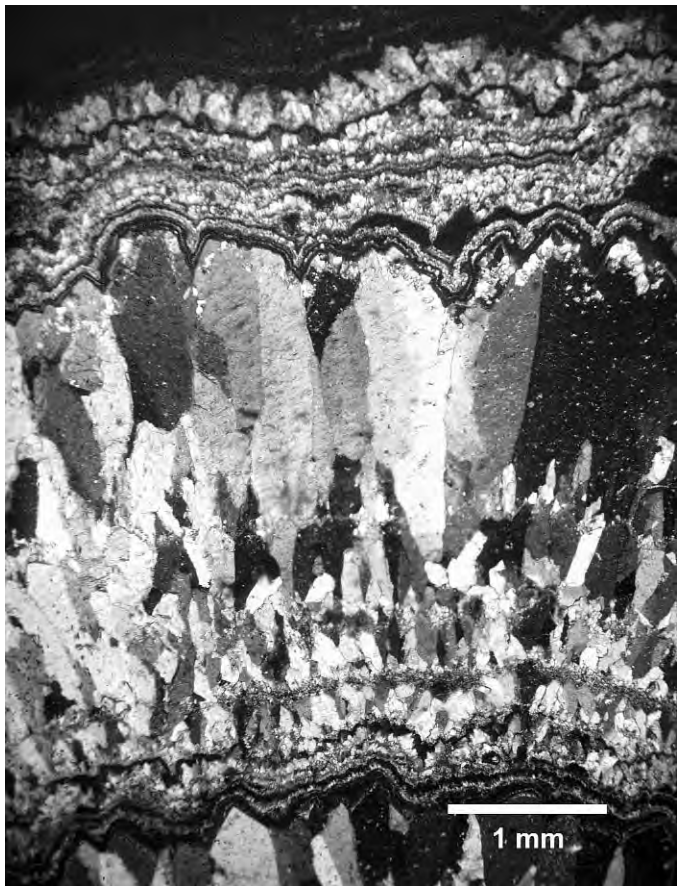


Figure 21. Polarized thin section of spherulitic aggregate texture in a calcite flowstone, Wind Cave, South Dakota. Note the repeated episodes of geometric selection after growth interruptions. Photo by Peg Palmer.

(2.1.2B) Irregular Spherulites. If the substrate is irregular, geometric selection causes a spherulitic texture to appear in the aggregate around each substrate protrusion. Such spherulitic crusts can develop in a subaqueous environment (e.g., pool spar) or in a subaerial environment (e.g., flowstone). If the supply of material is by diffusion of solute or by laminar flow of the feeding solution, the thickening crust will trend toward parallel-columnar growth (Fig. 21). This is normal in the case of pool spar and for flowstone deposited on very gentle slopes. On steeper slopes, turbulent flow promotes rapid growth on substrate protrusions and the development of microgours. On steep walls, the seepage water collects into rivulets that (because of an increased feeding rate) produce a locally thicker crust or even draperies.

(2.1.3) Radial-Fibrous Aggregates. Radial-fibrous aggregates are an important variation on both parallel-columnar and spherulitic aggregates where some (or all) of the individuals have begun to split. They make up the texture of many speleothem types, including flowstone and dripstone. Commonly they are interlayered with parallel-columnar (or spherulitic) aggregate crystals in these speleothems (Folk & Assereto 1976; Kendall & Broughton 1977, 1978; Kendall

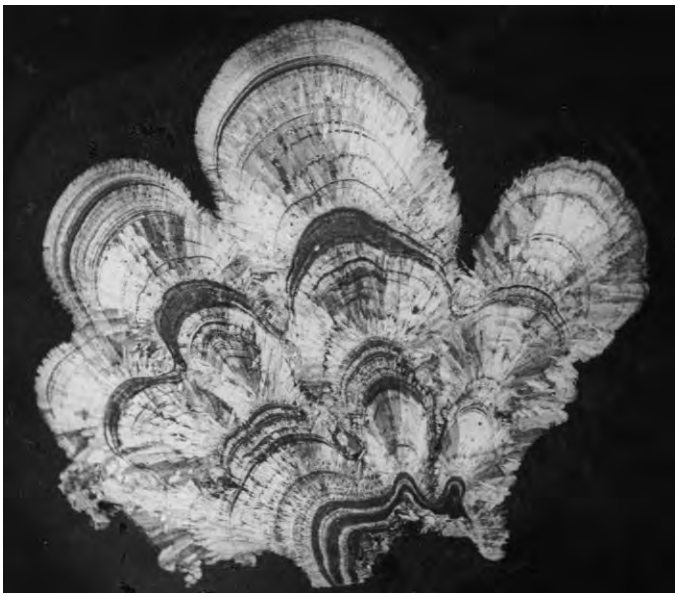


Figure 23. An early stage of branching of coralloids showing their subindividual structure in a thin-section photo (crossed polarizers, 24 mm across). Calcite cave coral from Soldiers Cave, California. Photo by George Moore.

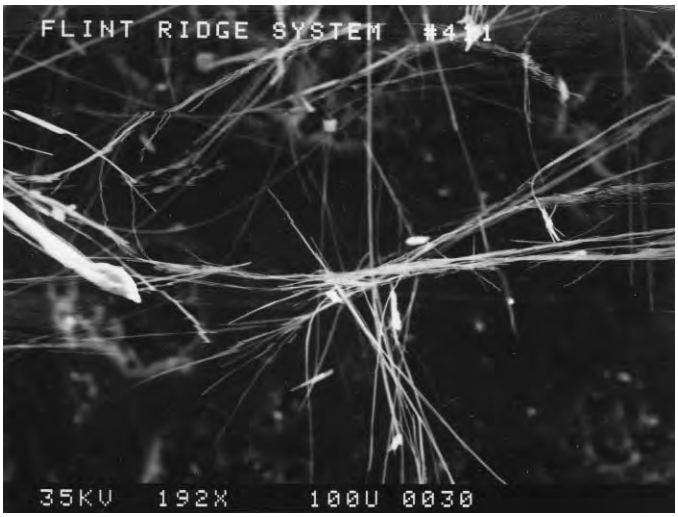


Figure 27. Scanning electron microscope image of individual filamentary crystals of cave cotton, Mammoth Cave, Kentucky. Photo by Will White.

1985) (Fig. 22: p. 148). The change to radial-fibrous texture is due to a decrease in solution supply, the mass-transfer of solutions changing from gravitational flow to a gravitation-influenced capillary thin-film flow. If the solution supply decreases further, radial-fibrous texture may lead to interruptions in growth.

(2.1.4) Branching Aggregates. A great variety of branching aggregates grow by evaporation in a capillary film environment. These include corallites, crystallictites, and many intermediate forms. Branching aggregates are aggregates of crystals displaying a compound branching form (Fig. 23). They are not the same as dendritic individuals (section 1.2.6), which display a branching pattern due to the splitting and skeletonization of crystals (compare Figs. 15 and 24, p. 148).

The competition in the case of branching aggregates is indirect and includes competition between nearby branches on the same bush. Molecules of solvent (water vapor and CO_2) leaving one branch adhere to neighboring branches, thus slowing their growth. For this reason, competing branches *never* touch each other and the strongest growth is always out towards the open void of the cave (Fig. 24: p. 148). For a single aggregate, there is competition between individuals but not selection. The situation changes when these aggregates grow together in close proximity. Substrate selection very strongly favors growth from protrusions (Fig. 25: p. 148), and aggregates situated there develop rapidly (Slyotov 1985). Less favorably situated aggregates find it increasingly difficult to lose solvent molecules, and their growth is suppressed or distorted away from nearby large bushes. The effect of substrate selection is very much stronger in the capillary film environment than in the subaqueous environment because of this need to lose solvent molecules. If solvent is not lost, the capillary film cannot supply new solution (and new solute) and the aggregate cannot grow.

(2.1.4A) Corallites. Corallites are aggregates composed of spheroidalite individuals and so have a rounded form and a branching pattern due to the uneven growth and bent splitting of spheroidalites (Fig. 23). They are the product of thin capillary water films that have a condensation origin or appear because of the slow spread of water due to very weak trickling. Prime examples of corallites are thin-film-generated varieties of coralloids (popcorn and cave coral). Note that *corallite* is an ontogeny term and should not be confused with the speleothem type "coralloid" of Hill & Forti (1997).

(2.1.4B) Crystallictites. Crystallictites are branching aggregates built from faced crystals (Serban *et al*. 1961; Moroshkin 1976). They form in a capillary film environment as an analog of corallites, but without the splitting of individuals that is characteristic of corallites. The branching of crystallictites is usually noncrystallographic–it is due to branching of the aggregates themselves. However, a full range of intermediate forms exists between corallites and crystallictites (Fig. 26: p. 148), displaying different degrees of crystal splitting. Also, there can be interconversions between corallites and crystallictites. Because the type and propensity for crystal splitting depends on mineral species, crystallictite aggregates are typical for minerals such as gypsum and aragonite, whereas corallite aggregates are more characteristic of calcite. Aragonite frostwork is a prime example of a crystallictite (Fig. 24: p. 148).

(2.1.5) Fibrous Aggregates. Fibrous aggregates are built from filamentary individuals (Fig. 27**),** and grow from a porous substrate that may be solid (such as the cave walls or breakdown blocks within a cave) or plastic (such as cave sediments, particularly clays). In the West, fibrous aggregates

have many fanciful names such as "hair", "cotton" (Fig. 28: p. 149), "beards", "flowers", and "needles" (Hill & Forti 1997), but in Russia they are known collectively as "antholites" (not to be confused with the speleothem type "anthodite"). Fibrous aggregates are always composed of soluble minerals such as gypsum, epsomite, mirabilite, or halite. The reason why no calcite "flowers" and "needles" exist is because carbonate solutions simply do not carry enough solute.

The growth mechanism of fibrous aggregates is purely by evaporation of the solvent and takes place close to the ends of pores in the substrate. The unique feature of fibrous aggregates is that they grow from the base, with new growth pushing the previous growth out into the cave void (Fig. 29: p. 149). This growth mechanism means that selection between individuals is impossible and there is only competition between pores. For growth from a solid substrate, the pores feeding the center of an aggregate often have a stronger supply than those feeding the periphery, leading to different growth rates. For well connected aggregates such as gypsum flowers, this causes the aggregate to burst into separate curving "petals". For loosely connected aggregates such as hair, the fibers may become tangled and form beards.

For growth from a plastic substrate such as cave clay, competition between pores leads to a very different situation. The capillary pressure and the crystallization pressure together press the substrate, causing only certain favorable pores to remain open while other surrounding pores collapse. This is a very specific type of selection for plastic substrates and explains the wide separation between individuals (e.g., selenite needles) in this environment compared with growth from a solid substrate (e.g., beards).

(2.1.6) Interactive Aggregates. The growth of any aggregate depends on environmental factors that are local to the growth front of the individuals of which it is composed. In most cases, these environmental factors are identical to those affecting other nearby aggregates, so we can talk of a *parent environment* controlling mineral growth over a significant part of a cave. However, not all mineral aggregates are passive products of a parent crystallization environment. There is a class of minor mineral bodies, called *interactive aggregates*, which grow under local conditions that the MMB itself creates. These local conditions are significantly different from the general environmental conditions of the crystallization space as a whole. In the case of helictites (and shields), a high capillary pressure is maintained in their central channels, which results in solute deposition when the feeding solution loses pressure in the open void of the cave. For this reason, helictites grow without regard to the force of gravity or the direction best suited for evaporation in the capillary film environment.

There are many different types of eccentric MMBs that are included in the speleothem term "helictite" (Hill & Forti 1997). In a detailed study (Slyotov 1985), one particularly common type was shown to be a parallel co-growth of spherulite bunches, tightly bonded and growing in strictly defined sectors (Figs. 15 and 30, p. 149). A fine central channel supplies a local capillary film spot on the helictite's tip, where there is competition for solute between the sectors but *not* selection. Small local variations affecting the wetted spot promote different growth rates between the sectors, but the sector boundaries are strictly maintained. This results in sudden changes in growth direction for the aggregate as a whole (so helictites can twist or turn in any direction). Moreover these variations are unique to each helictite; when groups of ordinary calcite helictites were studied by Moore (1954, 1999), their growth-front azimuths proved to be random.

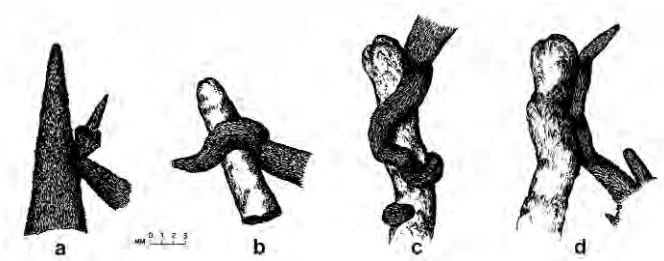


Figure 31. The "behavior" of helictites when meeting an obstacle: (a) reflection, (b) rounding, (c) sliding without separation, and (d) sliding with separation. From Slyotov (1985).

Interactive aggregates have a most peculiar additional property termed *behavior* when interacting with obstacles. According to Slyotov (1985), when a growing helictite makes a perpendicular impact on an obstacle, growth is stopped. If the approach is oblique, the aggregate may show reflection, rounding, or adherence to the obstacle's surface (Fig. 31). The reason for this may be found in a property of spherulite individuals, whereby when their growth surface is mechanically blocked (see section 1.2.1A, Fig. 7), the unobstructed rays of the spherulite serve as the focus for new growth. Exactly the same thing happens for spherulite bunches. In the case of helictites, changes in the growth of the bunch impacting an obstacle causes a change in growth direction for the aggregate as a whole.

For most aggregates, interaction only occurs between individuals (in the form of competition). For branching aggregates, there is some limited interaction with obstacles in that mineral growth slows down and stops before impact (due to an inability to lose solvent molecules). Interactive aggregates, however, are fully interactive with the general environment in which they grow, because their growth processes are not directly controlled by that environment.

(2.1.7) Other Aggregates. In addition to the main aggregate types described above, we will briefly mention some others. *Granular aggregates* form when a mineral species (or mineral habit) has similar growth speeds in different directions, or when frequent interruptions of growth combine with recrystallization or new nucleation to subvert the role of geometric selection. Granular aggregates commonly occur during bulk crystallization from viscous solutions and melts, whereas

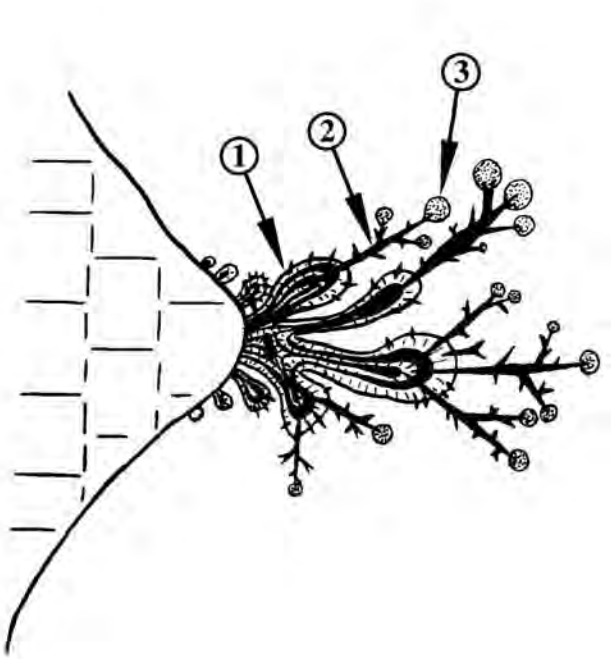


Figure 32. Drawing of a multicorallite bush: (1) calcite popcorn, (2) aragonite crystallictite needle, (3) hydromagnesite efflorescence. By Vladimir Maltsev, from an unpublished manuscript.

in caves with seasonal humidity cycles, they can be found in the evaporative deposition of soluble species such as gypsum.

Ice is a common cave mineral, forming many of the aggregate types described above. Ice can also form *sublimation aggregates*, which are built from skeleton crystals but branched in a special manner. *Plastic-substrate aggregates* of ice or gypsum have special textures and grow deep within clay sediments. *Monocrystalline aggregates* are the result of total recrystallization into one single individual; flaws within the new individual often retain traces of the previous aggregate texture. *Hybrid aggregates* have textures intermediate between the main types described above; they will be discussed later (section 2.2.3).

In all the above examples, crystallization takes place on an inert substrate. For *controlled-nucleation aggregates*, the orientation of individuals is predetermined. One example is autoepitaxial growth on a textured substrate (e.g., gypsum growing from gypsum crystals in the wall rock, typical for the caves of Podolia, Ukraine). Another is the growth of some varieties of cave rafts, where individuals align perpendicular to the surface because of electric forces associated with surface tension. This category is not so important for cave mineralogy, but growth on textured substrates is very important in ore mineralogy.

(2.2) Multiaggregates. *Multiaggregate* is a new category in minor mineral body hierarchy. It was first introduced by Maltsev (1996b), although the concept was originally suggested by Stepanov (1973) as "typical paragenetic pairs of aggregates." Multiaggregates are an intergrowth or co-growth of different types of aggregates that form simultaneously and syngenetically in the same crystallization environment. They are either polymineral or polytextural, as compared to simple aggregates, which are always monomineral and texturally homogeneous.

(2.2.1) Polymineral Multiaggregates. A typical multicorallite is a branching MMB that is formed of calcite popcorn from which grows aragonite frostwork that is often tipped with a soluble mineral such as hydromagnesite (Figs. 32 and 39, p. 152). All three mineral species form simultaneously from the same capillary solution and in the same crystallization environment. However, because of evaporation the Mg/Ca ratio of the capillary film steadily increases from the base of each multicorallite branch toward the tip. In this way, a multicorallite changes the chemistry of its feeding solution, giving rise to changes in morphology, crystal-splitting grade, and even the mineralogy of the crystals being deposited. In such speleothems, continuous recrystallization clearly also takes place, otherwise hydromagnesite would coat all the surface of the aragonite needles and not just remain on the growing needle tips. Because of continuous growth throughout all parts of the multicorallite, magnesium is also redissolved in the root part of each branch. This recycling of the Mg ion, even if from a rather low original concentration, creates the conditions whereby aragonite growth becomes possible (inasmuch as the Mg ion promotes aragonite growth but is not significantly incorporated within the mineral itself). Complete evaporation of the remaining solution on the tips of the aragonite needles allows high-Mg minerals such as hydromagnesite or huntite to be deposited.

Another example is a pseudohelictite, a type of solid quill anthodite consisting of a central aragonite needle sheathed in spherulitic aggregate calcite (Fig. 33: p. 150). Both minerals grow simultaneously. The aragonite needle defines the general geometry of the multiaggregate and the branching directions, while the calcite overgrowth suppresses the crystalline defects of the needle and, thus, limits the branching frequency.

(2.2.2) Polytextural Multiaggregates. Multiaggregates do not need to involve the co-growth of different mineral species. There are also monomineral multiaggregates that are polytextural. The most common example of this is the ubiquitous cone-shaped calcite stalactite. This speleothem contains the mineral calcite simultaneously growing as a "crown" of skeleton crystals that forms at the tip of the stalactite from drip water due to mechanical agitation and CO_2 loss during dripping (Fig. 34: p. 150), a monocrystalline tube that forms by recrystallization of these skeleton crystals, and a spherulitic aggregate outer layer that is deposited as a result of regular degassing of CO_2 (Maltsev 1997c). Soda straw stalactites are also multiaggregates since they contain both skeleton crystals and monocrystalline growth. It is important to note that conical stalactites are not soda straws overgrown by a later surface crust–the three textures form together and simultaneously.

(2.2.3) Hybrid Multiaggregates. One of the central tenets of ontogeny is that the texture of a minor mineral body is directly related to its crystallization environment. However, the boundary between different crystallization environments is not always clearly defined. For example, corallites grow in the capillary film environment by evaporation. If the feeding supply is sufficiently strong to cause slow dripping from the aggregate, a hybrid MMB (a corlactite) may form with features of both a corallite and a stalactite–the branches of the corlactite are partially cemented together, and the statistical trend of their orientation shows a weak gravitational control. Crystallictites similarly hybridize with stalactites, to form crystlactites. Names for these hybrid textures were first proposed by Victor Stepanov in 1983, but only appeared in print when part of his archive was published posthumously (Stepanov 1997).

If significant evaporation occurs in a gravitational water environment, similar hybrid textures may be expected. However, conical stalactites are multiaggregates of three textures, not all of which are available for hybridization. Only the outer spherulitic aggregate part can hybridize with corallites (or crystallictites), so the resulting MMB looks somewhat like a corlactite but with a soda straw inside (Maltsev 1997c). By contrast, stalagmites are simple spherulitic aggregates and so can fully hybridize with corallites. Depending on the balance between dripping and evaporation, a range of hybrid forms from almost "pure" stalagmite to almost "pure" corallite is possible. Hybridization between helictites and soda straws is also known.

Hybridization of texture is an important concept because it explains how some of the most interesting and unusual speleothems grow (Fig. 35: p. 150). However, speleothems can change texture as a result of a change in environmental conditions. Care needs to be taken to distinguish between true hybridization caused by a combined (or mixed) environment, and a sequential change of texture.

(2.3) Pseudoaggregates. Some speleothems are disordered and have no "through" structure. They cannot be considered as true aggregates and do not fit into the hierarchy of MMB. However, these anomalous mineral bodies can take part in the formation of higher levels of the MMB hierarchy (koras and ensembles), and so behave as if they were some form of aggregate. Such anomalous mineral bodies are called *pseudoaggregates.*

A consistent feature of pseudoaggregates is that the original place of nucleation of any crystal individual is different from its final resting place on a substrate. This produces a chaotic arrangement of crystals, for which there can be no "through" structure. For tufaceous deposits and chemogenic moonmilk, the crystallization displacement is usually quite small. But in the case of cave cones, where sunken cave rafts accumulate at the bottom of a pool, this distance can be measured in meters. Cave rafts are true aggregates, having structural and textural regularities. A jumbled pile of rafts does not collectively possess these features, but a cave cone does have a definite morphology that repeats itself in the cave environment (which itself is a textural feature). It clearly forms from the same crystallization conditions as rafts and shelfstone, and so can join with those speleothems in the higher levels of MMB hierarchy.

(2.3.1) Tufaceous Mineral Bodies. Some of the most massive stalactites, stalagmites, and flowstones in caves are formed not of hard crystalline calcite, but of a light and porous calcareous material composed of disordered microcrystals. It is common to find such tufaceous material alternating with crystalline layers. Such speleothems may be of a purely mineral (nonorganic) composition, but they commonly have a significant organic (bacterial or algal) content, particularly in the daylight zone of caves where calcite deposition is aided by photosynthesis. Tufaceous deposits in caves are usually made of calcite, but in metaliferous mines many other mineral species have been identified.

Tufaceous mineral bodies tend to grow massively and rapidly, with new nucleation outpacing the development of "through" structure. Such bodies are formed from turbulent gravitational water streams, where oversaturation of the feeding solution is caused by mechanical agitation and CO_2 degassing. This leads to nucleation of calcite crystals within the feeding solution, mainly around cavitation bubbles, rather than directly on the substrate surface. There is no opportunity for competition to start (such competition would lead to the formation of a regular aggregate), and the crystals coagulate together in a disorderly manner, producing light and porous speleothems. The nature of the dripping water environment allows the morphology of these tufaceous MMBs to mimic those made from crystalline material, so all of the common (laminar flow) gravitational water speleothems have their tufaceous analogs. In addition, most rimstone dams (gours) are built of tufaceous calcite because turbulent flow over their rims causes mechanical agitation and rapid degassing. Tufaceous mineral bodies can also form as a result of sudden pressure or temperature changes, for example from crack-fed solutions in artificial structures such as tunnels, bridges, etc. (Fig. 36: p. 151).

(2.3.2) Moonmilk. Moonmilk is a microcrystalline to nanocrystalline coagulation of disordered acicular individuals, porous and plastic in nature, and containing 40-80% water by weight. Moonmilk may be of biogenic origin, chemogenic origin, a residual precipitate of bedrock or speleothem weathering, or of mixed origin (Hill & Forti 1997). Moonmilk deposits are often composed of calcite, but they can also be composed of other carbonate, sulfate, phosphate, or silicate minerals. Chemogenic moonmilk forms under conditions of high oversaturation in a dripping/flowing water environment, and so can form speleothems similar (but on a far smaller scale) to tufaceous deposits (Fig. 37: p. 151).

At present, only chemogenic carbonate moonmilk has been studied from an ontogenetic perspective (Stepanov 1997). A case could be made for considering speleothems of biogenic origin as a specific environment within ontogeny, but this is a

debate for the future. Weathering residues are sediments and therefore cannot be studied in ontogeny.

(3) THIRD LEVEL: Assemblages of Aggregates. The division of physical mineral bodies into individuals and aggregates is an 18th Century concept. However, *aggregate* was then a very broad term, even including rocks within its scope. This situation was not resolved until Stepanov (1970) found a new formulation of *aggregate texture* that excluded rocks. This led directly to the concept of minor mineral bodies and the understanding that an aggregate is a relatively low-ranking MMB within a larger hierarchy. This larger hierarchy is still poorly known among mineralogists, even in Russia, inasmuch as it has been derived mainly from observations of speleothems in caves. Above the level of aggregate, there seemed to be a class of MMB that had the same sense of texture as an aggregate, but lacking the structure of an aggregate. This new and more complicated type of MMB was given the name *kora* by Russian speleologists.

(3.1) Koras. Kora is a Russian word meaning "crust" in a broad sense. For Russian mineralogists, the term has two meanings: As an aggregate term and as a hierarchy term. ("Crust" is also used more loosely in English texts as a speleothem term; Hill & Forti 1997.) Here, we use *kora* strictly as a hierarchy term.

A kora is an assemblage of texturally similar aggregates, growing together at the same time and in the same crystallization space, and forming from the same environmental conditions. The concept was first suggested by Fersman & Shcherbakov (1925) as a term uniting the different forms of stalactites, stalagmites, draperies and flowstones that grow together in a dripping water environment–they called this "the stalactite-stalagmite kora of calcite" (Fig. 38: p. 151). Stepanov's great contribution was to extend the concept of kora to other aggregate assemblages. Examples include the tufaceous calcite kora, the corallite kora, the antholite kora, etc. (Stepanov 1971, 1997).

A strict definition of kora was given by Stepanov (1997): "A kora is an association of aggregates that appears in all the space of synchronous crystallization, during episodes of the crystallization cycle when the phase state of the crystallization medium remains constant for significant intervals of time." In current usage, aggregates, multiaggregates and pseudoaggregates can all be included in koras, because at this level there is no distinction between them. We must note that for koras, the concept of "through" *structure* no longer applies–only "through" *texture*. In the case of polytextural multiaggregates such as conical stalactites, the dominant spherulitic aggregate texture is kora-forming and allows them to join with stalagmites and flowstones (which have only this texture).

The great advantage of studying koras, as compared to aggregates, is that variations in structure become apparent when the whole crystallization space is studied as a unit. For example, in a capillary film environment crystallictites may grow in one part of a chamber, corallites in another part, and intermediate forms in between. Without the kora concept, this would seem to be two groups of aggregates with some hybrid forms. With the kora concept, it becomes obvious that corallites and crystallictites are texturally the same and that the only difference between them is the degree of crystal splitting in the structure of the individuals that form the aggregate. This is an example of variations of structure within a crystallictite-corallite kora.

The concept of kora denotes the union of texturally similar crystallization products generated together by the same environment. However, over very long periods of time the cave environment can change. As different mediums of crystallization replace one another, new koras can be generated thereby initiating a change in textures throughout the whole space of synchronous crystallization. For example, corallites growing on stalactites and corallites growing from rock walls can together form a corallite kora (if they are of the same generation), but the stalactites themselves are not part of that kora–they are from an earlier stalactite-stalagmite kora.

(4) FOURTH LEVEL: Assemblages of Koras. A fourth hierarchy level in mineral ontogeny was first suggested by Stepanov in a series of lectures given at Moscow State University during the 1970s. He named this new and more complex minor mineral body an *ensemble*. Some years after Stepanov's death, the term was introduced into print by Maltsev (1993).

(4.1) Ensembles. The ensemble concept is fundamentally different from that of other terms used in MMB hierarchy. The factor of a regular change is involved. Crystallization environments evolve over long periods of time, becoming successively drier until a new wet phase marks the start of the next crystallization cycle. These cycles are not always complete, but the sequence remains the same (Stepanov 1971). For the first three levels in MMB hierarchy, the mineral bodies form in a stable crystallization environment during a single episode and from one feeding mechanism. To study an ensemble, we must examine all the mineral growth of the current crystallization cycle; i.e., since the last general inundation of the crystallization space, or its last general drying out. For ensembles, the concept of "through" texture is different because it involves a sequence of textures evolving through time (Fig. 39: p. 151). An ensemble is usually described by a "diagnostic set" of minerals or speleothems and can include any MMB.

In many limestone caves fed by meteoric water, the crystallization cycle begins with stalactites, stalagmites, and flowstone. Later in the cycle, this dripstone and flowstone may become overgrown by knobby popcorn concretions. Here a stalactite-stalagmite kora is replaced by a corallite kora as a dripping (gravitational) environment dries out and becomes a capillary film (evaporitic) environment. The overgrowth may be sharply defined, as in this example, or it can be a gradual transition (crystalline stalactite-stalagmite kora, seasonal overgrowth of radial-fibrous aggregates, continuous radial-fibrous aggregates, corallite kora).

Each cave or cave system, because of its own particular set of environmental parameters, has only a limited number of ensembles. Generally, these are different for different caves, although some ensembles may be typical for an entire cave region. For example, the caves of the Guadalupe Mountains, New Mexico, were developed in dolomitic limestone by a sulfuric acid mechanism. In these caves, there is a particularly well-displayed ensemble comprising gypsum blocks deposited during the original sulfuric acid speleogenesis episode, and younger gypsum stalactites (chandeliers) and stalagmites derived from reworked material (Fig. 35: p. 150). The caves of Crimea (Ukraine) are typical of limestone caves fed by meteoric water, and are abundantly decorated by speleothems showing the following sequence: tufaceous stalactite-stalagmite kora, crystalline calcite stalactite-stalagmite kora, corallite kora, antholite kora (Stepanov 1971).

An ensemble is, therefore, very different from other MMBs. It is an expression of the mineralogic landscape of a cave or cave passage. Because of differences in the chemistry of the host rock or the mineralizing solution, a great many possible ensembles can be found in caves. However, within any one cave, or within a small karst region, they are relatively few in number. One weakness of the ensemble concept is that it is not transitive; i.e., in different cave regions the crystallization products and their evolution are different. A stalactite is much the same in all caves, as is a multicorallite or an antholite kora. Ensembles rarely repeat themselves exactly.

Ontogeny is concerned only with minerals deposited during a single crystallization cycle. Very old speleothems, formed during several cycles of deposition, have no "through" regularities and are not MMBs. The separate phases of deposition can be studied using ontogeny techniques (e.g., Stepanov 1971), but such speleothems as a whole must be classed as *rocks* and studied by petrographic techniques.

CONCLUSION

In this paper, we have shown how crystal individuals combine together to form aggregates, and how associations of aggregates build the higher levels of the minor mineral body hierarchy–koras and ensembles. These more complex MMBs are best understood by building parallels to regular mineralogy. Multiaggregates may be viewed as the MMB equivalent of paragenesis, koras of associations, and ensembles of sequences.

Curiously, the higher levels of the MMB hierarchy are readily understood by non-mineralogists. Most members of the general public know that stalactites and stalagmites "go together", which (with textural considerations) is the kora concept. Experienced cavers will describe stalagmites covered with popcorn corallites as "old-looking", this being the ensemble concept of one kora replacing another as a crystallization cycle progresses. The historical problem for cave scientists has been how to deconstruct the mineralogical landscape, to break it down into simpler units. But without the concepts of ontogeny, any studies of MMB texture suffer greatly, as was the case for the first thorough study of speleothems (Prinz 1908).

Another apparent problem for studies of ontogeny is that the detailed structure and texture of speleothems can only be seen by microscopic examination of cut sections. However, once this determination has been made and described, the specific form of many common speleothems can be recognized simply by eye. Cavers with a small amount of mineralogic experience are, therefore, able to accurately identify the stage in a development cycle of the mineral growth in any newly discovered cave passage.

Ontogeny of minerals is not simply a new classification system for minerals. It is a method by which past crystallization environments can be interpreted from the mineral bodies that were deposited. The structure and texture of minor mineral bodies can be directly related to environmental factors, and speleothems are ideal subjects for this type of study.

ACKNOWLEDGMENTS

The conceptual framework of this paper belongs to our colleague Vladimir Maltsev, who worked with us on an earlier version of the text. The ideas presented here have been developed from the (largely unpublished) work of the late Victor Stepanov. We would like to acknowledge Donald Davis, Paolo Forti, George Moore, Bogdan Onac, Victor Polyak, and William White for their helpful reviews during the preparation of this paper, and to thank the many who contributed photographs and drawings.

REFERENCES

Broughton, P.L., 1983a, Lattice deformation and curvature in stalactitic carbonate: International Journal of Speleology, v. 13, n. 1-4, p. 19-30.

Broughton, P.L., 1983b, Environmental implications of competitive growth fabrics in stalactitic carbonate: International Journal of Speleology, v. 13, n. 1-4, p. 31-42.

Broughton, P.L., 1983c, Secondary origin of the radial fabric in stalactitic carbonate: International Journal of Speleology, v. 13, n. 1-4, p. 43-66.

Dana, J.D., 1837, A system of mineralogy (1st ed.): Durrie & Peck, New Haven, 452 p.

Fersman, A.E., 1935, Achievements of Soviet mineralogy and geochemistry during recent years, 1929-1934: Moscow-Leningrad, Izdatel'stvo A.N. SSSR. In Russian.

Fersman, A.E., & Shcherbakov, D.I., 1925, The Tyuya-Muyun deposit of radium ore in Fergana: Moscow. In Russian.

Folk, R.L., 1965, Some aspects of recrystallization in ancient limestones, *in* Pray, L. C., & Murray, R. C. (eds.), Dolomitization and limestone diagenesis: Society of Economic Paleontologists and Mineralogists Special Publication 13, p. 14-48.

Folk, R.L., & Assereto, R., 1976, Comparative fabrics of length-slow and length-fast calcite and calcitized aragonite in a Holocene speleothem, Carlsbad Caverns, New Mexico: Journal of Sedimentary Petrology, v. 46, n. 3, p. 486-496.

Godovikov, A.A., Ripenen, O.I., & Stepanov, V.I., 1989, Spherolites, spherocrystals and spheroidalites: New data on minerals: Nauka, Moscow, v. 36, p. 82-89. In Russian.

Grigor'ev, D.P., 1961, Ontogeny of minerals: Lvov, Izdatel'stvo L'vovskogo Univ. In Russian. English translation 1965, Israel Program for Scientific Translations, 250 p.

Grigor'ev, D.P., & Zhabin, A.G., 1975, Ontogeny of minerals. Individuals: Nauka, Moscow, 200 p. In Russian.

Hill, C.A., & Forti, P., 1997, Cave minerals of the world (2nd ed.): National Speleological Society, Huntsville, Alabama, 463 p.

Jones, B., & Kahle, C.F., 1993, Morphology, relationship, and origin of fiber and dendrite calcite crystals: Journal of Sedimentary Petrology, v. 63, n. 6, p. 1018-1031.

Jushkin, N.P., 1973, The theory of micro-blocked crystal growth in natural heterogenic environments: Syktyvkar NC, 74 p. In Russian.

Kantor, B.Z., 1997, Besedi o mineralakh (Discussions about minerals): Nazran, Astrel, 136 p. In Russian. Republished in English 2003, as Crystal growth and development interpreted from a mineral's present form: Mineralogical Almanac, v. 6.

Kendall, A.C., 1977, Fascicular-optic calcite: a replacement of bundled acicular carbonate cements: Journal of Sedimentary Petrology, v. 47, n. 3, p. 1056-1062.

Kendall, A.C., 1985, Radiaxial fibrous calcite: A reappraisal, *in* Schneiderman, N., and Harris, P.M. (eds.); Carbonate Cements, Society of Economic Petrologists and Mineralogists Special Publication no. 36, p. 59-77.

Kendall, A.C., 1993, Discussion: Columnar calcite in speleothems: Journal of Sedimentary Petrology, v. 63, n. 3, p. 550-552.

Kendall, A.C., & Broughton, P.L., 1977, Discussion: Calcite and aragonite fabrics, Carlsbad Caverns: Journal of Sedimentary Petrology, v. 47, n. 3, p. 1397-1400.

Kendall, A.C., & Broughton, P.L., 1978, Origin of fabrics in speleothems composed of columnar calcite crystals: Journal of Sedimentary Petrology, v. 48, n. 2, p. 519-538.

Korshunov, V.V., & Shavrina, E.V., 1998, Gypsum speleothems of freezing origin: Journal of Cave and Karst Studies, v. 60, n. 3, p. 146-150.

Maleev, M.N., 1971, Properties and genesis of natural filamentary crystals and their aggregates: Nauka, Moscow, 180 p. In Russian.

Maleev, M.N., 1972, Diagnostic features of spherulites formed by splitting of a single crystal nucleus. Growth mechanism of chalcedony: Tschermaks Mineralogische und Petrographische Mitteilungen, v. 18, p. 1-16.

Maltsev, V.A., 1989, The influence of season changes of the cave microclimate to the gypsum genesis: Proceedings of the 10th International Congress of Speleology, Budapest, v. 3, p. 813-814.

Maltsev, V.A., 1993, Minerals of the Cupp Coutunn karst cave system, southeast Turkmenistan: World of Stones, Moscow, v. 1, p. 5-30.

Maltsev, V.A., 1996a, Filamentary gypsum crystals from the Cupp-Coutunn Cave: Journal of Cave and Karst Studies, v. 58, n. 3, p. 204.

Maltsev, V.A., 1996b, New levels in the minor mineral bodies hierarchy: Journal of Cave and Karst Studies, v. 58, n. 3, p. 204-205.

Maltsev, V.A., 1996c, Sulphate filamentary crystals and their aggregates in caves: Proceedings of the University of Bristol Spelaeological Society, v. 20, n. 3, p. 171-186.

Maltsev, V.A., 1997a, A model of structure and genesis for the gypsum "nest" found in the Geophysicheskaya Cave (Kugitangtou Mountains, Turkmenistan): Journal of Cave and Karst Studies, v. 59, n. 2, p. 87-90.

Maltsev, V.N., 1997b, Overview of cave minerals onthogeny: Proceedings of the 12th International Congress of Speleology, La Chaux-de-Fonds, Switzerland, v. 1, p. 219-222.

Maltsev, V.A., 1997c, Stalactites, crystlactites, corlactites, tuflactites – 4 types of "stalactite-like" formations, generated from crystallization environments with different physical properties: Proceedings of the 12th International Congress of Speleology, La Chaux-de-Fonds, Switzerland, v. 1, p. 267-270.

Maltsev, V.A., 1998, Stalactites with "internal" and "external" feeding: Proceedings of the University of Bristol Spelaeological Society, v. 21, n. 2, p.149-158.

Moore, G.W., 1952, Speleothem – A new cave term: National Speleological Society News, v. 10, n. 6, p. 2.

Moore, G.W., 1954, The origin of helictites: National Speleological Society, Occasional Papers, n. 1, 16 p.

Moore, G.W., 1999, Discussion: Helictites, *in* V. A. Slyotov, Cave Geology, v. 2, n. 4, p. 196.

Moroshkin, V.V., 1976, On genesis of crystallictite types of aggregates: Nauka, Novye Dannye o Mineralakh SSSR, v. 25, Moscow. In Russian.

Moroshkin, V.V., 1986, Karstotypic mineralization: Mineralogickeskiy Journal, Kiev, v. 8, no. 5, p. 10-20. In Russian.

Polyak, V.J., 1992, The mineralogy, petrography, and diagenesis of carbonate speleothems from caves in the Guadalupe Mountains, New Mexico: Unpublished MS thesis, Texas Tech University, Lubbock, 165 p.

Prinz, W., 1908, Les cristallisations des grottes de Belgique: Nouveau Memoire de la Societie Belge de Geologie, ser. 4, n. 2, 90 p. In French. English translation 1980, Cave Geology, v. 1, n. 7, p. 191-258.

Serban, M., Viehmann, I., & Coman, D., 1961, Caves of Romania: Meridiane, Bucharest. In Romanian, Russian, French, and German editions.

Shafranovskiy, I.I., 1961, Crystals of minerals: Curved-faced, skeletal and granular forms: Gosgeoltekhizdrt, Moscow, 230 p. In Russian.

Shubnikov, A.V, 1935, How crystals grow: Izdatel'stvo AN SSSR, Moscow-Leningrad. In Russian.

Slyotov (Sletov), V.A., 1985, Concerning the ontogeny of crystallictite and helictite aggregates of calcite and aragonite from the karst caves of southern Fergana: Novye Dannye o Mineralakh CCCP (New Data on Minerals), Nauka, Moscow, v. 32, p. 119-127. In Russian. English translation 1999, Cave Geology, v. 2, no. 4, p. 196-208.

Stepanov, V.I., 1965. Exploration de la succession de crystallisation des agregats mineraux comme l'une des facon d'etude de l'histoire de la formation des grottes a concretions calcaires (abst.): 4th International Congress of Speleology, Ljubljana, Yugoslavia. Summaries of lectures, p. 54-55. In French.

Stepanov, V.I., 1970, On the genesis of so-named "collomorphic" mineral aggregates, *in* Ontogenetic methods of studying minerals: Nauka, Moscow, p. 198-206. In Russian.

Stepanov, V.I., 1971, Crystallization processes periodicity in karst caves: Trudy Mineralogicheskogo Muzeya imini A.E. Fersmana, Moscow, n. 20, p. 198-206. In Russian. English translation, 1999, Cave Geology, v. 2, no. 4, p. 209-220.

Stepanov, V.I., 1973, On aims and methods when studying crystallization sequences in ore mineral aggregates; *in* Issledovaniya voblasty prikladney mineralogii i kristallokimiie: Institute of Geology, Geochemistry, and Crystallography of Rare Elements, Moscow, p. 3-10. In Russian.

Stepanov, V.I., 1997, Notes on mineral growth from the archive of V. I. Stepanov (1924-1988): Proceedings of the University of Bristol Spelaeological Society, v. 21, n. 1, p. 25-42.

Zhabin, A.G.,1979, Ontogeny of minerals. Aggregates: Nauka, Moscow, 300 p. In Russian.



Figure 2. (A - top) A single spar crystal of hydrothermal calcite on a passage wall, Carlsbad Cavern, New Mexico. Photo by Cyndi Mosch. (B - bottom) Gypsum individuals on the side of a pseudohelictite, Cupp-Coutunn Cave, Turkmenistan. Photo by Vladimir Maltsev.

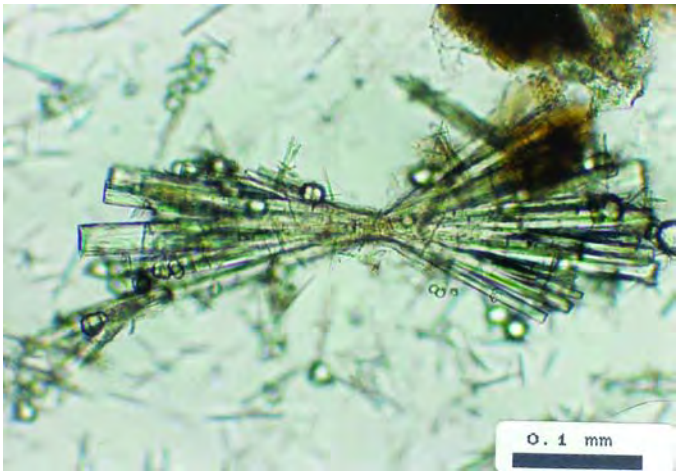
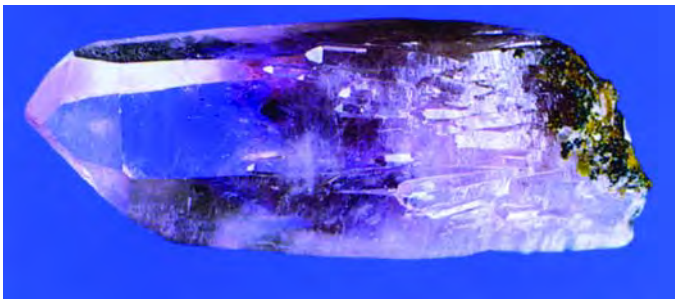
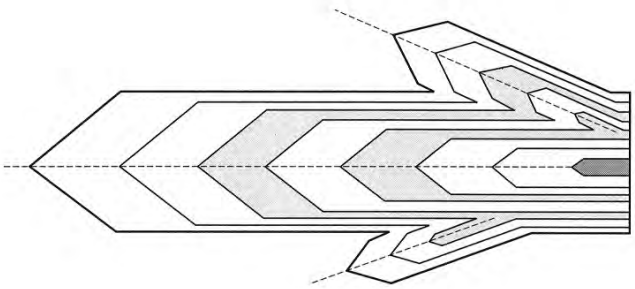


Figure 3. Thin-section photomicrograph of a split crystal of aragonite growing from a single nucleus (the small round structures in the photo are spherules of monohydrocalcite). Precipitation was achieved under laboratory conditions. From Polyak (1992).

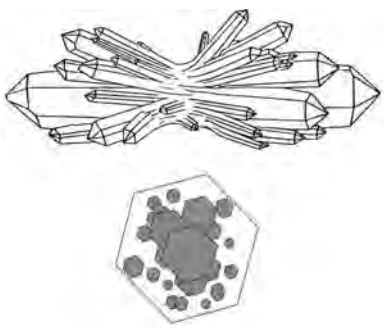


Figure 6. Spherulites of wavellite, an aluminium phosphate mineral (non-cave photo). From Kantor (1997).











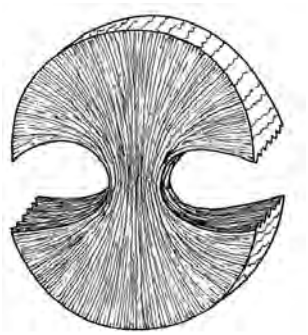


Figure 5.
Photos and representative drawings of :
(A - top) late stage simple splitting of a quartz crystal;
(B - center) early stage "sheaf" splitting of a quartz crystal,
(C - bottom) "twin leaf" continuous splitting of stellerite, a mineral of the zeolite group (non-cave photos).
From Kantor (1997).





Figure 8.
(A - left) Growth of an aragonite beaded helictite, Carlsbad Cavern, New Mexico. Note the tip of the helictite where split crystals are poised to begin a new bead. Photo by Cyndi Mosch.
(B - right) A pseudostalactite (a type of aragonite spathite), Cupp-Coutunn Cave, Turkmenistan. Photo by C. Self, courtesy of University of Bristol Speleological Society.

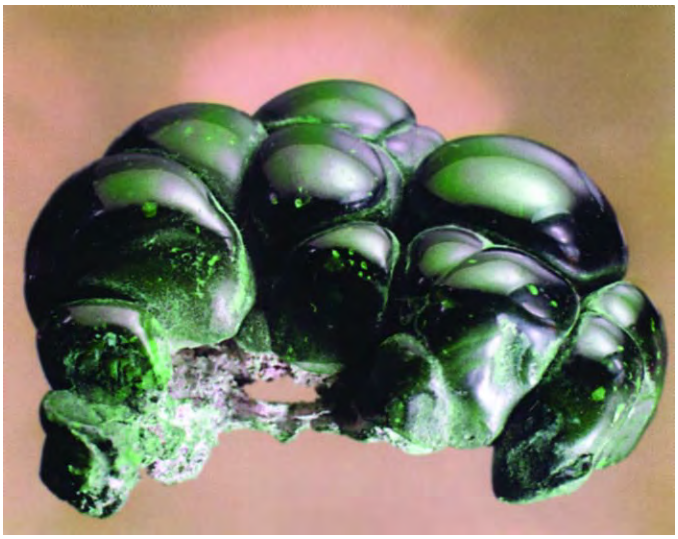


Figure 10. The smooth, bright surface of malachite, which is composed of several spherocrystals (not a cave photo). From Kantor (1997).



Figure 11. A sublimation ice crystal aggregate, Eiskogelhöhle, Tennengebirge, Austria. Note the skeletal nature of these crystals. The largest crystal on the left is ~9 cm in diameter. Photo by W. Hartman.



Figure 12 (left). A twin crystal of selenite (gypsum) from Fort Stanton Cave, New Mexico. Note the symmetrical growth around the "twin plane" (central line along the crystal). The crystal is ~4 cm long. Photo by Alan Hill.

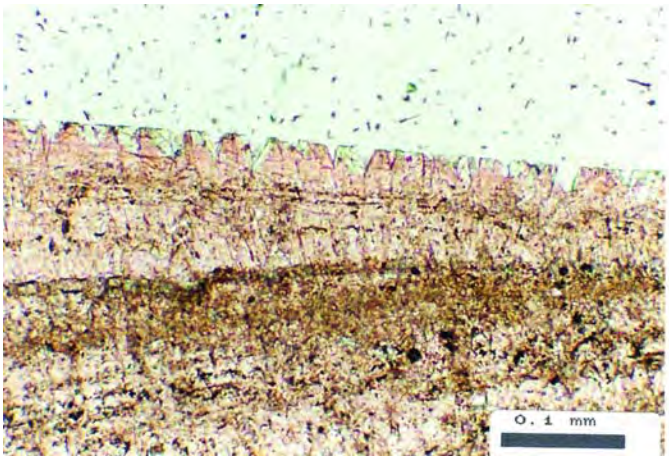


Figure 16. Thin-section photomicrograph showing crystal terminations on the surface of a stalactite, ABC Cave, New Mexico. From Polyak (1992).

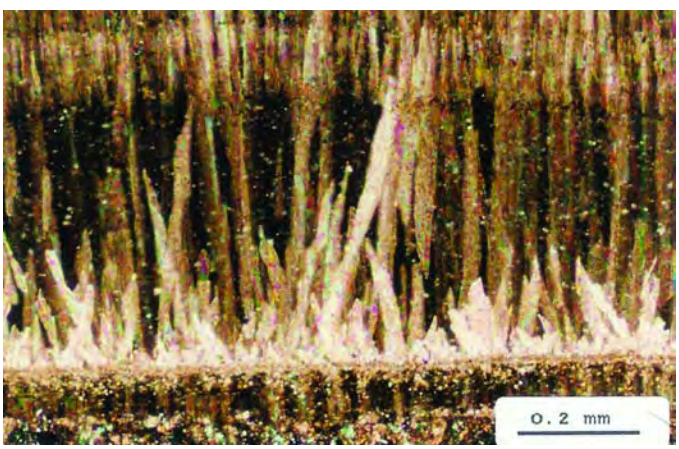


Figure 18. Thin-section photomicrograph showing competitive growth of calcite and a transition from randomly oriented to parallel-columnar texture, from a cave in New Mexico. From Polyak (1992).

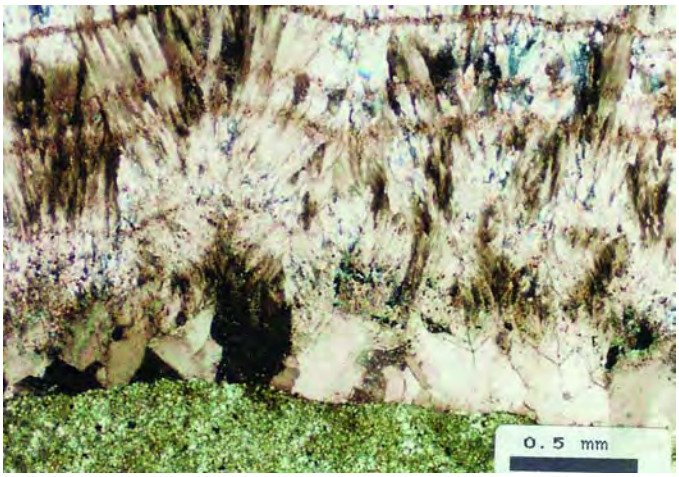


Figure 22. Thin-section photomicrograph of parallel-columnar texture (spar crystals at growth surface) changing to radial-fibrous texture ("felted" or "coconut-meat" crystals overlying spar), from Endless Cave, New Mexico. The horizontal "lines" may be due to interruptions of growth where "dirt" accumulated on the surface of the growing speleothem. From Polyak (1992).



Figure 24. Aragonite crystallictites growing from a stalagmitic floor crust, Cueva del Nacimiento, Spain. Note that the separate branches never touch each other. Photo by C. Self.



Figure 25 (left). Corallites growing on a bear's skull, Piatra Altarului Cave, Romania. Note that the strongest growth is on the more convex surface at the back of the head. Photo by Cristian Lascu.



Figure 26 (above). A calcite crystallictite overgrowth on a stalactite, Cueva del Nacimiento, Spain. The curved crystal faces are probably due to chemical splitting at the molecular level (in a similar manner to that of spherocrystals). Photo by C. Self.



Figure 28. Gypsum cotton (on ceiling) and hair (on and over ledge) in a Grand Canyon cave, Arizona. Photo by Alan Hill.



Figure 29. Epsomite (left) and gypsum (right) flowers in Torgac Cave, New Mexico. Note the shard of rock (in center of photo directly below caliper) that has been pushed outward from the wall by mineral growth. Photo by Alan Hill.



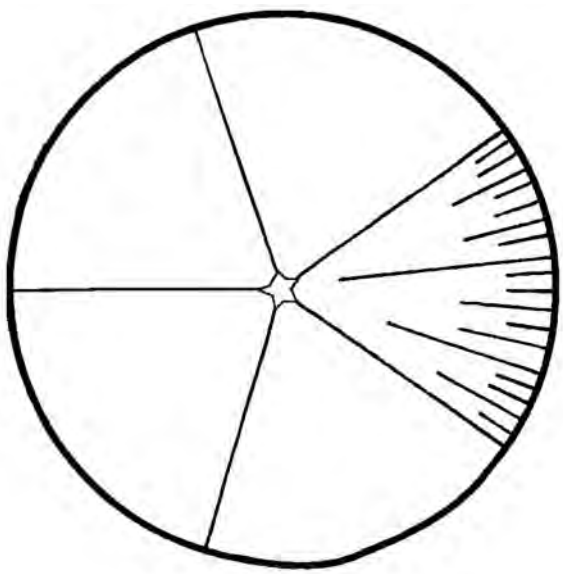


Figure 30. (A - top) Aragonite "cut" helictites, The Blue Cave (a Roman copper mine), France, showing parallel co-growth of 4 spherulite bunches. Photo by Patrick Cabrol. From *Cave Minerals of the World, Second Edition* Copyright 1997, National Speleological Society, Inc. Used with permission. (B - bottom) Sketch cross section of a helictite built from 5 spherulite bunches (for clarity, subindividuals are shown in only 1 of the 5 spherulite sectors).



Figure 33. Pseudohelictites with partial overgrowth of gypsum crystals, Cupp-Coutunn Cave, Turkmenistan. Photo by C. Self.

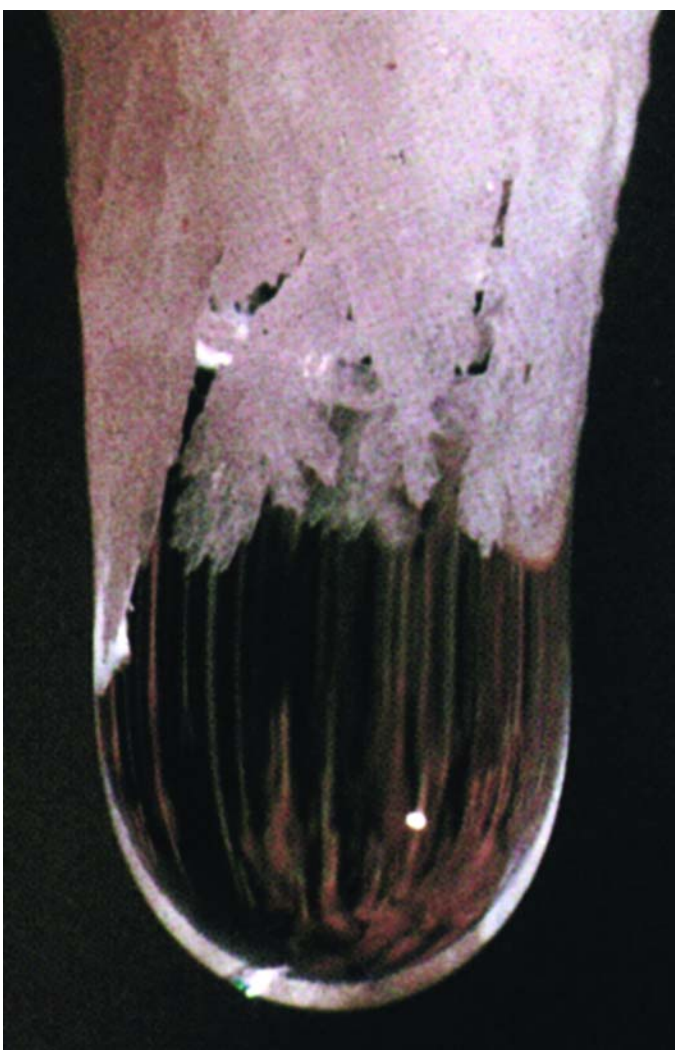


Figure 34. The growth tip of a calcite stalactite from Moravia, Czech Republic, showing skeleton crystals. Photo by Igor Audy.



Figure 35. Gypsum chandeliers, Lechuguilla Cave, New Mexico. Because gypsum is precipitated by evaporation, not as a result of CO_2 loss during dripping, it is normal for crystlactites to form rather than regular stalactites. Photo by Urs Widmer.



Figure 36. Tufaceous calcite soda straws in the cellar of a house in Bristol, England. Photo by Geoff Wood.



Figure 37. A flowstone "river" of hydromagnesite moonmilk, Pink Dragon Cave, New Mexico. Photo by Alan Hill.



Figure 38. A "stalactite-stalagmite kora of calcite", Carlsbad Cavern, New Mexico. Photo by Urs Widmer.

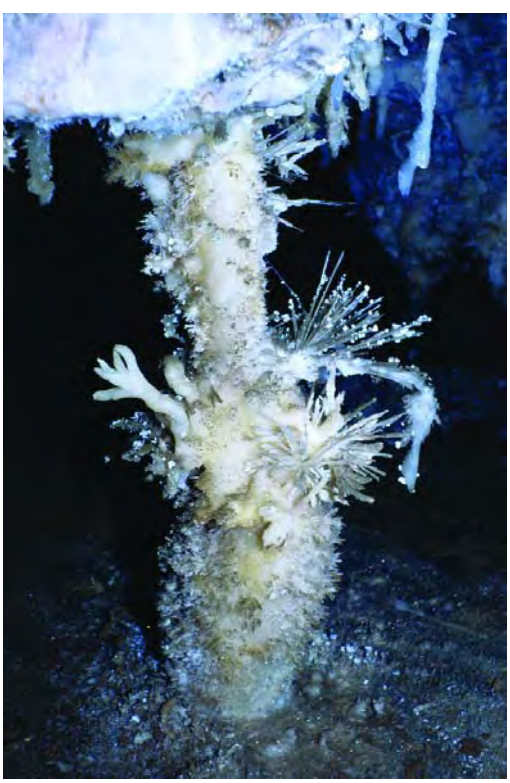


Figure 39. An ensemble of a stalactite-stalagmite kora overgrown by a corallite kora, Cupp-Coutunn Cave, Turkmenistan. Also present in the overgrowth are multicorallites, a branching aragonite helictite (left), and a multicorallite/pseudostalactite hybrid (right). The presence of pseudostalactites (a type of spathite) growing independently on the cave roof suggests that the progression from a gravitational to a capillary film environment is not yet complete. Photo by C. Self.

JOURNAL ACHIEVES MILESTONE

The staff of the Journal of Cave and Karst Sciences is very proud to announce that the *Journal of Cave and Karst Studies* has been accepted by the Institute for Scientific Information (ISI) for coverage in the following ISI products beginning with vol. 65(1) 2003:

Current Contents/Physical, Chemical & Earth Sciences
Science Citation Index-Expanded (SCIE), including the *Web of Science*
Research Alert

For cave and karst researchers, particularly those working in the publish-or-perish academic world, this achievement will dramatically enhance the prestige of any articles they publish in the *Journal* and help with tenure and promotion considerations.

EXPLORATION EDITOR NEEDED BY *JCKS*

The *Journal of Cave and Karst Studies* seeks a new Associate Editor for Exploration. The responsibilities of the Associate Editors include soliciting articles, arranging for appropriate reviews of papers in their fields of expertise, working with authors to prepare their manuscripts for publication, making recommendations concerning acceptance and rejection of submitted papers, and assisting the Editor in gathering material for the non-refereed section of the *Journal*. Advice from the Associate Editors, along with the *Journal*'s Advisory Board, is commonly solicited on editorial policy decisions.

The *Journal* desires a pro-active caver with contacts in the cave exploration community and experience with scholarly publishing. Interested candidates are asked to send a letter of interest by September 30, 2003 to the editor at: LHose@cemrc.org.

NEW MEXICO TECH
SCIENCE • ENGINEERING • RESEARCH • UNIVERSITY

NCKRI SCIENCE COORDINATOR

NEW MEXICO INSTITUTE OF MINING AND TECHNOLOGY seeks a NCKRI Science Coordinator to provide science coordination, leadership, and scientific direction for the National Cave and Karst Research Institute located in Carlsbad, N.M. Reports to NCKRI Director on issues pertaining to science advancement goals, funding strategies, and scope of NCKRI science activities. Master's degree required; Ph.D. preferred subject relevant to speleology. Familiarity with at least one aspect of speleological science required. Familiarity with more than one aspect of speleological science desired. Must be familiar with the cave and karst scientific community. Familiarity with the general scientific community desired. Ability to write well required. Experience with grant proposals to agencies and private foundations desired. Experience as college faculty member and teaching at college level desired. Good verbal communication ability required. Transcripts required. Applicants should send a resume, transcripts, and the names, email addresses and phone numbers of three employment references to: New Mexico Institute of Mining and Technology, 801 Leroy Pl., Human Resources Wells Hall Box 93, Socorro, NM 87801. For information about New Mexico Tech, visit our web page http://www.nmt.edu/. E-mail applications **NOT** accepted. AAEOE

Paid Advertisement

HELP WANTED - *JOURNAL OF CAVE AND KARST STUDIES* EDITOR

The NSS *Journal of Cave and Karst Studies* (*JCKS*) seeks a new Editor-in-Chief. Interested applicants should send a curriculum vitae to NSS Executive Vice President Don Paquette at: speleo@reliable-net.net

The *JCKS* is published three times annually during April, August, and December. It is the refereed, multi-disciplinary publication of the National Speleological Society accepting papers on cave and karst related research. The Editor's responsibilities include maintaining the level of scientific integrity with the eight associate editors (Life Sciences, Conservation, Exploration, Earth Sciences/Journal Index, Paleontology, Social Sciences, Anthropology, and Book Reviews), confirmation of publication via the Production Editor and interfacing with the nine member Advisory Board. The *JCKS* Editor submits and is responsible for an annual budget and reports to the Executive Vice President at least three times per year. *JCKS* annual meetings are generally held during the NSS Convention.